

A Stochastic Framework for Ground Vehicle Simulation

Justin Madsen

Under the Supervision of Prof. Dan Negruț

At the University of Wisconsin - Madison

Over the last decade, simulation-based engineering in the form of virtual prototyping has been increasingly utilized by engineers in the design process of mechanical systems. Benefits of computer-aided engineering include reduced prototype costs, lower time to market and the ability to run “what if?” studies. As computing power has steadily increased in the past years, models have become larger, more complex and simulations are expected to run in less time. This is evident in the field of ground vehicle modeling and simulation. In the past, small sets of simulations were run to understand the general behavior of deterministic vehicle system models. In recent years there has been an increasing demand to understand complex problems such as uncertainty propagation, sensitivity analysis and reliability prediction. As such, single deterministic vehicle and operating environment models must be extended into stochastic sets of models and simulations in order to capture the added dimensionality that is associated with these types of problems. To address these issues, methods and tools were created to utilize existing models that are simulated in commercial software that enabled a stochastic simulation framework. Deterministic vehicle and environment models are extended into

sets of stochastic models and simulations using the tools in conjunction with information about the nature of the uncertainty.

The description and application of these methods and tools is the premise of this work. The original motivation for creating the tools stems from a joint research project between the author and engineers at GP Technologies, where the effect of various uncertainties on the reliability calculations of a light truck model was investigated. The creation of the vehicle and road models and simulations will be discussed, with an emphasis on the stochastic simulation framework which was developed. Proven simulation software used in industry is used to create a single vehicle system model, and the developed tools use this model in conjunction with the uncertainty information of interest to run the large number of simulations that are required to handle the high-dimensionality inherent in uncertainty propagation and sensitivity analysis problems. The tools that were created and presented were meant to be able to be extended to different types of ground vehicle systems with relative ease. To demonstrate this ability, they were applied to a tracked vehicle model which operated on a soft soil model. The goal in this example is to understand how the uncertainty in the measurements used to define parameters in the soft soil model affect the range of responses. The application of the stochastic framework on these new vehicle and terrain models is discussed and results are presented to illustrate the impact of uncertainty on the mobility and reliability of the tracked vehicle.

Acknowledgments

I would like to acknowledge all the current and past members of the Simulation Based Engineering Lab for their wisdom and support over the past two years: Makarand Datar, Nick Schafer, Naresh Khude, Martin Tupy, Philipp Hahn, Gene Shiau, Kyle Schmitt, Arman Pazouki, Hamid Ardeh, Hammad Mazhar, Dan Melanz, Yakira Braden and Toby Heyn.

A special thanks goes to my adviser and head of the Simulation Based Engineering Lab, Dr. Dan Negrut, for being the best boss a student could hope for and for giving me great advice about beaches.

Of course no acknowledgement page can be complete without thanking my parents, Geraldene and Curt, for their love, emotional and financial support.

Saving the best for last, I have to thank the love of my life, Julie Elizabeth Jackson, for saying yes to the most important question I have ever asked another human being.

Table of Contents

Abstract.....	i
Acknowledgments	iii
Table of Contents	iv
List of Figures.....	viii
List of Tables	x
Chapter 1: Introduction and Objectives	1
1.1 Introduction	1
1.2 Ground Vehicle Simulation	2
1.3 Sources of Model Uncertainty	4
1.4 Motivation and Objectives.....	6
1.5 Thesis Outline	7
Chapter 2: Terrain Models	9
2.1 Introduction.....	9
2.2 Hard-Soil Model	11
2.3 Deformable-Soil Models.....	15
2.3.1 Soil Stresses Due to External Loading.....	16
2.3.2 Soil Stress Due to Soil Deformation.....	19
2.3.3 Consideration for Repetitive Loading.....	23
2.4 Summary	24
Chapter 3: Wheeled Vehicle Description and Model	26
3.1 Introduction.....	26
3.2 Wheeled Vehicle Description	27
3.2.1 Steering	27
3.2.2 Suspension	28
3.2.3 Roll Stabilization	32
3.2.4 Powertrain	33

3.2.5	Tires	33
3.3	Wheeled Vehicle Model	33
3.4	Tire and Road Models.....	37
3.5	Summary	40
Chapter 4:	Stochastic Wheeled Vehicle Simulation	41
4.1	Introduction.....	41
4.2	Stochastic Process applied to Vehicle and Road Models	41
4.3	Post-Processing Method.....	47
4.4	Summary	47
Chapter 5:	Tracked Vehicle Description and Model	48
5.1	Introduction and Nomenclature	48
5.2	Methods for Tracked Vehicle Analysis	49
5.2.1	Empirical Methods.....	49
5.2.2	Super-element Model.....	50
5.2.3	Multi-body Approach.....	52
5.3	Tracked Vehicle Description	53
5.3.1	Suspension Unit and Road Wheel.....	54
5.3.2	Tensioning System and Idler	54
5.3.3	Drive Sprocket and Powertrain.....	56
5.3.4	Track Shoe	58
5.3.5	Compliant Track Chain.....	60
5.4	Tracked Vehicle Model.....	62
5.4.1	Assembly Topology	63
5.4.2	Rigid Body Frictional Contacts	64
5.5	Summary	67
Chapter 6:	Application 1: Reliability Prediction using a HMMWV Model.....	69
6.1	Introduction and Objectives.....	69
6.2	Stochastic Operating Environment Models	72

6.3	Stochastic Vehicle Models.....	74
6.4	HMMWV Simulation Results.....	76
6.4.1	Category 2 Results – Original Vehicle Model.....	77
6.4.2	Category 3 Results – Original Vehicle Model.....	79
6.4.3	Category 2 Results – Degraded Vehicle Model.....	82
6.4.4	Category 3 Results – Degraded Vehicle Model.....	84
6.4	Summary	86
Chapter 7: Application 2: Tracked Vehicle Response		
Sensitivity to Soft Soil Parameters.....		88
7.1	Introduction and Objectives	88
7.2	Stochastic Tracked Vehicle Simulation	89
7.3	Latin Hypercube Sampling Design	91
7.4	Tracked Vehicle Simulation Results.....	93
7.4.1	Tracked Vehicle Results: Mobility	93
7.4.2	Tracked Vehicle Results: Bushing Forces	96
7.5	Summary	99
Chapter 8: Summary and Conclusions.....		101
References		103
Appendix A: ADAMS Post-Processing Commands		106
Appendix B: Latin Hypercube Design Values		111

List of Figures

Fig. 2.1. Road height as a function of width and length plotted as a mesh in MATLAB	12
Fig. 2.2. Road profile defined with a mesh of triangular elements	13
Fig. 2.3. Section of road in ADAMS/Car RDF format and after a conversion to the FTire RGR format	15
Fig. 2.4. Subsurface stresses due to a vertical and horizontal load	17
Fig. 2.5. Pressure-sinkage behavior of selected soils, $b = 10$ cm.....	20
Fig. 2.6. Shear displacement j of the terrain increases from the front to the rear of the vehicle	21
Fig. 2.7. Shear-stress curves according to Eq.(2.10)	22
Fig. 2.8 Repetitive loading of a sandy terrain.....	24
Fig. 3.1. Front suspension and steering system of the HMMWV in the multibody dynamics software ADAMS/Car.....	28
Fig. 3.2. Front left suspension unit, front view	30
Fig. 3.3. Front left suspension unit, left side view	30
Fig. 3.4. Front suspension damper force as a function of shock velocity	31
Fig. 3.5. Rear suspension damper force as a function of shock velocity	31
Fig. 3.6. Bumpstop force as a function of deformation	32
Fig. 3.7. HMMWV vehicle model as seen in ADAMS/Car	35
Fig. 3.8. Subsystems part of the full vehicle assembly.....	36
Fig. 3.9. HMMWV and tires traversing the exit lip of a hill	38
Fig. 3.10. Illustration of the FTire modeling approach.....	39
Fig. 4.1. Data flow diagram for a single simulation	42
Fig. 4.2. Data flow diagram for stochastic simulations.....	43
Fig. 4.3. Section of the ADM file which specifies the spring stiffness of the shock absorber in the rear left suspension subsystem.....	44
Fig. 4.4. Code snippet of MATLAB script used to write multiple instances of an ADM file with modified values of the spring spline shown in Fig. 4.3.....	46

Fig. 5.1. CAD view of tracked vehicle model	48
Fig. 5.2. Components of a bevameter	50
Fig. 5.3. Schematic diagram of road wheel and suspension unit	55
Fig. 5.4. Schematic diagram of idler and tensioning system	56
Fig. 5.5. Drive sprocket on the left track system consists of two identical gears	57
Fig. 5.6. Left drive sprocket gear engaging multiple track shoes	58
Fig. 5.7. Individual track shoe	59
Fig. 5.8. Collision geometry that contacts the rolling parts and the terrain.....	59
Fig. 5.9. References frames for track shoes.....	62
Fig. 5.10. Subsystems that are part of the full tracked vehicle assembly.....	63
Fig. 5.11. Two colliding spheres with raidus r and penetration depth d	66
Fig. 6.1. Transition from a deterministic reliability prediction to a stochastic reliability approach.....	71
Fig. 6.2. Road surface models with high and low spatial correlations.....	74
Fig. 6.3. Tire deflections of the front-left tire	78
Fig. 6.4. Zoomed in section of Fig. 6.3 illustrate tire deflection when traversing an obstacle	79
Fig 6.5. Effect of rolling hills topology on chassis pitch for the medium roughness road.....	80
Fig. 6.6. Chassis pitch for medium and high roughness road simulations	80
Fig. 6.7. Shock absorber force for medium and high roughness roads.....	81
Fig. 6.8. LCA ball joint vertical force for medium and high roughness roads	81
Fig. 6.9. UCA ball joint lateral force for medium and high roughness roads.....	82
Fig. 6.10. Front left shock spring force is lower in the degraded model simulation	83
Fig. 6.11. Vertical force in the LCA ball joint is lower and higher in the degraded model	83
Fig. 6.12. Chassis pitch angles of the degraded and original vehicle model	84
Fig. 6.13. Chassis pitch angular acceleration of the degraded and original vehicle model.....	85
Fig. 6.14. Damper force comparison for roads with rolling hills topology	86
Fig. 6.15. UCA ball joint lateral force in the original and degraded vehicles	86
Fig. 7.1. Data flow diagram for a stochastic set of tracked vehicle simulations.....	90

Fig. 7.2. Tracked half-vehicle model shown on the flat road profile	91
Fig. 7.3. An example of a non-space filling LH design for the soft-soil samples.....	92
Fig. 7.4. Average longitudinal velocity of the tracked vehicle.....	94
Fig. 7.5. Individual chassis velocities during quasi-steady state operation.....	95
Fig. 7.6. Standard deviation of chassis velocity during quasi-steady state operation.....	95
Fig. 7.7. Standard deviation of chassis velocity during initial acceleration	96
Fig. 7.8. Simulation screen shots of the selected track shoe.....	97
Fig. 7.9 Bushing force of the track shoe shown in Fig. 7.8	97
Fig. 7.10. Maximum, minimum and average bushing forces	98
Fig. 7.11. Standard deviation of bushing forces during quasi-steady state operation	99

List of Tables

Table 2.1 Pressure-sinkage parameters (sources: [15, 18])	19
Table 3.1. Input data used for the FTire front and rear tires.....	40
Table 6.1. Example set of random distribution coefficients for a suspension unit.....	76
Table 6.2. Selected stochastic variable factors.	78
Table B.1. Nominal soft-soil parameters for dry sand model.....	111
Table B.2. LH sample values for soft-soil parameters.....	111

Chapter 1

Introduction and Objectives

1.1 Introduction

Over the last decade, simulation-based engineering in the form of virtual prototyping has been increasingly utilized by engineers in the design process of mechanical systems. Benefits of computer-aided engineering include reduced prototype costs, lower time to market and the ability to run “what if?” studies. As computing power has steadily increased in the past years, models have become larger, more complex and simulations are expected to run in less time. This is evident in the field of ground vehicle modeling and simulation, where in the past simplified vehicle models with only a few bodies and degrees of freedom (DOFs) have progressed into complex and accurate representations with many bodies and DOFs, which results in extremely large sets of equations that must be solved multiple times. For example, the High Mobility Multi-Wheeled Vehicle (HMMWV) light truck model presented in this work has 76 bodies and 101 DOFs which results in a set of 1895 equations that are solved at every integration step. It should be noted that a co-simulation environment is used where the tires and road are handled with a separate simulation program, and the values above only apply to the vehicle model. Descriptions of the vehicle and tire simulation software packages utilized are discussed in sections 3.3 and 3.4, respectively. A brief introduction to the modeling and simulation of ground vehicles is presented to highlight the trends and problems that are encountered with an emphasis on off-road vehicles which are used in this work.

1.2 Ground Vehicle Simulation

Both tracked and wheeled vehicles fall into the same category of vehicles; ground vehicles, with the main difference being that tracked vehicles are specifically designed for unprepared terrain whereas wheeled vehicles are not. Although many wheeled vehicles can go off-road, e.g. SUVs and HMMWVs, they are usually limited to dry, hard packed off-road terrain. This is due to the main difference between the two vehicles; the ground contact area the running gear (track chain/tires) makes with the terrain. As will be discussed in subsequent sections, both wheeled and tracked vehicles have a large weight to terrain contact area ratio. Wheeled vehicles are preferred to tracked vehicles when high operating speeds or lower amounts of maintenance are desired because of their transportation productivity and efficiency. This is due to the fact that the running gear of a tracked vehicle is complex and heavy, leading to a high overall mass which requires large forces to move, which leads to equipment failure more quickly.

Since World War II, there has been considerable interest shown in the way vehicles operate on unprepared or off-road terrain. Scientists and engineers are concerned with the principles that affect the performance of off-road vehicles in order to create new and improved designs that will lead to increased performance, efficiency and reliability of the vehicles. As a result an entire field of study, known as terramechanics, has emerged which is focused on the performance of off-road vehicles in relation to their operating environment. Terramechanics plays an important role in the study of off-road vehicles and especially tracked vehicles, which are designed to operate on unprepared and off-road terrain.

The interaction between off-road vehicles and terrain is difficult to model accurately due to the complexity of the problem. Early empirical methods utilized terrain measurement techniques such as the cone penetrometer test to determine if vehicle mobility was possible over a given terrain. These methods were pioneered in WWII by the U.S. Army Waterways Experiment Station and were subsequently used as a basis for the NATO Reference Mobility Model, which correlates vehicle performance with the terrain measurement parameter and its derivatives [1]. It is this importance between the interaction of the vehicle and terrain that motivates the tracked vehicle section of this paper. When using a high fidelity soft-soil model with an accurate vehicle model the dynamics of the system are dominated by the terramechanics. As such, experimental error in the terrain measurements such as sensor error or non-homogeneity of the soil could possibly have a large impact on the outcome of any tracked vehicle simulation.

As the trend to simulate vehicle models with increasing complexity and computational problem size accelerates, there is an inherent need to understand how certain modeling elements and their parameter values affect the outputs of interest. This knowledge is especially important when physical test data is used to define parameter values or when models have highly non-linear behavior. Thus uncertainty and sensitivity to uncertainty becomes more important as the trend towards larger and more complex models continues. Various common sources of uncertainty are detailed in the following section.

1.3 Sources of Model Uncertainty

In vehicle modeling and simulation, there are numerous sources of uncertainty. Generally, sources of uncertainty fall under two categories: modeling uncertainty and lack of data effects. These types of uncertainty are not mutually exclusive and many modeling elements can fall under both categories. Descriptions of both types of uncertainty will be presented and examples of uncertainty effects in ground vehicle simulations will be discussed.

When parts of a vehicle system (vehicle and operating environment, i.e. road profile) are simplified from a continuous to discrete representation there is error associated when the simulation must interpolate values between the discrete data points. This type of uncertainty is referred to as a “lack of data” effect. For example, road profiles are commonly modeled as a mesh of triangular elements created from a set of nodes. The nodes are height measurements taken at various locations on the road profile. To exactly model the road surface profile, one would have to take infinitely many measurements, and the simulation would have to store an infinitely large road description file. Since both of these situations are unfeasible, road profile measurements are usually taken at intervals that retain sufficient accuracy of the road profile while requiring a reasonable number of experimental measurements. The density of the road profile height measurements will invariably impact the final results, and methods for assessing the uncertainty of Gaussian and non-Gaussian variations in the road profile have been presented by Datar [2] and Madsen [3], respectively. Similarly, variable friction coefficients can be applied to each triangle in a road profile mesh to model effects such as

snow and ice. In this case the size of each triangle will dictate the level of fidelity of the road surface friction model. Sampling techniques for quantifying the level of uncertainty stemming from this type of lack of data effect were discussed by Schmitt [4].

Another type of uncertainty arises from assumptions or simplifications. For example, a shock absorber in a truck is commonly modeled by a spring and damper element. The spring may be modeled as a force element that changes linearly with displacement, which is almost never true in reality. In the context of a simulation a non-linear spring may be approximated by a linear model if the spring operates in a range that is nearly linear [5]. However, this linearization introduces another source of uncertainty in the model. This is known as modeling error, which can have a varying degree of impact on vehicle simulations.

Representing uncertainty in vehicle simulations can be addressed using several techniques, each having positive and negative attributes depending on the application. Random sampling methods such as Monte-Carlo and Latin-hypercube sampling methods [6, 7] are easy to implement but computationally expensive since the estimation of variance converges with the inverse square root of the number of runs. Methods such as generalized polynomial chaos theory are more elegant, but make the assumption that the equations that define the system can be represented as polynomials [8]. This approach is not amiable for simulations that have a large number of uncertain parameters since the complexity of the technique greatly increases with an increased number of uncertain parameters. In this context, the approaches that are utilized in this paper are of the Monte-

Carlo and Latin-hypercube type, as the tracked and wheeled system models utilized in the application examples have 7 and 54 uncertain variables, respectively.

1.4 Motivation and Objectives

The original motivation for creating the tools which implement a stochastic simulation framework stems from a research project which will be discussed in Chapter 6, where the effect of various uncertainties on the reliability calculations of a HMMWV truck model was investigated. A key aspect of this framework is that it is meant to be applied to a single deterministic model and creates a large number of models which are then subsequently simulated. The output from these numerous simulations can then be used in a sensitivity analysis or to understand the range of certain outputs of interest. Outputs can also be used as inputs into a second stage of analysis, e.g. Finite Element Analysis programs, to evaluate component stress cycles from the dynamic responses of the vehicle. In this work, the framework is applied in the commercial simulation program MSC/ADAMS, but it can be modified and applied to any vehicle simulation program.

Tools were created to extend a single model to multiple models and simulations, and to also handle the large amount of output data that result from running large numbers of simulations. In order to run large numbers of simulations in an efficient manner, the tools had to automate many of the steps in the model manipulation process. The tools created do just that, and were successfully applied to a simulation project that required a single vehicle model to be varied and simulated over 500 times. Furthermore, dynamic vehicle analysis is usually just one step in a longer process that involves component stress analyses in order to predict fatigue and damage failures, as was the case with the

HMMWV project. Thus, tools were also created that automatically post process results and extract graphical plots and data files that are subsequently used for FEA analysis. Finally, the tools should be able to be extended to multiple models and vehicle types with relative ease. After a slight modification, they were successfully applied to a tracked vehicle model in order to understand how the experimental uncertainty in the soft soil model affects the range of responses of certain forces and accelerations of interest.

1.5 Thesis Outline

Since both application examples of the stochastic framework deal with uncertainty stemming from the road and terrain, a brief introduction on the commonly used approaches for representing both hard and soft terrains is given in Chapter 2. Also, the elastoplastic stress theory of deformable soils is presented followed by its role in the deformable soil models utilized for the tracked vehicle investigation. A key element in the HMMWV project was to create a representative and dynamically accurate model from actual measurements and tests. A description of the vehicle systems of importance which are included in the dynamic simulations are given in Chapter 3, with an explanation of the modeling methodologies of the selected software packages used in the project. Chapter 4 details the steps necessary for creating large sets of models from a single deterministic model file in order to run stochastic simulations. Both pre- and post-processing methods and examples are given to highlight the approach taken when creating the tools which automate the model and results data manipulation for the large number of simulations. Chapter 5 presents the tracked vehicle model used for the soft-soil investigation and is analogous in nature to Chapter 3. The tracked vehicle simulations are

heavily influenced by rigid-body frictional contacts and the formulation in ADAMS is presented. Application examples of the stochastic framework are presented in Chapters 6 and 7 for the HMMWV and tracked vehicles, respectively. Both chapters motivate the need for analyzing uncertainty in their respective systems, and details on how this analysis was carried out using the developed tools are given. Sample results will be presented with comments on future work that should be carried out in both cases. Finally, Chapter 8 concludes the work with an emphasis on possible future applications of the tools developed herein.

Chapter 2

Terrain Models

2.1 Introduction

Although many ground vehicles operate on paved roads, there are many reasons for operating on unpaved or unprepared terrain. Vehicles involved in mining, logging or cross-country military operations spend a majority of their time operating on unpaved terrain. The type of material contained in off-road terrain ranges from dry sand to wet mud and clay, each of which has different material properties and may or may not deform substantially under vehicle loads. Soil material properties have a large impact on the performance of an off-road vehicle, which is why knowledge of terramechanics is essential when predicting the terrain-vehicle interaction. Hard soil models relate to hard packed or paved roads that are assumed not to deform under vehicle loads, while soft soil models relate to unprepared and deformable terrain.

When simulating vehicles for mobility or durability purposes, paved or hard packed roads are usually represented by a three-dimensional surface with the assumption that the road does not deform. Hence, the vehicle-terrain interaction can be modeled as a rigid body or flexible-rigid body contact problem depending on the type of running gear. Ground vehicles that operate on these types of roads are mostly comprised of wheeled vehicles, due to their cost and time efficiency of transportation. Hence, the vehicle-terrain interaction that dominates the dynamic response of the vehicle is the tire-road relationship. Moreover, the road is assumed to be rigid while the tire is pneumatic and can undergo large deformations. This leads to the conclusion that the vehicle-terrain

interaction on paved roads is dominated by the mechanics of pneumatic tires [1]. Discussion of the tire model and details on its implementation will be given in Chapter 3.

Terrain that is comprised of deformable soil has a road profile that is represented in a similar fashion as the hard soil models. However, the description of the undeformed road surface is not as important as the mechanics of the soil itself. Vertical and horizontal loads that can be sustained by a soft soil vary depending on many factors including soil material properties and soil deformation.

Hard soil models are mostly concerned with an accurate representation of the road profile, and computer simulations of vehicles on paved or hard packed roads also require a computationally efficient model. The steps in creating a computationally efficient road model for a widely used commercial off-the-shelf (COTS) vehicle simulation software from a set of input data will be discussed. Experimental measurements are necessary to procure road profile data, and some of the common methods to get the input data sets will be introduced. Soft soil models require an accurate representation of the road surface profile as well, but also have to account for the mechanics of the soil itself. First, the stress distribution in soft soils due to applied forces is discussed. The vertical and shear stress-strain models used in vehicle simulations are presented. An explanation of the effects of repetitive loading will also be included. Bulldozing effects are not discussed in detail since the soft soil model implementation assumes these forces to be negligible. Finally, implementation details for a soft soil model for vehicle mobility and reliability simulations will be discussed.

2.2 Hard Soil Model

In order to represent a non-flat 3D road profile, physical measurements must be taken from the actual road using either satellite maps or road profilers. Satellite maps do not have the level of resolution required for vehicle simulations that predict durability and reliability. Therefore, road profilers must be used in the field if the roads are to be used in high fidelity vehicle simulations. There are many sources of experimental error in road profilers, including dropouts that insert outliers in the data, the dynamics of the vehicle carrying the profiler and trends caused by gyro error [9]. A pre-processor step is needed to filter out some of the errors caused by the instruments; however, this introduces additional error from the filter and removes some information. Road profilers take measurements in straight lines, and therefore any one pass of a road profiler is one-dimensional. Once the data is pre-processed, a Power Spectral Density (PSD) is obtained by taking the fast Fourier Transform (FFT) of a window (typically Hanning) of the data. The PSD is typically assumed to be stationary along the length of the road, and multiple PSDs are averaged to reduce the variance [9]. Although the PSD is not unique, by assuming it is stationary and Gaussian, one can recreate a road profile that is a 2D map of the height data. An example of the road height as a function of the length and width along the road as plotted in MATLAB is shown in Fig. 2.1.

Once road profile data is ready to be used in a simulation, it must be posed in a filetype that is recognized by the simulation software. In the vehicle simulation software ADAMS/Car it is typically defined by a text based Road Data File (RDF) type. The road profile can be defined in a number of ways. A triangle mesh is generally used to define a

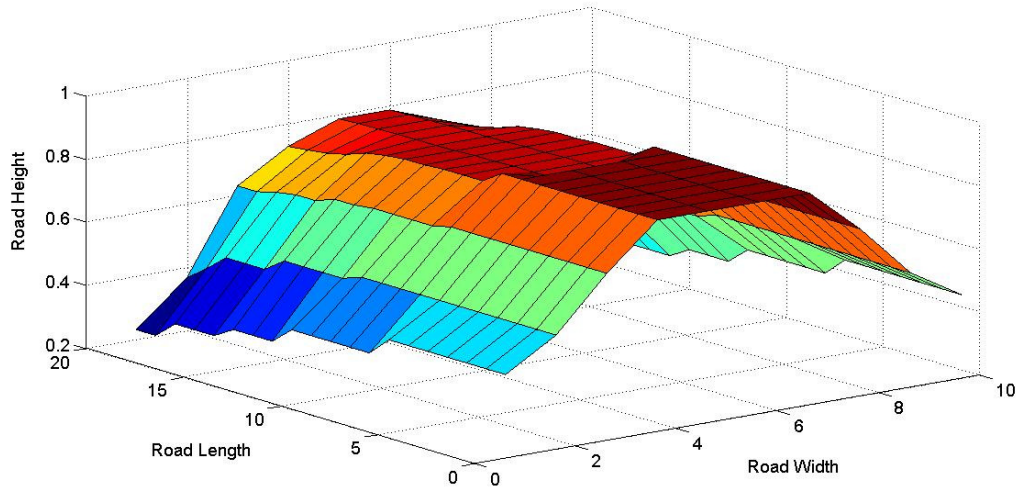


Fig. 2.1. Road height as a function of width and length plotted as a mesh in MATLAB.
Units are not to scale.

road with varying elevation in both the longitudinal and lateral directions. Each input data point represents a vertex; sets of vertices are then grouped to define triangles that make up the mesh. Fig. 2.2 shows a section of road made up of this type of triangle mesh.

Although the level of fidelity of the road model can be as high as the total number of known vertices, the simulation time required per time step using the RDF file type increases quadratically with the number of triangles in the mesh. This is due to the fact that for each time step, the simulation has to check every triangle for contact with the tire patch. For example, a road profile defined with 200,000 data points results in 350,000+ triangular elements, making this standard approach infeasible.

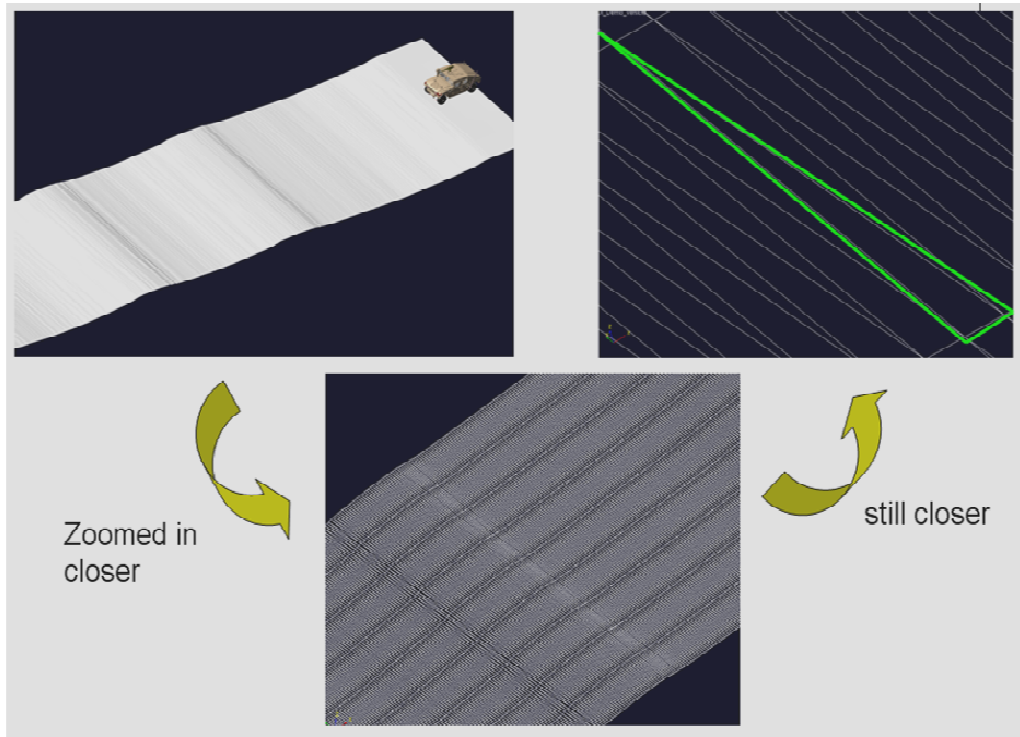


Fig. 2.2. Road profile defined with a mesh of triangular elements

In order to simulate large road profiles with high fidelity in a computationally efficient manner, the road profile data can be stored so that each line represents a lateral strip of data points. This takes advantage of data locality in that the vehicle generally travels in the longitudinal direction, which is perpendicular to the lateral direction. Rather than doing an extensive contact search to determine the location of the tire-road interface, only a few of the nearby lines of data need to be searched to find the location of the tire contact patch. Thus, the computational complexity is reduced from quadratic to constant time as the size of the road profile increases. By assuming that the data points are equally spaced in the x- and y- directions, each data point can be reduced from a set of 3 coordinates to a single height value. This pre-processing step results in a fast lookup and

interpolation routine during simulation and is independent of the amount of road profile data. The FTire specific Regular Grid Road (RGR) data file format is the result of this type of pre-processing step. FTire is a commercially available tire simulation package that will be discussed in detail in section 3.4. Under the assumption that the input road data points are equally spaced in the lateral and longitudinal directions, a conversion from a triangle mesh to a regular grid road file type is possible [10]. The disadvantage of using this type of road data file is that a conversion is necessary and if incorrect parameters are chosen, the file size can balloon or the accuracy of the road profile can diminish. However, the time required to convert from RDF to RGR format is linear with respect to the size of the input data file, and is much more amiable for road profiles with a large number of input data points. The similarity between a section of road in RDF and RGR file types when conversion parameters are carefully selected can be seen in Fig. 2.3.

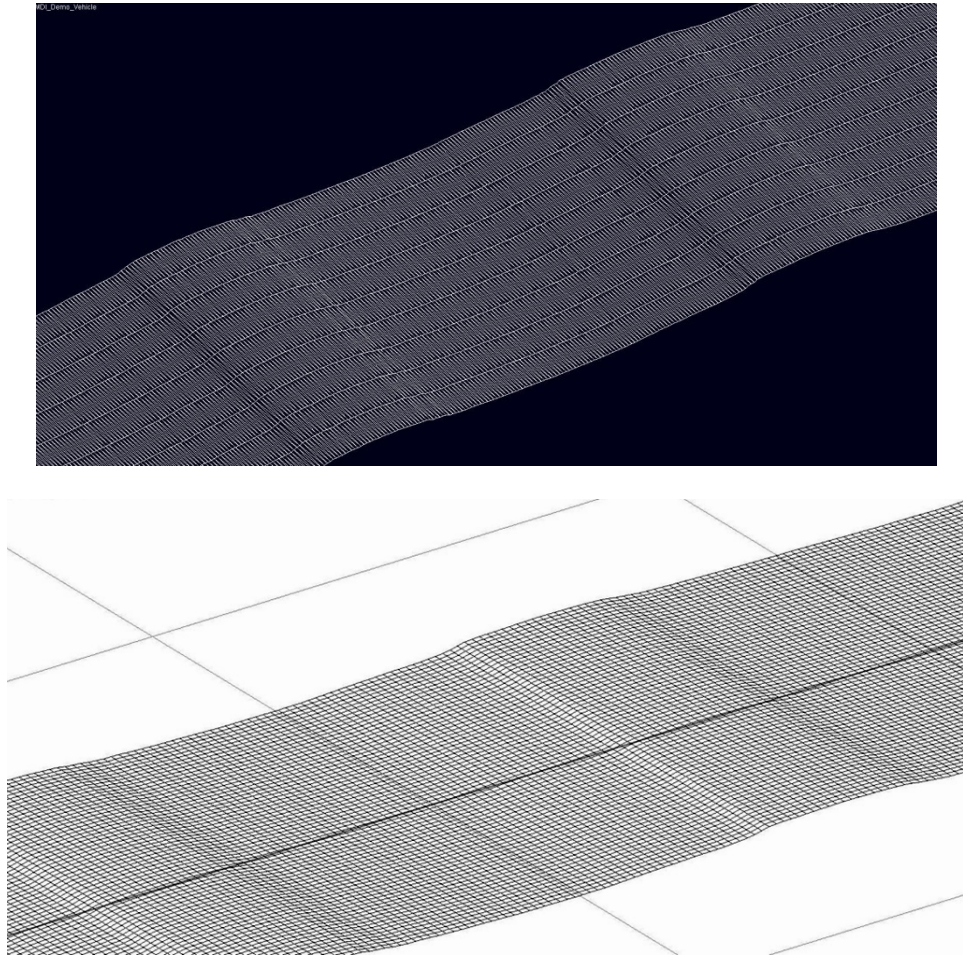


Fig. 2.3. Section of road in ADAMS/Car RDF format (top) and after a conversion to the FTire RGR format (bottom)

2.3 Deformable Soil Models

Road profile measurement data is required as an input to deformable soil models just as it is for hard soil models. However, as indicated by its name, the road surface deforms under vehicle loading and thus the initial road profile procured from measured data persists for a very short time once it is encountered by the vehicle. While the accuracy of the road profile is still important, the mechanics of the soil and the way it deforms dominates the dynamic response of vehicles simulated on soft soils. Thus an

accurate physics based soil model based on soil mechanics must be used when simulating vehicles on terrain that deforms. The stress propagation in soil due to various types of loading is introduced to clarify the elastoplastic behavior of deformable soil. Stress-strain relationships are used to create terrain-vehicle interaction models that define the normal and shear forces that the soft soil exerts on the vehicle. Repetitive vertical and shear loading effects are also taken into consideration in the soft soil model used for vehicle simulations.

2.3.1 Soil Stresses Due to External Loading

Terrain that is deformable is typically compared to an ideal elastoplastic material with a stress-strain relationship whose stress increases linearly in the elastic range, and remains constant once the plastic deformation occurs. The effects of a point load on a soil operating in the elastic range that is assumed to be semi-infinite, homogeneous and isotropic was first developed by Boussinesq [1], and predicts the vertical stress σ_z at a given depth z and radial distance r from the applied point load W as shown in Fig. 2.4.:

$$\sigma_z = \frac{3}{2\pi} \frac{1}{[1 + (r/z)^2]^{5/2}} \frac{W}{z^2} \quad (2.1)$$

Radial stress σ_r is best expressed using polar coordinates since it is axisymmetrical,

where $r = \sqrt{x^2 + y^2}$, $R = \sqrt{z^2 + r^2}$ and $\cos \theta = \frac{z}{R}$:

$$\sigma_r = \frac{3W}{2\pi R^2} \cos \theta \quad (2.2)$$

and is also shown in Fig. 2.4. Boussinesq's elasticity model can be extended to forces applied over an area by using the concept of superposition[11].

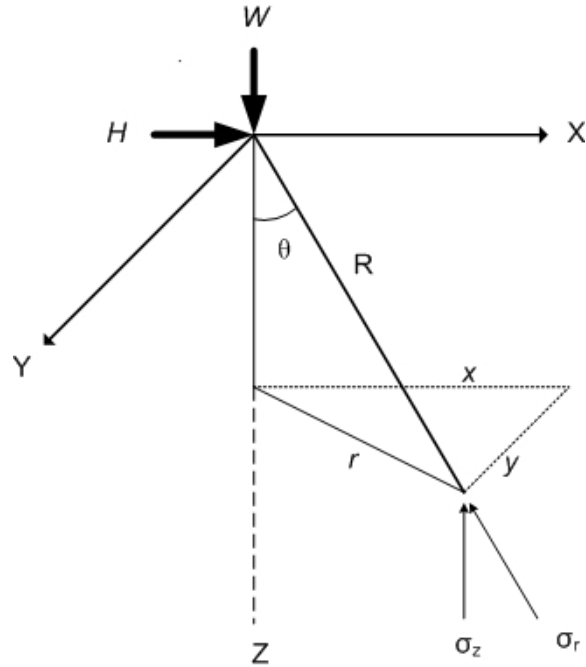


Fig. 2.4. Subsurface stresses due to a vertical and horizontal load

The stresses calculated in Eqs. (2.1) and (2.2) are only valid for points some distance from the applied force, as the soil behaves plastically near the applied force. Also, the stress in the soil tends to concentrate directly under the loading axis in actual soils, and the degree of concentration depends on the cohesiveness of the soil and the moisture content. Fröhlich introduced a concentration factor ν that is applied to Boussinesq's equations that compensates for the stress concentration under the loading axis [12]. The modified vertical and radial stress equations become, respectively:

$$\sigma_z = \frac{\nu W}{2\pi z^2} \cos^{\nu+2} \theta \quad (2.3)$$

$$\sigma_r = \frac{\nu W}{2\pi R^2} \cos^{\nu-2} \theta \quad (2.4)$$

where the value of the concentration factor varies slightly depending on the literature referenced. For example, for hard, normal and soft soil, $\nu=3,4$, and 5, respectively according to Koolen and Kuipers [13], or $\nu=4,5$ and 6 according to Wong [1] and Ayers [14].

Moving vehicles apply horizontal forces on the soil in order to accelerate/decelerate and to provide turning forces. These horizontal forces in the longitudinal and lateral direction are known to cause subsurface stresses in all three directions. Cerruti was the first to develop methods for calculating the stress distribution in an elastic medium due to a horizontal point load on the surface. The medium is assumed to be semi-infinite, homogeneous and isotropic. Since the horizontal load H shown in Fig. 2.4 does not result in an axisymmetric case, the stress equations are expressed in Cartesian coordinates [15]:

$$\sigma_x = \frac{3Hx^3}{2\pi R^5} \quad (2.5)$$

$$\sigma_y = \frac{3Hxy^2}{2\pi R^5} \quad (2.6)$$

$$\sigma_z = \frac{3Hxz^2}{2\pi R^5} \quad (2.7)$$

The stresses calculated in equations (2.5)-(2.7) are added with the stresses calculated in equations (2.3) and (2.4) (since the medium is considered linear) to produce the total stress at a subsurface point.

2.3.2 Soil Stress Due to Soil Deformation

Bekker proposed an empirical pressure-sinkage relationship for terrains under the assumption that the terrain is homogenous in the depth range of operation and is characterized by the following equation [16]:

$$p = \left(\frac{k_c}{b} + k_\varphi \right) z^n \quad (2.8)$$

where p is pressure, b is the width of the smaller edge of the contact area patch e.g. the width of the track shoe, z is vertical sinkage, and n , k_c , k_φ are pressure-sinkage parameters experimentally obtained for each type of soil. k_c is the parameter associated with cohesion and k_φ represents the frictional quality of the soil. A common technique for measuring the response of the terrain to obtain these types of soil parameters is known as the bevameter technique [16-18]. Example values for the pressure-sinkage parameters of sand, clay and snow are given in Table 2.1. The pressure-sinkage relationship of these three different types of soil is plotted in Fig. 2.5 with a plate width of $b=10$ cm.

Table 2.1 Pressure-sinkage parameters (sources: [16, 19])

Terrain Type	Moisture Content [%]	n [-]	k_c [kN/m ⁿ⁺¹]	k_φ [kN/m ⁿ⁺²]
Dry Sand	0	1.1	0.99	1528.43
Heavy Clay	40	0.11	1.84	103.27
Snow	n/a	1.6	4.37	196.72

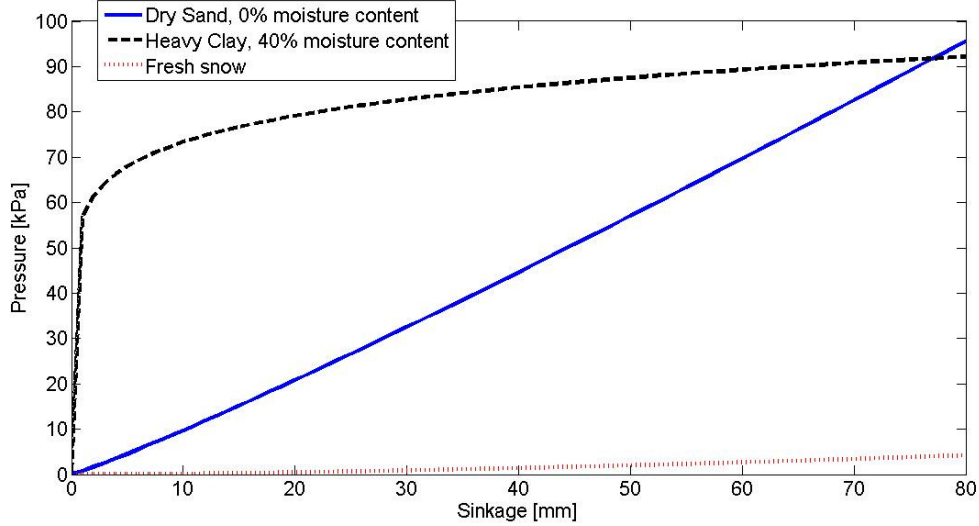


Fig. 2.5. Pressure-sinkage behavior of selected soils, $b = 10$ cm

The tractive force of a vehicle is a function of the shearing of the terrain. The maximum shear stress that a terrain can produce is given by [20]:

$$\tau_{\max} = c + p \tan \varphi \quad (2.9)$$

where τ_{\max} is the maximum shear stress, p is the normal stress and c and φ are the cohesion and the angle of internal shearing resistance of the terrain, respectively. The actual tractive effort of a tracked vehicle is dependent on the shear displacement of the terrain. Bekker noticed that shear stress is a function of shear displacement; hence terrain that has just come into contact with the vehicle running gear exerts no shear stress since the shear displacement is initially zero. The shear displacement increases to a maximum at the back end of the vehicle's running gear, as shown in Fig. 2.6. Note that in reality, the maximum shear displacement is reached quickly depending on the type of soil and vehicle system.

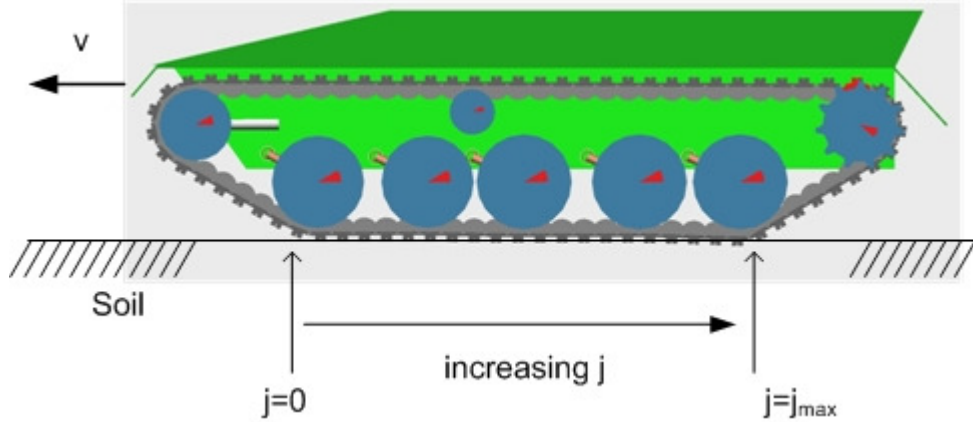


Fig. 2.6. Shear displacement j of the terrain increases from the front to the rear of the vehicle

For most distributed soils, i.e. terrains composed of sand, clay or fresh snow, the shear stress-shear displacement relationship proposed by Janosi and Hanamoto [16, 20] is typically used. The equation for the actual shear stress becomes:

$$\begin{aligned}\tau &= \tau_{\max} (1 - e^{-j/K}) \\ \tau &= (c + p \tan \varphi) (1 - e^{-j/K})\end{aligned}\quad (2.10)$$

where j is the shear displacement and K is the shear deformation modulus, which is a measure of the magnitude of the shear displacement required to develop the maximum shear stress [21]. Shear stress initially increases with shear displacement at a rate determined by K , and then reaches a constant value for any increase in shear displacement, as shown in Fig. 2.7. Equation (2.10) can be used to determine the approximate tractive force of a vehicle on a given terrain. For example, the tractive force of a tracked vehicle with a track length in contact with the terrain, l , and track width b ,

can be calculated by integrating the shear stress τ calculated by equation (2.10) over the length of the track multiplied by the track width as follows [1]:

$$\begin{aligned} F &= b \int_0^l \tau dx \\ F &= b \int_0^l (c + p \tan \phi)(1 - e^{-j/K}) dx \end{aligned} \quad (2.11)$$

This equation depends on the normal pressure distribution along the length of the track, and any function for normal pressure can be used for p .

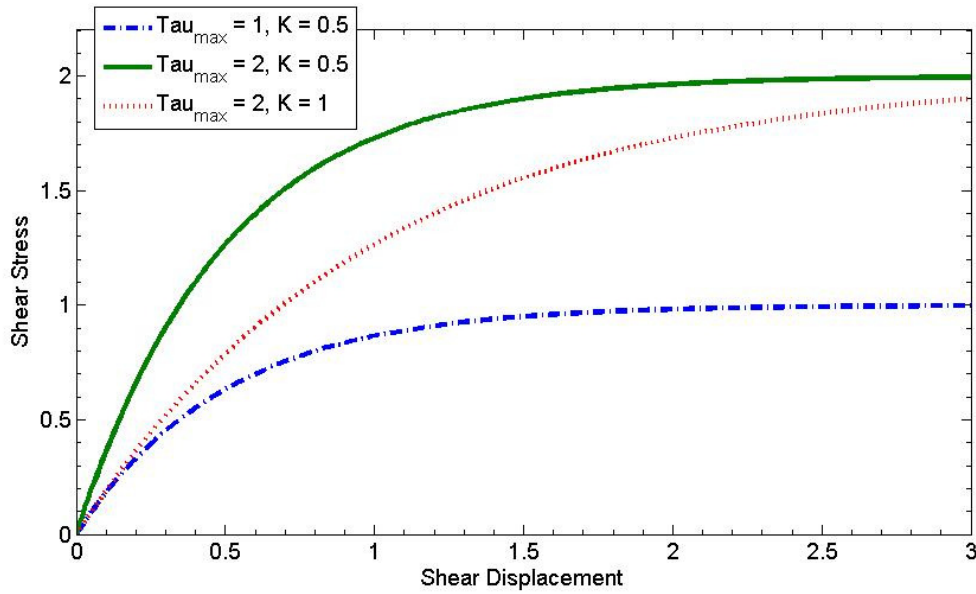


Fig. 2.7. Shear-stress curves according to Eq. (2.10)

2.3.3 Considerations for Repetitive Loading

Tires or tracks of off-road vehicles have a tendency to encounter the same section of terrain multiple times. For example, a wheeled vehicle traveling in a straight line will encounter the same terrain twice as the rear tires pass over terrain already encountered by the front tires. Due to the elastoplastic nature of the soil there will be a certain amount of permanent plastic deformation as well as elastic deformation which rebounds when an element of soil is initially loaded then unloaded. This element of soil will then experience reloading when successive wheels or tracks travel over it.

Experimental observations have shown that the unloading-reloading cycle can be approximated by a linear pressure-sinkage relationship which is assumed to be the average response of the terrain [20, 22]:

$$p = p_u - k_u(z_u - z) \quad (2.12)$$

where p and z are the pressure and sinkage, respectively during either unloading or reloading; p_u and z_u are the pressure and sinkage, respectively, when unloading begins and k_u is the average slope of the unloading-reloading line. The degree of elastic rebound is represented by the k_u parameter; as the soil behavior become more plastic and less elastic, the slope represented by k_u approaches a vertical line. Experimental measurements have shown that the value of k_u is dependent on z_u , and an approximate relationship can be expressed as [20, 22]

$$k_u = k_0 + A_u z_u \quad (2.13)$$

where k_0 and A_u are soil specific parameters and z_u is the depth of sinkage where unloading begins. Fig. 2.8 illustrates the repetitive loading behavior of a type of sandy terrain. As the soil is initially loaded along the curve 0-A, it follows the pressure-sinkage relationship of equation(2.8). Curve A-B represents the response of the terrain as it is unloaded to zero pressure as given by equation (2.12). As the terrain is reloaded, it follows the same curve A-B, and then resumes the pressure-sinkage relationship given by equation(2.8) along curve A-C once point A is reached during reloading.

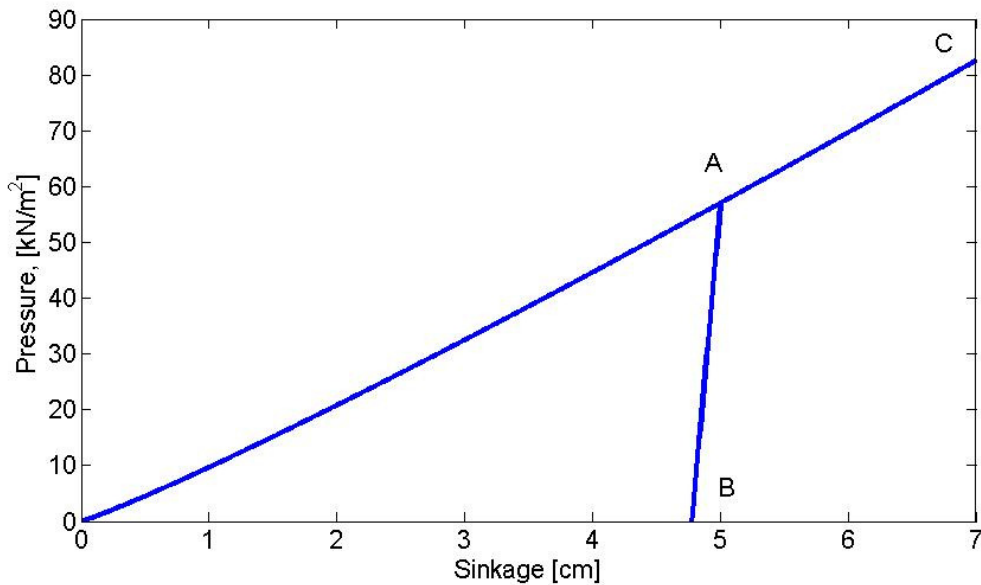


Fig. 2.8 Repetitive loading of a sandy terrain

2.4 Summary

One of the most important aspects of ground vehicle simulation other than the vehicle itself is the vehicle-terrain interaction. An entire field of study known as terramechanics is dedicated to understanding the performance of vehicles in relation to

the terrain it operates on. When dealing with hard-packed or paved terrain, the assumption that the terrain does not deform is generally made to simplify the simulation and the main concern is to create an accurate and efficient representation of the road profile from measurement data. However, when the vehicle operates on soft soil, the terrain deforms and it becomes necessary to understand the mechanics of the soil under various types of loads. Most soil mechanics theories treat deformable soil as an ideal elastoplastic material, and various formulas for predicting the stress distribution of soil under loads operating in the elastic range were presented. Due to vehicle loads, soils deform plastically as well, and the soil stress varies with the deformation. Parametric models that capture the deformation-pressure relationships are derived from measurement data and are ultimately used in the tracked vehicle simulations discussed in Chapters 5-7. Due to the combined elastic-plastic behavior of soil, repetitive loading effects can be substantial and their effects on the vehicle-terrain stresses were discussed.

Chapter 3

Wheeled Vehicle Description and Model

3.1 Introduction

The first step in the stochastic framework is to create a deterministic model which captures the dynamic behavior of the vehicle system. The wheeled vehicle model used herein is a high-fidelity and representative model of the U.S. Army HMMWV which is based off of a model that was used in a simulation project which investigated the physics of failure of a ball joint in the rear suspension [23]. First, the overall vehicle and its individual subsystems as they appear in the ADAMS/Car model will be described in-depth. Next, the implementation of the vehicle model and the ADAMS/Car modeling methodology are presented. Due to the possibility of short wavelength variations in the road profile in the vehicle simulations, a robust tire model must be used. This is one of the reasons for using the tire modeling software FTire. The tire model and the modeling methodology used for the tire will be introduced. Details of the road model were described in section 2.2, which is also handled by FTire. Chapter 4 will discuss the steps taken to implement and run a set of simulations using the models described in this chapter by leveraging the stochastic framework. Chapter 7 will show simulation results of this model being used in the stochastic framework.

3.2 Wheeled Vehicle Description

The U.S. Army's High-Mobility Multipurpose Wheeled Vehicle (HMMWV) was selected for the wheeled vehicle simulations due to its ability to navigate on-road and off-road terrains. Specifically, model number M966 (TOW Missile Carrier, Basic Armor without weapons) was selected since values of the total vehicle inertia were available [23]. The vehicle is driven with 4x4 wheel drive which is powered by a 145-hp engine. Only the major subsystems which were included in the dynamic model will be described, which include: parallel link steering with a pitman arm, double A-arm suspension, chassis, roll stabilization bar, powertrain and tires. The chassis is analogous to the hull of the tracked vehicle from section 3.2, and is a single rigid body with mass and inertia properties. Subsystems for the brakes and wheels were also included in the multi-body model but will not be described due to their minor role in the simulations.

3.2.1 Steering

The HMMWV utilizes a power-assisted parallel link steering system. A pitman arm transfers the steering inputs from the steering wheel to the steering link through a recirculating ball, worm and nut device with a 13/16:1 gear ratio. An idler arm keeps the steering link at the desired height, and tie rods transmit the steering input to the upright arms located in the suspension subsystem. The parallel link is connected to the tie rods with a convol joint. This type of constraint allows two rotational DOFs of one body with respect to the other, keeping the bodies coincident and also maintaining constant velocity between the spin axes. Topology of the steering system as modeled in the software can be seen in context with the suspension, anti-roll bar and wheels in Fig. 3.1.

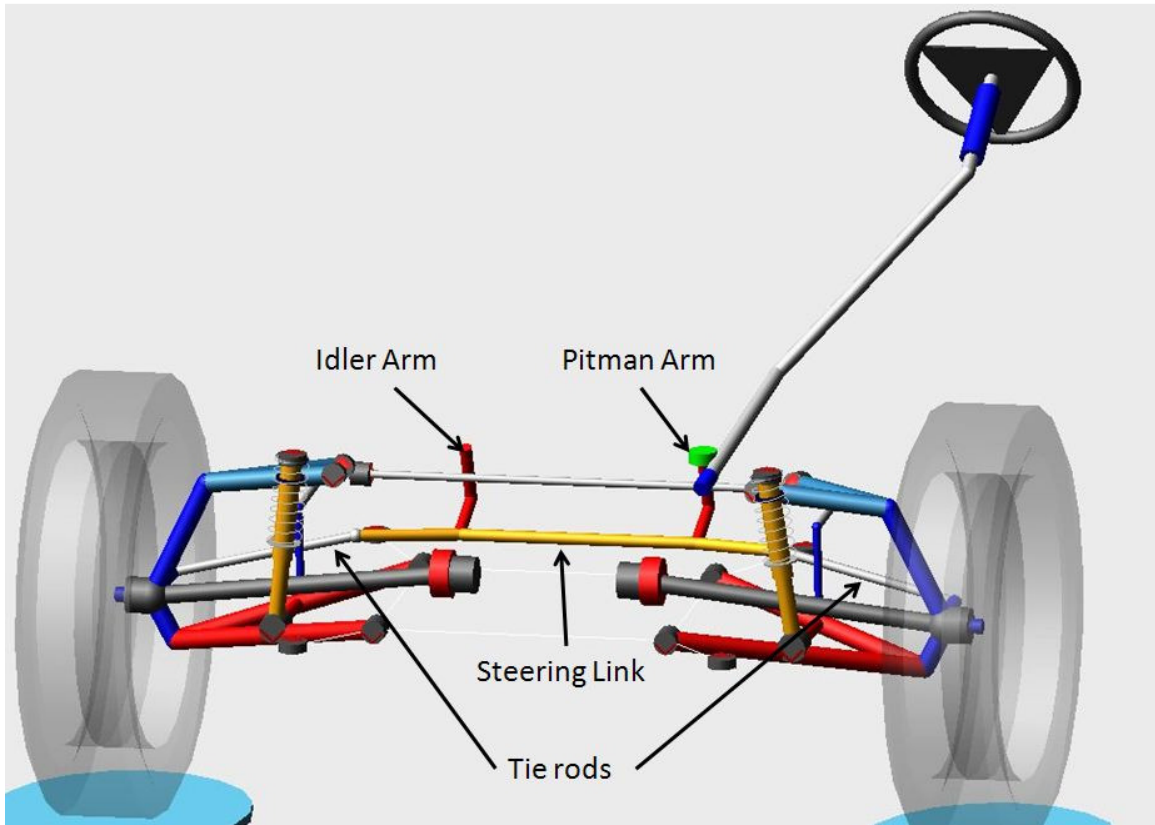


Fig. 3.1. Front suspension and steering system of the HMMWV in the multibody dynamics software ADAMS/Car.

3.2.2 Suspension

A double Ackerman Arm type suspension unit is used on the HMMWV, one for each wheel. Dimensions and locations of the suspension elements differ between the front and rear subsystems; however, the topology remains the same. Both the Upper Control Arm (UCA) and Lower Control Arm (LCA) are connected to the upright arm with ball joints, which allow three rotational DOFs. This is due to the ball joint being modeled as a spherical joint constraint, where a point on each body is required to coincide. This removes all three translational DOFs, but allows for rotation about all 3

axes. The upright arm connects the wheel spindle to the suspension units with a revolute joint. Rear radius rods are connected between the chassis to the rear suspension and control the rear wheel static toe angle, and are fixed to the chassis. Front tie rods attach the steering subsystem with the front suspension and control the wheel steer angle.

Important design configurations of the front and rear suspensions include a design kingpin angle of 12 degrees resulting in a kingpin offset of 2.14 inches. Kingpin angle is the rotation of a vector connecting the center of the UCA and LCA balljoints from a vertical line, as shown in Fig. 3.2. The kingpin offset is the horizontal distance between the point where the vector connecting the balljoints intersects the ground and where the centerline of the tire intersects the ground when viewing the suspension from the front. A positive kingpin offset indicates that the centerline of the tire is further from the centerline of the vehicle. The front suspension has a caster angle of 3 degrees and a caster offset of 0.857 inches. Caster angle and offset is very similar to the kingpin except that the angle is defined by a vector between the UCA balljoint and the center of the wheel when viewed from the side, shown in Fig. 3.3.

Shock absorber units are located on each suspension unit, are attached between the lower control arm and chassis with bushings, and can be seen in Fig. 3.2 and 3.3. Each shock absorber is comprised of three elements: a spring, a damper and a bumpstop. At the specified design load and height, the springs are assumed to have linear elastic behavior. The dampers and bumpstops, on the other hand, are not linear. Dissipative forces are proportional to the relative velocity between the piston and cylinder of the shock. Both front and rear springs and dampers were modeled in a similar way, but using

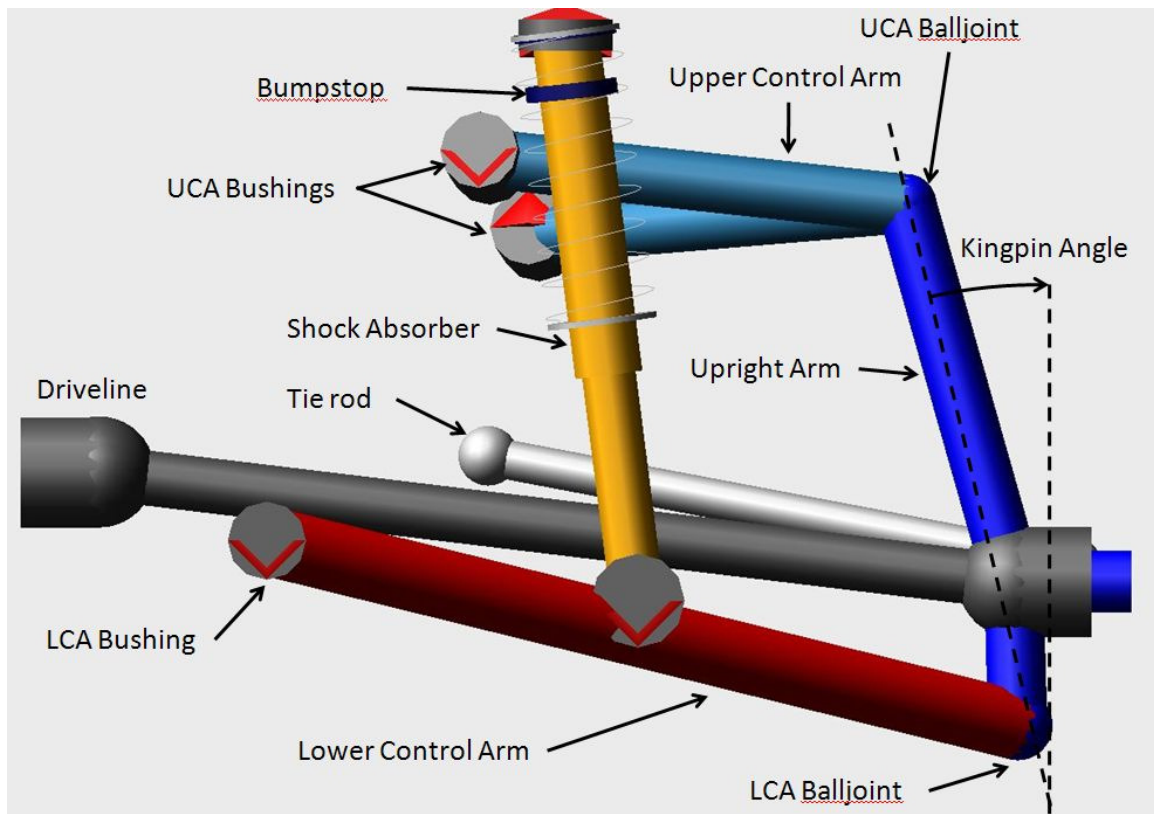


Fig. 3.2. Front left suspension unit, front view

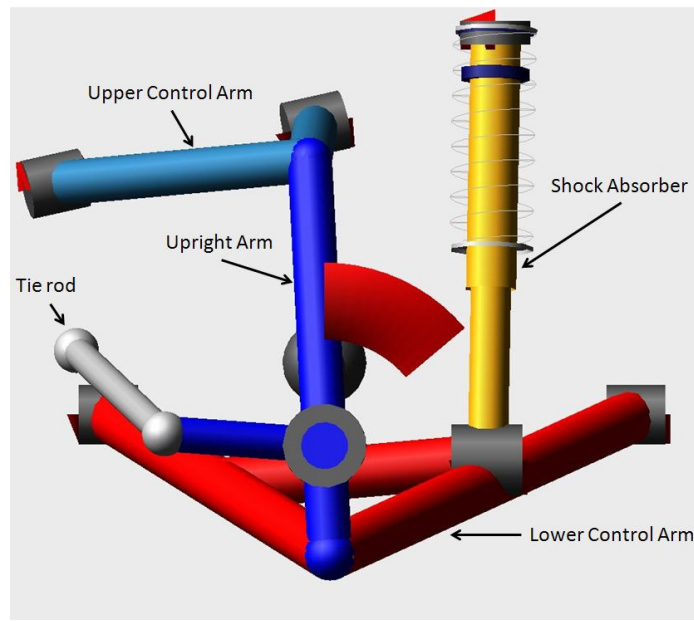


Fig. 3.3. Front left suspension unit, left side view

different data as the rear springs and dampers are designed for larger operating loads. The front and rear spring constants used in this model were 954 lb/in and 1,728 lb/in, respectively. Front and rear damper forces are modeled as a third order polynomial from measurement data found in [23], and are shown in Figs. 3.4 and 3.5.

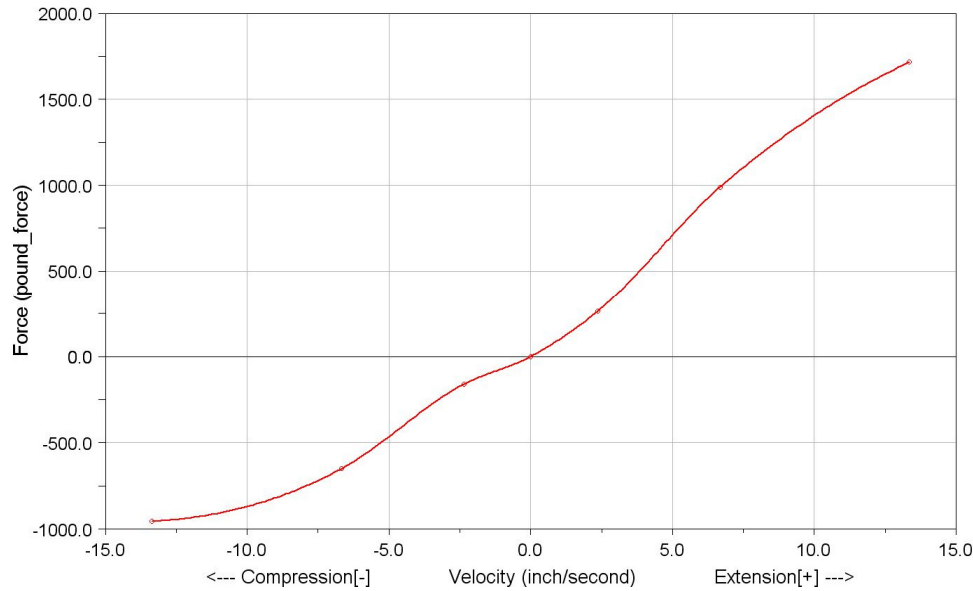


Fig. 3.4. Front suspension damper force as a function of shock velocity

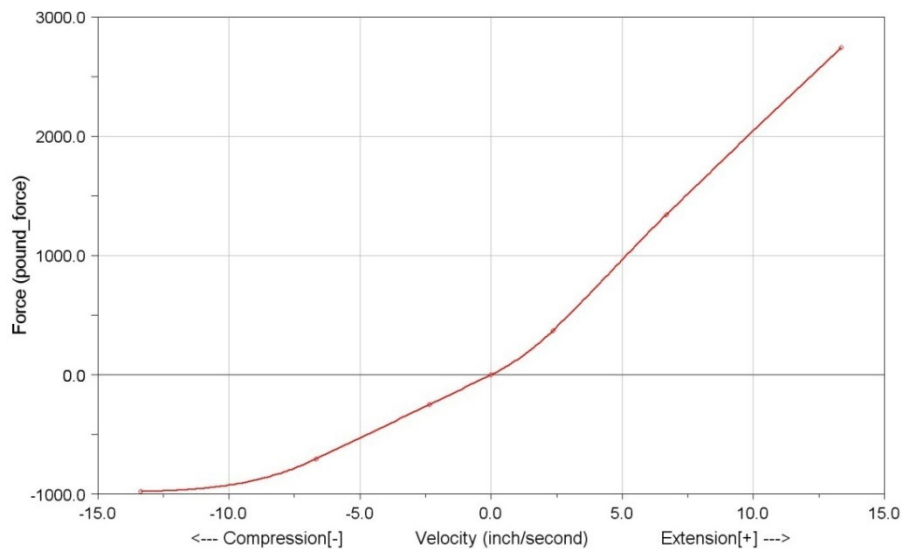


Fig. 3.5. Rear suspension damper force as a function of shock velocity

Bumpstops are located on the end of the shocks and provide an additional spring force in the shocks as shown in Fig. 3.6. They are engaged only after a displacement of 1.2 inches occurs between the piston and cylinder of the shock absorber, measured relative to the design height.

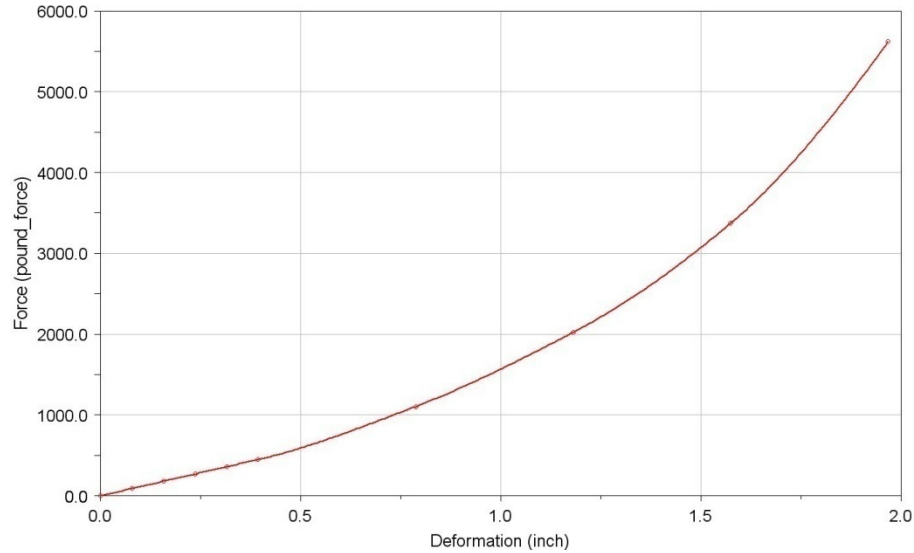


Fig. 3.6. Bumpstop force as a function of deformation

3.2.3 Roll Stabilization

Auxiliary roll stiffness is provided by an anti-roll bar that is present only in the front suspension and is attached between the lower control arms. Suspension roll is defined as the rotation of the vehicle's sprung mass about the fore-aft centerline with respect to a transverse axis that passes through the left and right wheel centers. Given a suspension roll angle, the anti-roll bar provides an auxiliary roll stabilization force on each lower control arm. The roll bar is modeled as a torsional spring and the torque is

assumed to increase linearly with respect to the roll bar twist angle at a rate of 2443 in-lb/deg [23].

3.2.4 Powertrain

The HMMWV is powered by a 6.5L V-8 diesel engine that is rated at 160-hp. An engine map controls the torque at various engine speeds and reaches its maximum torque of 300 ft-lb at 1600 rpm [24]. Engine torque is transferred through a clutch to the 4-speed automatic transmission. Power is then transferred through the differential and an equal amount of power is transferred to each wheel.

3.2.5 Tires

Tires used on all four wheels of the vehicle were the bias-type 36x12.5-16.5 LT. Front tire pressures of 20 pounds per square inch (psi) and rear tire pressures of 30 psi were maintained on the HMMWV. By using a tire simulation template modeling scheme, only a select number of tire size, geometry and specification parameters were needed as input into the tire model; other characteristics such as carcass mass/damping/stiffness, tread and friction information were either inherited from a light truck tire template or calculated with a tire simulation pre-processor routine. Details on the tire modeling scheme will be discussed in Section 3.4.

3.3 Wheeled Vehicle Model

In this work the vehicle simulation software package ADAMS/Car is used to investigate the behavior of the rigid multi-body model of the HMMWV. There are three main reasons for using a COTS simulation package such as ADAMS/Car to model and

simulate a vehicle. First, there is Graphic User Interface (GUI) support that allows the user to visually create and modify parts and apply forces and constraints to the model. Second, the resulting Equations of Motion (EOMs) are automatically assembled from the information (i.e. part masses, inertias, constraints, force elements, etc.) that the user prescribes when building the model. ADAMS uses generalized Cartesian coordinates, thus the assembled EOMs are a set of Differential Algebraic Equations of index three [25]. Finally, ADAMS has a variety of robust and efficient integration algorithms that solve the DAEs over a specified time interval, which yields the time-evolution of the mechanical system. The integrators and supporting algorithms (e.g., nonlinear solvers) are a part of a standalone program called ADAMS/Solver, which carries out the actual simulation of the model and creates output files which contain the results of the simulation.

The modeling methodology of ADAMS/Car divides a vehicle into subsystems that are modeled independently. Sets of subsystems are invoked and integrated together to create a vehicle assembly at simulation time to represent the vehicle model. The subsystems present in the model include: a chassis, front and rear suspension, anti-roll bar, steering, brakes, a powertrain and four wheels. Note that only the wheels and not the tires are present in the multi-body vehicle model. Also, all the major subsystems (front/rear suspension, steering, roll bar and powertrain) are connected to the chassis with compliant bushing elements. The entire HMMWV model as seen in the vehicle simulation software is shown in Fig. 3.7 (chassis geometry is partially transparent), and the combination of the various subsystems to create the full assembly is illustrated in Fig.

3.8. CAD geometry is applied to the chassis and tires to make the vehicle look realistic for animation purposes. The geometry has no bearing on the dynamic behavior of the vehicle.

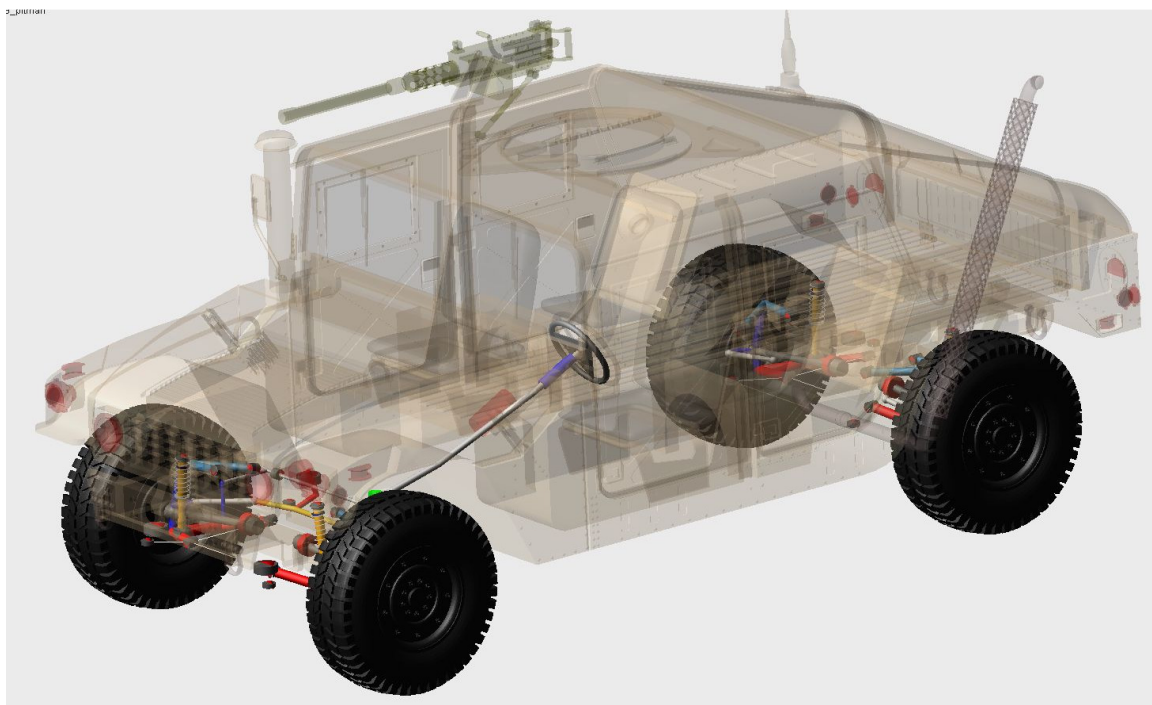


Fig. 3.7. HMMWV vehicle model as seen in ADAMS/Car

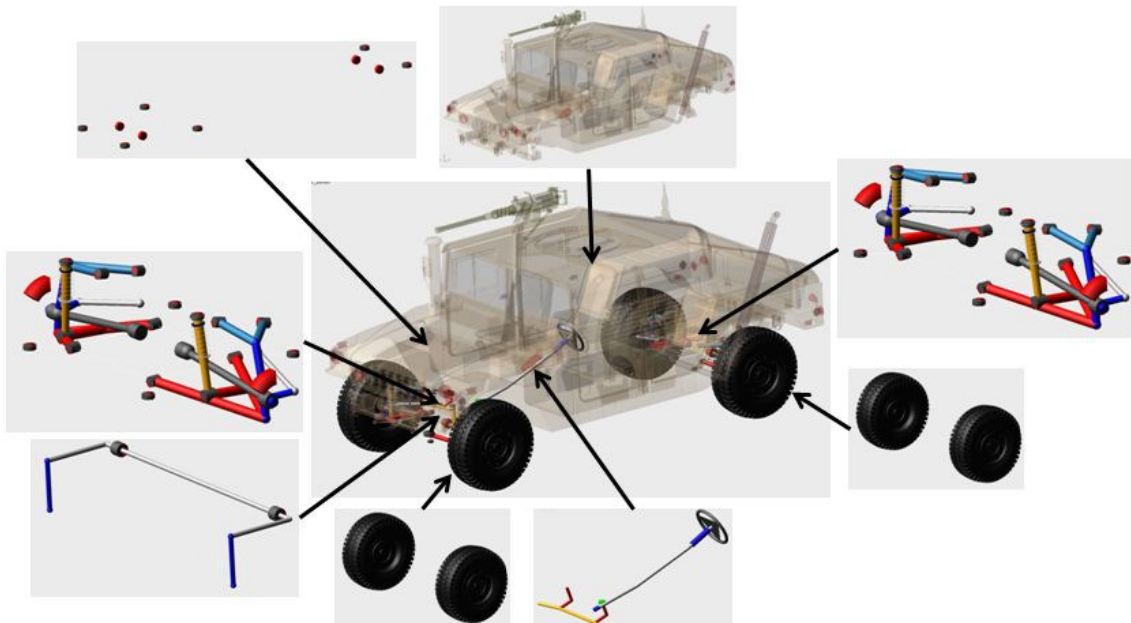


Fig. 3.8. Subsystems part of the full vehicle assembly. Subsystems present in the HMMWV vehicle model, from the top-left clockwise: powertrain, chassis, rear suspension, rear wheels, steering, front wheels, anti-roll bar and front suspension. The brake subsystem is not shown but present in the model.

To run a large number of simulations from a base model, the various file types and their format involved in the simulation must be understood in order to be manipulated properly. After the model has been completely defined, two important files are created that are subsequently used by ADAMS/Solver to run the simulation. A filetype called the Adams Command File (ACF) is used as an input to the Solver to specify the simulation settings used by the integrator, as well as the name of the Adams Dataset Model (ADM). The ADM filetype contains all of the model specific data used by the Solver to assemble the EOMs.

An important note to make is that the Name (NAM) filetype may also be created before simulation if the Solver is instructed to save Request (REQ) information. The simulation output can be modified to save any of the three following files: Request (REQ), Result (RES) and Message (MSG). By default, only the result file is saved, as this is a complete set of all the body specific data (e.g. position, velocity, acceleration) and forces that are acquired at each time step of the simulation. If only a specific subset of the results is desired for analysis, a set of Requests are created in the model, and these files are saved in the REQ output filetype. The NAM file is created when the REQ filetype is desired, and its sole purpose is to indicate to the Solver which output data to save. The message file gives detailed information on the status of the simulation at various stages of the solution process. In summary, ACF, ADM and possibly NAM files are created as input to the Solver routine. The RES, REQ and/or MSG are saved as output files, depending on the selected settings.

3.4 Tire and Road Models

Due to the variation of the three vehicle operating conditions in the HMMWV simulations which will be discussed in Chapter 7 (micro- and macro-scale road profile variation and vehicle velocity), situations may occur where the vehicle encounters a short-wavelength obstacle at high speed. A robust tire modeling and simulation program, FTire, was used because it has shown the ability to handle these types of obstacles while experiencing large tire deflections. Figure 3.9 gives an example of the vehicle and tire models traversing the exit lip of a hill at moderate speed. It operates in a co-simulation environment with the vehicle model in ADAMS/Car. At each integration step,

information at the wheel is used by FTire, which calculates the reaction force at each wheel, which in turn is a function of a road input and the tire parameters.

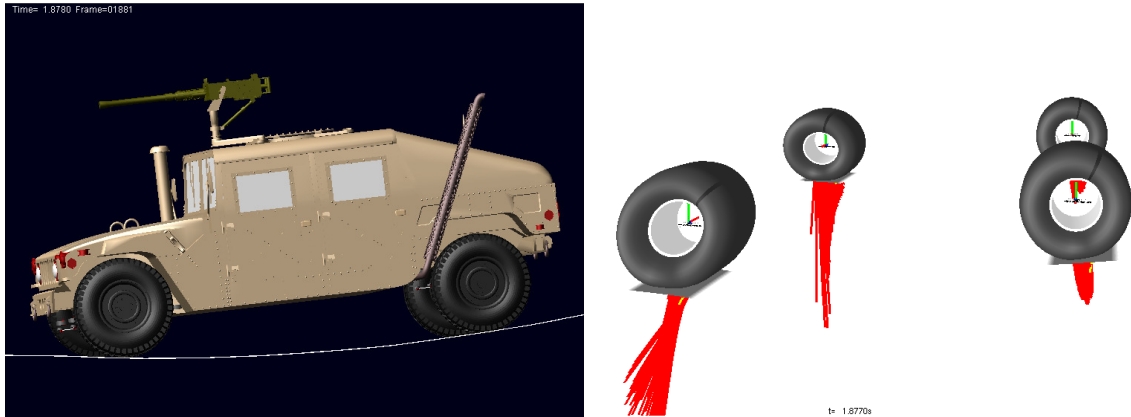


Fig. 3.9. HMMWV (left) and tires (right) traversing the exit lip of a hill

The FTire [26] model serves as a sophisticated tire force element and can be used in multi-body models for vehicle ride comfort investigations as well as other vehicle dynamics simulations on three dimensional roadways. Specifically, the tire model used is designed for vehicle comfort simulations and performs well even on obstacle wave lengths as small as half the width of the tire footprint. At the same time, it serves as a physically based, highly nonlinear dynamic tire model for investigating handling characteristics under the above-mentioned excitation conditions [27]. Computationally the tire model is fast, running only 10 to 20 times slower than real time. The tire belt is described as an extensible and flexible ring carrying bending loads, elastically founded on the rim by distributed dynamic stiffness values in the radial, tangential, and lateral directions. The degrees of freedom of the ring are such that both in-plane and out-of-plane rim movements are possible. The ring is numerically approximated by a finite number of discrete masses called belt elements. These belt elements are coupled with

their direct neighbors by stiff springs with in- and out-of-plane bending stiffness [26].

Figure 3.10 illustrates this lumped mass modeling approach. Each belt element contains a certain number of massless tread blocks which convey the nonlinear stiffness and damping in the radial, tangential and lateral directions.

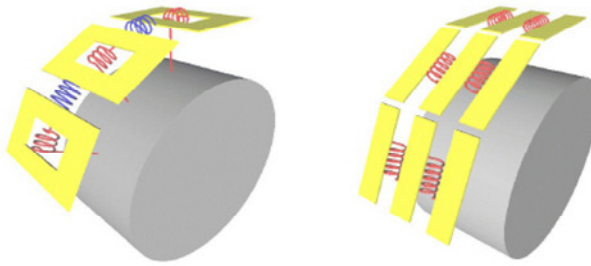


Fig. 3.10. Illustration of the FTire modeling approach

The mechanics of a tire model are dependent on a set of input parameters that can be specified directly in the tire model file (TIR), whose file path is referenced in the vehicle's ADM file, or by using a toolset provided by FTire. The toolset is intended for applying field test data to the model to refine its properties. However, only a small amount of basic tire data is required to create a representative tire model because the program provides high-fidelity templates of common tire types such as those for passenger cars and light trucks. The input data used for the front and rear tire models is shown in Table 3.1 and was applied to a light truck tire template. Once the data is specified in the TIR file, FTire runs a preprocessor routine which extracts some of the important modal properties and updates the TIR file with these values. After the preprocessor routine is run, the tire model is ready for co-simulation with the vehicle model.

Table 3.1. Input data used for the FTire front and rear tires

Input Parameter	Front Tires	Rear Tires
Inflation Pressure [bar]	1.4	2.1
Tire section Width [mm]	317	317
Aspect Ratio [%]	78	78
Rim Diameter [mm]	419.1	419.1
Load Index [-]	120	120
Speed Rating [-]	R	R
Rim Width [mm]	208.28	208.28
Tire Mass [kg]	40	40

3.5 Summary

Creating a deterministic vehicle and tire model which is representative of their physical counterparts is an important first step in the stochastic framework. This chapter presented a representative HMMWV vehicle model with in-depth descriptions of the components used in dynamic simulations which are discussed further in chapters 4 and 7. The modeling methodology of a popular COTS simulation software ADAMS/Car was illustrated using the HMMWV model developed. Leveraging modeling methodologies which can accurately simulate the system when various model parameters are changed is also an important aspect. Due to the possibility of short-wavelength features in the road profiles, the high-fidelity tire modeling software FTire was used to create tire models. The modeling methodology of FTire was also briefly discussed. Models described in this section are used as inputs into the stochastic simulation framework which is described in the next chapter.

Chapter 4

Stochastic Wheeled Vehicle Simulation

4.1 Introduction

This chapter details the necessary steps for implementing the stochastic simulation framework from a single deterministic set of input files for a wheeled vehicle simulation. As discussed in Chapter 1, the reasons for moving from a deterministic to stochastic framework for vehicle simulation varies from running an uncertainty analysis to understanding the sensitivity of certain outputs to varying inputs.

The HMMWV vehicle model is implemented in the vehicle software package ADAMS/Car and the tire models are implemented using the FTire software package in a co-simulation environment as described in chapter 3. First, the original model files are manipulated using scripting tools and saved as a new set of files. Next, a batch simulation is set up to simulate some or all of the newly created files. Once the simulations are completed, the post-processing to export plots and datasets is automated by creating another set of script files. This stochastic framework is applied to the HMMWV model and results are discussed in detail in chapter 6, which also includes a discussion of the uncertain inputs considered. The same framework is applied to the tracked vehicle model and results are presented in chapter 7.

4.2 Stochastic Process Applied to Vehicle and Road Models

In order to illustrate the extra steps involved in creating a batch of stochastic simulations from a single set of model files, a data flow diagram for a single vehicle

simulation is shown in Fig. 4.1. It is assumed that road profile data is available as a set of 3D vertices, vehicle and tire models have already been created and the associated files are ready to be simulated. In this example a specific set of results is desired, thus a request output file (REQ) is preferred over the full result file. The ADAMS/Solver routine is called using the ACF file as an input argument, which initiates the simulation using the model information contained in the ADM, NAM (not shown in Fig. 4.1), RGR and TIR files. Only the requested subset of outputs is saved.

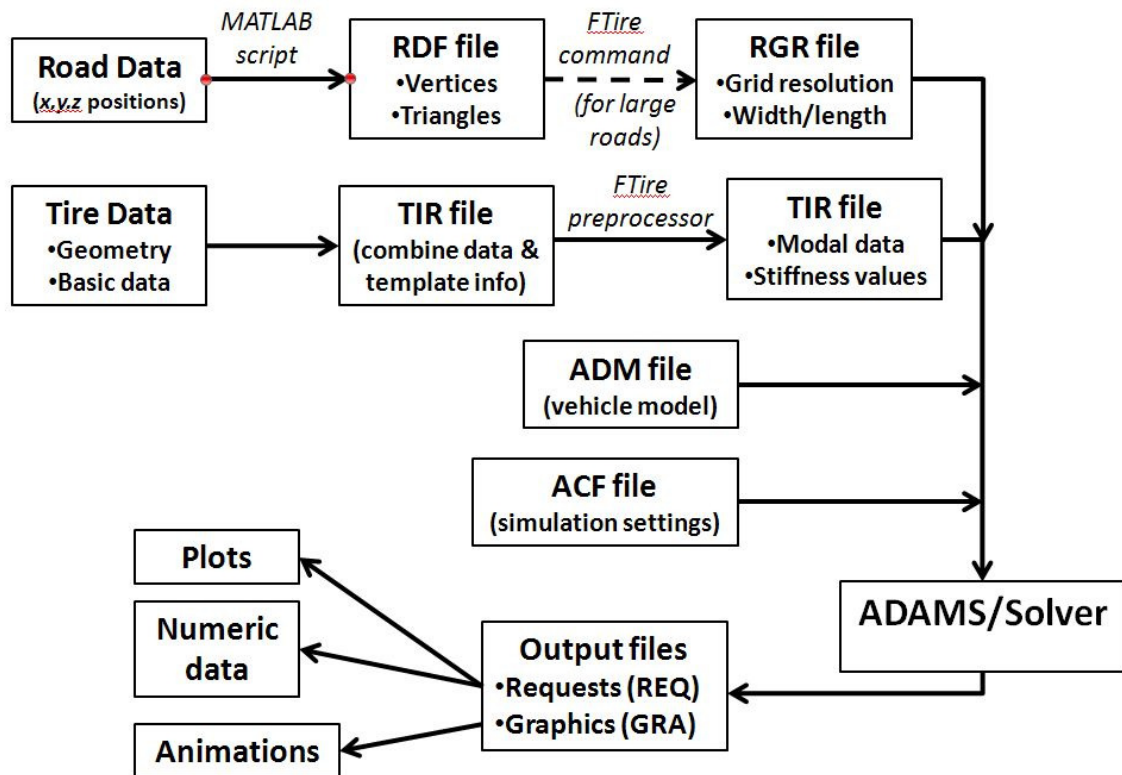


Fig. 4.1. Data flow diagram for a single simulation. Dotted lines indicate optional steps

The modified data flow diagram is shown in Fig. 4.2. Assuming that the integrator options remain the same for every additional simulation, the only change that needs to be made to the modified ACF file is the name of the ADM file which it references, located on the second line of the ACF file. Since this example uses request files as an output, the accompanying NAM input file also needs a simple modification. Assuming that the same results are to be saved for every additional simulation, the NAM file can be copied directly; only the filename is changed to match that of the ACF file. Thus, in Fig. 4.2 the NAM files are assumed to be produced in the same fashion as the ACF files and are omitted in Fig. 4.2 to avoid clutter. The MATLAB batch simulation script in Fig. 4.2 is simply a script that consecutively initializes all the simulations by invoking the ADAMS/Solver with each ACF file, one after the next as simulations are finished.

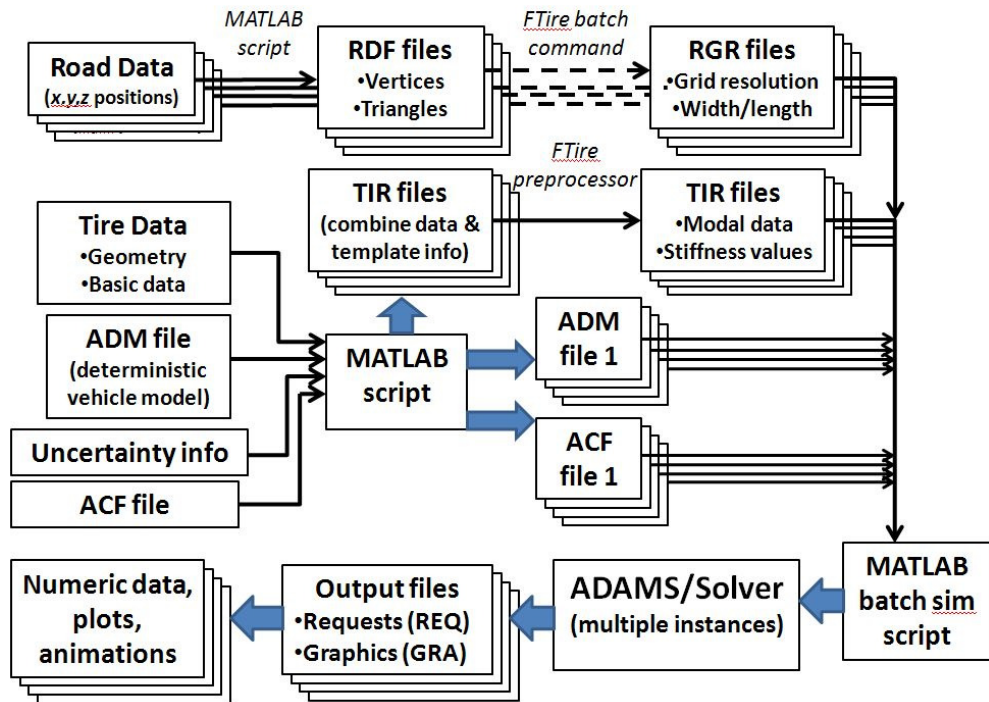


Fig. 4.2. Data flow diagram for stochastic simulations. Dotted lines indicate optional steps

The only major modifications that are generally made to ADAMS/Solver input files are in the ADM and TIR files. The ADM file is organized as follows. Each modeling element (i.e. points, coordinate systems, parts, strings, data arrays) has a header indicating its name when viewed in the GUI, e.g. “!adams_view_name = ‘testrig.smart_driver_filename’”, followed by its type and unique number of that type, e.g. “STRING/3”, which is helpful for locating the value that will be modified. Next, the value of the type if given, e.g. ” STRING =test_accel.xml”. This example specifies the filename of the driver control file that is used during the simulation to steer the vehicle.

Although the modeling elements of interest (e.g., joint types and locations, spring stiffness values, damper values, etc.) are generally more complicated than the above example, the same elements are present in the same order and can be modified using any type of scripting program. For example, Fig. 4.3 shows a section of the HMMWV ADM file that describes the data which is used to define the spring stiffness of the shock in the rear left suspension subsystem.

```
!      adams_view_name='rear_suspension_stochastic.ns1_ride_spring.spline'
SPLINE/272
, X = -7.33, -6.7192, -6.1083, -5.4975, -4.8867, -4.2758, -3.665, -3.0542
, -2.4433, -1.8325, -1.2217, -0.6108, 0, 0.6108, 1.2217, 1.8325, 2.4433, 3.0542
, 3.665, 4.2758, 4.8867, 5.4975, 6.1083, 6.7192, 7.33
, Y = -12666.24, -11610.72, -10555.2, -9499.68, -8444.16, -7388.64, -6333.12
, -5277.6, -4222.08, -3166.56, -2111.04, -1055.52, 0, 1055.52, 2111.04, 3166.56
, 4222.08, 5277.6, 6333.12, 7388.64, 8444.16, 9499.68, 10555.2, 11610.72
, 12666.24
, LINEAR_EXTRAPOLATE
!
```

Fig. 4.3. Section of the ADM file which specifies the spring stiffness of the shock absorber in the rear left suspension subsystem

Similar to the above example, the first line specifies the name of the element in the GUI and the second line declares it as a spline data type with unique identifier of 272. The next three lines specify the x-coordinates of the spring data, and the following four lines describe the corresponding y-coordinates. The force F in the spring is linear, and is in the form $F = y = f(x)$. Finally, the last statement “LINEAR_EXTRAPOLATE” allows for this data type to linearly extrapolate beyond the upper and lower specified x-bounds.

A MATLAB script which modifies the spring spline in Fig. 4.3 and writes it to multiple instances of a base ADM file is shown in Fig. 4.4. The script makes use of the deterministic vehicle model and its ADM file, called the template, and an array named “spring” which contains the x- and y-values for the template spring stiffness spline. Lines 1150-1158 read data from the template file and write it to the new file until the name of the element in the GUI is found. Lines 1160-1174 write the x-values (which are constant in this case), line 1176 modifies the y-values by a variance coefficient matrix, and lines 1177-1189 write the remainder of the spline data type to the new ADM file. It should be noted that the script shown in Fig. 4.4 for writing the modified spring stiffness values can also be used to create and modify all the corresponding model input files (e.g. ACF, NAM and TIR files) in one sweep. Also, if any modifications are made to the tire data files, the pre-processing of the tire model must be repeated. FTire has a setting in the TIR file “append_pp_data“ which will automatically initialize the pre-processing routine and update the tire data files before running the simulation by setting this value to “1”.

```

1146 %
1147 % ***** ride_spring data *****
1148 %
1149 % write file until the data series is found
1150 while 1
1151     tline = fgetl(fidread);
1152     fprintf(fidwrite,'%s\n',tline);
1153     if( strcmp(springS, tline))
1154         break;
1155     end
1156 end
1157 tline=fgetl(fidread);
1158 fprintf(fidwrite,'%s\n',tline);
1159 % % write the X data (stays the same)
1160 l = length( spring(:,1) );
1161 fprintf(fidwrite,' X= %d, %d, %d, %d, %d\n',spring(1,1),spring(2,1),...
1162             spring(3,1),spring(4,1),spring(5,1));
1163 n = floor((l-5)/5);
1164 m = mod(l,5);
1165 for i=1:n
1166     fprintf(fidwrite,' %d, %d, %d, %d, %d\n',spring(5*i+1,1),...
1167             spring(5*i+2,1),spring(5*i+3,1),spring(5*i+4,1),spring(5*i+5,1));
1168 end
1169 for j=1:m
1170     fprintf(fidwrite,',%d',spring(5+n*5+j,1));
1171     if(j==m)
1172         fprintf(fidwrite,'\n');
1173     end
1174 end
1175 % % write the Y data (MODIFIED BY STOCHASTIC COEFS)
1176 spring(:,2) = spring(:,2).*coef(loop,1);
1177 fprintf(fidwrite,' Y= %d, %d, %d, %d, %d\n',spring(1,2),spring(2,2),...
1178             spring(3,2),spring(4,2),spring(5,2));
1179 for i=1:n
1180     fprintf(fidwrite,' %d, %d, %d, %d, %d\n',spring(5*i+1,2),...
1181             spring(5*i+2,2),spring(5*i+3,2),spring(5*i+4,2),spring(5*i+5,2));
1182 end
1183 for j=1:m
1184     fprintf(fidwrite,',%d',spring(5+n*5+j,2));
1185     if(j==m)
1186         fprintf(fidwrite,'\n');
1187     end
1188 end
1189 fprintf(fidwrite,' LINEAR_EXTRAPOLATE\n!\n');
1190

```

Fig. 4.4. Code snippet of MATLAB script used to write multiple instances of an ADM file with modified values of the spring spline shown in Fig. 4.3. Only a subsection of the script is shown.

4.3 Post-Processing Method

Once a single simulation is completed, the output data is easily plotted using the built-in ADAMS/Post-Processor Tool (PPT) GUI. Data can be exported using the File→Export menu option and the plots can be saved as pictures using an ADAMS command (provided in Appendix A) which takes a screen shot of every plot and saves a JPEG image. However, these methods will become tedious very quickly if a large number of simulations have been run. Running a command file which automatically loads, plots, exports plot data and pictures for all the simulations run is necessary. This type of command is specific to the ADAMS/Car software program, and will not be discussed in detail. However, the utilized command file is provided in Appendix A

4.4 Summary

In order to run any type of sensitivity or uncertainty analysis, multiple simulations must be run. However, manually creating sets of model files and running the subsequent simulations is time consuming and inefficient. A single deterministic set of input files for a wheeled vehicle simulation can be extended into a stochastic set of simulations by understanding the data structures associated with the model files and utilizing scripting tools as was discussed in this chapter. Tools specific to the simulation software program ADAMS/Car were also created to automate the post-processing of plots and datasets. Applications of this stochastic framework will be discussed in detail in chapters 6 and 7, where they are used with HMMWV and tracked vehicle models to understand the propagation of uncertainty from various sources.

Chapter 5

Tracked Vehicle Description and Model

5.1 Introduction and Nomenclature

The tracked vehicle model that will be used in this investigation is based on a high mobility military tracked vehicle, similar to the models seen in [28-31] and shown in Fig. 5.1. This class of military tracked vehicle is specifically designed to give a tactical advantage when traversing unprepared or off-road terrain and thus the vehicle-terrain interaction is of utmost importance when making design considerations. First, a literature review is presented which gives a brief overview of some of the methods that have been used for tracked vehicle analysis. Next, the vehicle and the individual subsystems which have a large impact on the dynamic response will be described. Finally, the topology of the entire vehicle system will be introduced, with special consideration given to the rigid body frictional contact forces which dominate the response of the system.

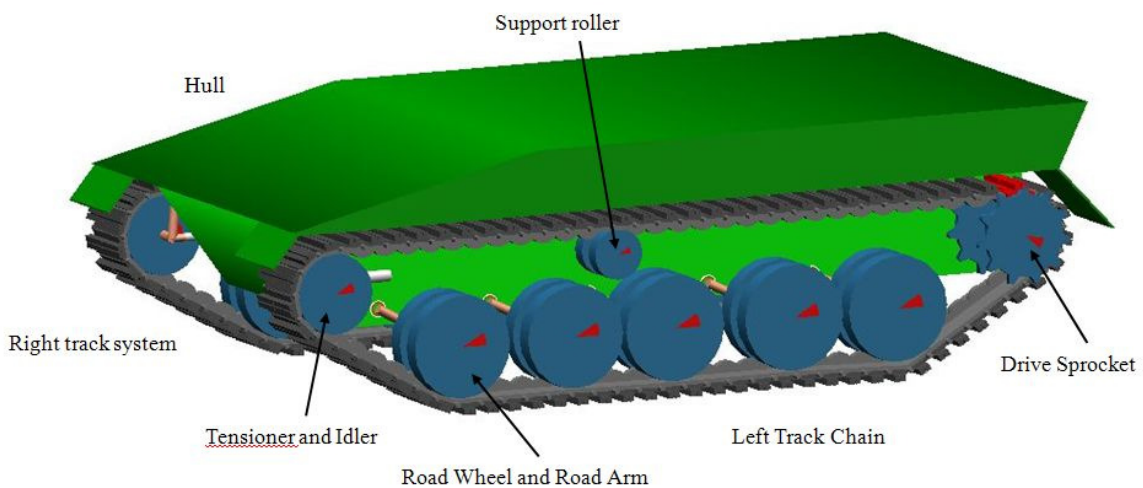


Fig. 5.1. CAD view of tracked vehicle model

5.2 Methods for Tracked Vehicle Analysis

In this section a handful of the most utilized models for the analysis and simulation of tracked vehicles are reviewed. One of the first methods used an empirical approach which was simply used to determine a “go/no-go” decision to drive a tracked vehicle on a given terrain. Other early models were proposed by Bekker [11, 16, 17], which assume that the running-gear in contact with the terrain be treated as a rigid footing. Many simplifying assumptions are made in this particular model as it is only useful as a preliminary assessment tool and does not apply to all types of tracked vehicles. With the advent of High Performance Computing (HPC) in recent decades, a number of computer-aided methods have been developed in order to create fully dynamic simulations of tracked vehicles. These models vary in complexity from “super-element” approaches which considers the track-shoe chain as a single flexible belt, to fully rigid body approaches which treats every track shoe as an individual rigid body.

5.2.1 *Empirical Methods*

Original methods for predicting off-road tracked vehicle performance can be traced back to WWII, when the Army Waterways Experiment Station (WES) created an empirical method to calculate the Mobility Index (MI) of given off-road vehicles using a simple cone penetrometer measurement of the terrain [32]. Essentially, the method determined if a vehicle would be able to successfully make a number (e.g., one or 50) of passes over a given terrain based on measurements of the soil taken by the cone penetrometer.

Bekker developed early terramechanics formulas as discussed in Section 2.3.2, which could be applied to tracked vehicles to create a parametric analysis method for tracked vehicles based on bevameter measurements of various terrains, shown in Fig. 5.2 [11, 16, 17]. However, large assumptions were made, such as the section of track in contact with the terrain was considered a rigid footing. This method calculated the motion resistance and the tractive effort of a tracked vehicle and allowed for rough calculations of drawbar pull. Both methods are empirical in nature and require experimental measurements of the terrain.

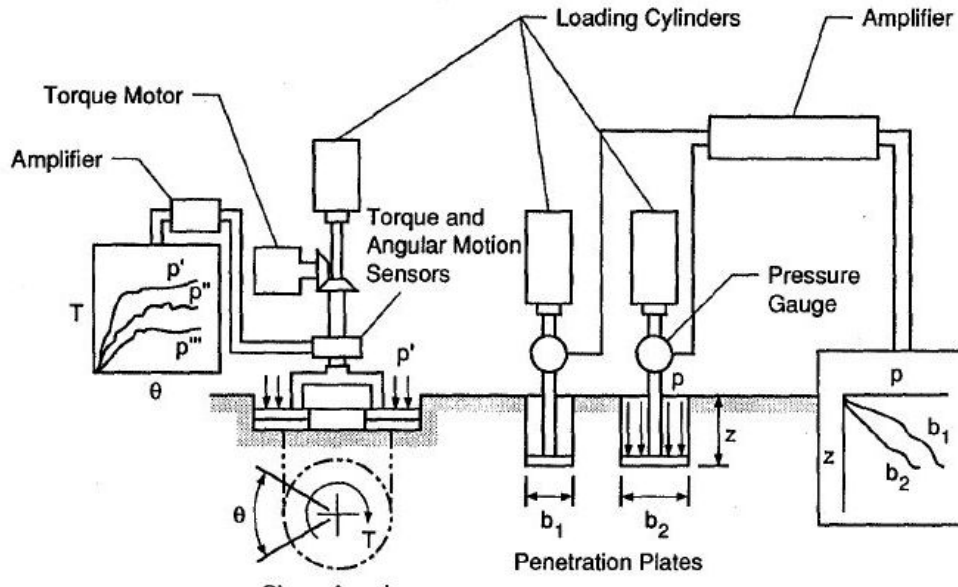


Fig. 5.2. Components of a bevameter [33]

5.2.2 Super-Element Models

Modern day computer-aided methods have allowed large and complex systems to be modeled and simulated accurately and efficiently. Engineers can leverage simulation

tools to understand not only the overall behavior of a tracked vehicle, but also important internal factors (e.g., forces on individual parts) that are important to the design.

A popular method known as the Super-Element model treats the track chain as a single flexible-band and the rest of the running gear as discrete rigid bodies (road wheels, support rollers, drive sprockets, idlers and chassis components) with kinematic constraints. This reduces the size of the problem because the track chain is reduced from a number of rigid bodies with frictional contacts to a single force super-element applied to each road-wheel. Early versions of this methodology include that by McCullough and Haug [34], where a 2D version of a flexible-band track model was developed.

Sandu and Freeman [35] use this modeling methodology for high-speed military tracked vehicles. The vehicle model proposed is a three-dimensional model which employs a trailing-arm suspension, a torque driven toothed sprocket with a track tension adjusting mechanism attached to the front idler. Using the assumption that the road wheel radius is large compared with the track pitch allows the track chain to be modeled as a continuous flexible belt which only has longitudinal elasticity. Thus the flexible belt has only one Degree of Freedom (DOF), which is the extension or compression of the length of the belt. This type of super-element model allows for the vehicle to be simulated on hard or soft soil terrains with obstacles, but is limited in that it cannot be used to simulate non-straight line runs, e.g. steering maneuvers. Other simplifying assumptions are made in [35], which include:

- The track does not slip on the toothed sprocket and idler
- The track is in a quasi-static state, with constant velocity

- The first and last road wheels are always in contact with the track.

These assumptions are realistic under most operating conditions, but limit the types of investigations that can be performed, e.g. acceleration maneuvers.

A variation of the super-element model was developed by Ma and Perkins [36] where the track chain is described as a continuous uniform elastic rod, and a finite element method is used to discretize the nonlinear problem. The forces in the track chain response can then be described with linear stiffness and viscous damping. Similar assumptions need to be made for this super-element model, but it has the advantage of capturing high-frequency content of the track-wheel-terrain interaction.

The objective of super-element models is to create high-fidelity simulations of the interaction between the track chain and other running gear components without the computational cost of implementing the track chain as a large number of rigid bodies with frictional contacts between the track-chain and terrain as well as the track-chain and road wheels. A number of simplifying assumptions are made for this type of model, and cannot be used if non-straight line maneuvers are to be simulated. In order to capture the dynamic response of a tracked vehicle as it makes non-straightline maneuvers, a fully multibody approach must be used.

5.2.3 Multibody Approach

There are a number of approaches for three-dimensional fully multibody models, where each track shoe is considered an individual rigid body. Rubinstein and Hitron [29] create a model which incorporates a detailed description of the track, suspension system and the dynamic interaction between its components. Each track shoe is considered a

rigid body and is connected to its neighboring track shoes via a kinematic revolute joint constraint. The road-wheel track-link interaction is described with three-dimensional contact force elements, and the track-link terrain interaction is modeled with a pressure-sinkage force relationship.

Ryu, Bae, Choi and Shabana [30] create a three-dimensional multibody model similar to that in [29], except that the vehicle has a compliant track chain. The revolute joints which connect track shoes with their neighbors are replaced with bushing elements which are described by stiffness and damping values. The model in [30] also includes fairly sophisticated hydro-pneumatic suspension units, and techniques for experimentally measuring the contact and bushing force parameters are presented. Ryu, Huh, Bae and Choi [31] build on the methodology proposed in [30] by further developing the contact force model to investigate the advantages of using an active track tensioner in the vehicle design.

5.3 Tracked Vehicle Description

This type of tracked vehicle has six major subsystems of interest. They include: the hull, suspension units and attached road wheels, a support roller, tensioning system and attached idler, drive sprocket and powertrain, and track shoe chain. The hull is simply a single rigid body with mass and inertia properties and will not be discussed in-depth. The support roller is similar in nature to the road wheels, but it has no road arm suspension and is simply connected to the hull via a revolute joint constraint. However, the four other subsystems are not trivial and warrant a more detailed illustration.

5.3.1 Suspension Unit and Road Wheel

The road wheel and suspension unit serve as the main load bearing mechanism between the vehicle hull and track chains. Each track system has five identical road wheel and suspension units. The type of suspension system is a trailing arm suspension, where the road wheel is connected to a rigid road arm. Road arms are connected to a torsion bar which is modeled as a rotational spring/damper. For simplicity, both the spring and damper forces have a linear relationship with respect to the rotation and rotational velocity of the road arms. A revolute constraint allows the road arm one rotational DOF with respect to the axis of rotation which is fixed to the hull.

Two concentric cylinders are used as the geometry for the road wheel with a gap in between to allow space for the guide tooth on each track shoe body. This design allows for three possible collision scenarios between the track shoe and road wheel. The outer circumferential surface of the road wheel can collide with either the flat surface of the track shoe or its guide tooth (or in extreme circumstances, both simultaneously). The inner circular surface of the road wheel can also come into contact with the track shoe guide tooth. During normal operating conditions, more than one of these scenarios can occur concurrently. Fig. 5.3 gives a schematic diagram of an individual road wheel with its trailing arm suspension unit.

5.3.2 Tensioning System and Idler

The tensioning system and idler is the mechanism that keeps the track chain in tension and the track shoes in contact with the inner running gear of the track system. As the vehicle traverses obstacles, the road wheels and suspension deflect to absorb the impact,

which decreases the wrap length of the track chain. The tensioner is modeled as a linear spring with a pre-load that is connected between the hull and the pivot arm, shown in Fig. 5.4. If the pre-load and stiffness of the tensioning system is not sufficient, the track chain may go slack resulting in possible damage to running gear. The pivot arm is connected to the hull with a revolute joint that allows one rotational DOF for the idler wheel.

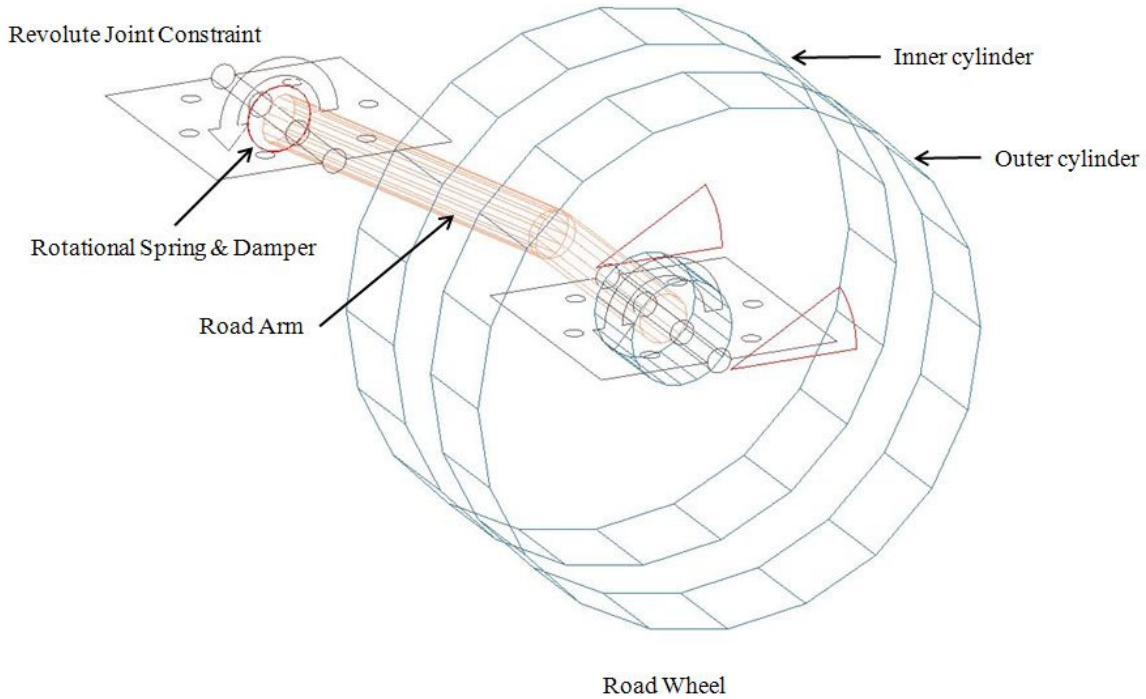


Fig. 5.3. Schematic diagram of road wheel and suspension unit

The geometry of the idler wheel used for collision calculations is similar in nature to that of the road wheels, which results in the same three possible collision scenarios between the idler wheel and track shoes. The diameter of the idler wheel is slightly smaller than that of the road wheels in this particular vehicle model.

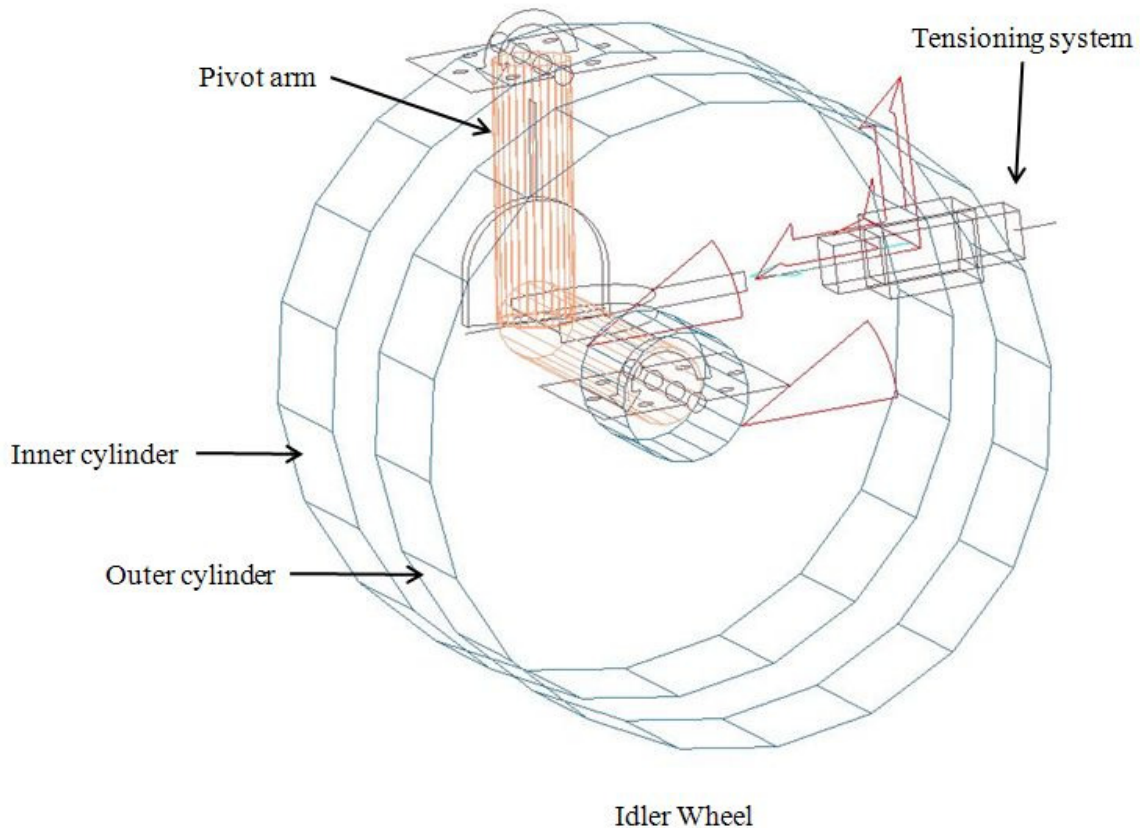


Fig. 5.4. Schematic diagram of idler and tensioning system

5.3.3 Drive Sprocket and Powertrain

Drive sprockets are present on both track chains and are driven by the vehicle powertrain. Each sprocket is connected directly to the hull with a revolute joint constraint which limits motion to one rotational DOF along the drive axle. Motion is imparted by imposing either a rotational motion or torque along the axle of the sprockets. Each drive sprocket is made up of two identical gears which move in unison when the vehicle is in motion. The gears used for this model have 11 teeth and engage the track

shoes on both ends of their connection pins. The drive sprocket on the left track system is shown in Fig. 5.5.

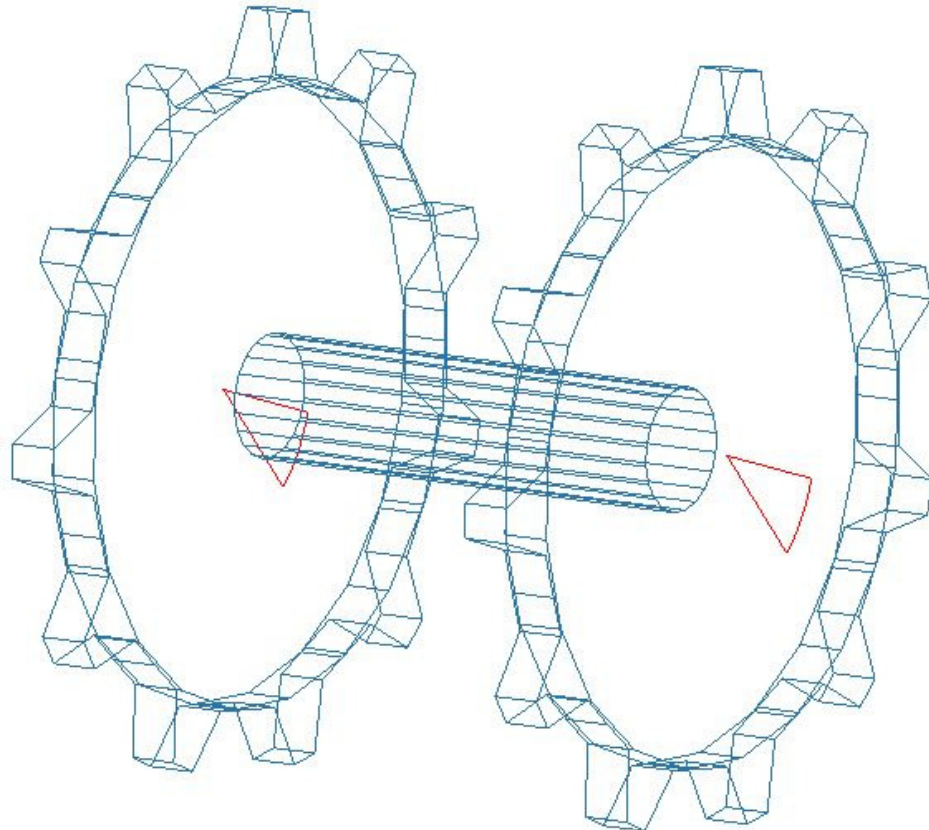


Fig. 5.5. Drive sprocket consists of two identical gears

Similar to [30], the gear teeth usually engage several track shoes simultaneously, as shown in Fig. 5.6. It is evident from the figure that the gear teeth are correctly in contact with the track shoe pins, but are penetrating the outer part of the track shoe. This is because there are two different sets of geometry used for calculating the collision forces between the rolling elements, track shoes and ground. The two sets of collision

geometry associated with each track shoe will be discussed in detail in the following section.

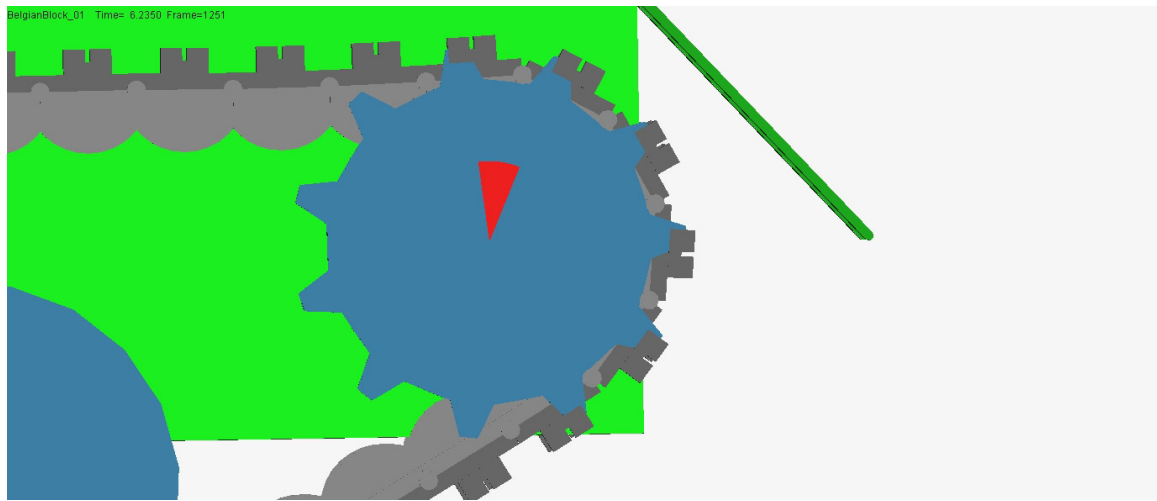


Fig. 5.6. Left drive sprocket gear engaging multiple track shoes

5.3.4 Track Shoe

In this model, there are a total of 73 identical track shoes in each track chain system. A single track shoe is shown in Fig. 5.7. Each track shoe has a few important properties that have already been mentioned in previous sections but will be summarized here. On the inner surface of the shoe is a guide tooth that keeps the entire chain in line with the various rolling elements. The bottom surface has a grouser which is intended to increase the maximum tractive effort of the vehicle.

There are two sets of collision geometry associated with each track shoe. The set on the inner surface is used for the contact forces between the inner surface of the track chain and the rolling elements, which includes two cylinders for the bushings, a semi-circle for the guide tooth, and a flat plane for the body of the shoe. The set on the outer

surface is used for contact between the track shoes and terrain, and only consists of the grouser and a flat plane for the body of the shoe. Both sets of geometry used for contact force calculations are shown in Fig 5.8.

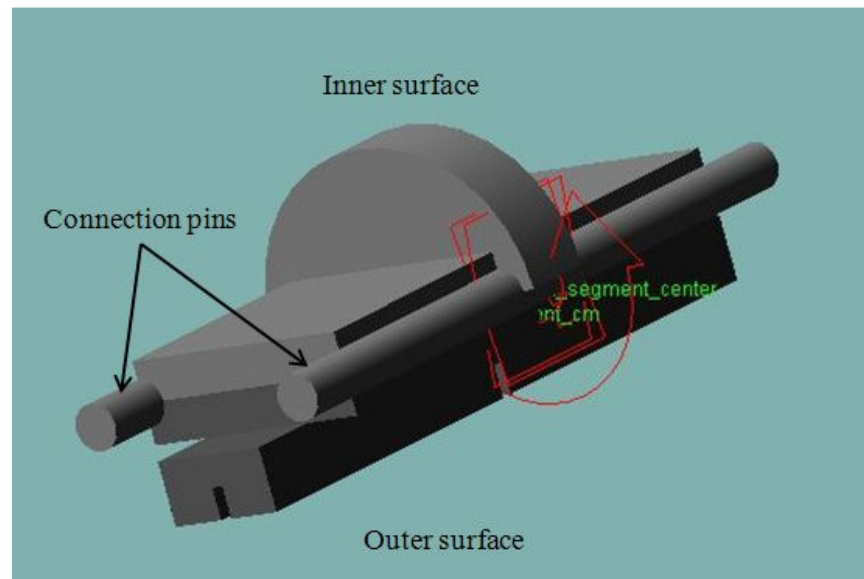


Fig. 5.7. Individual track shoe

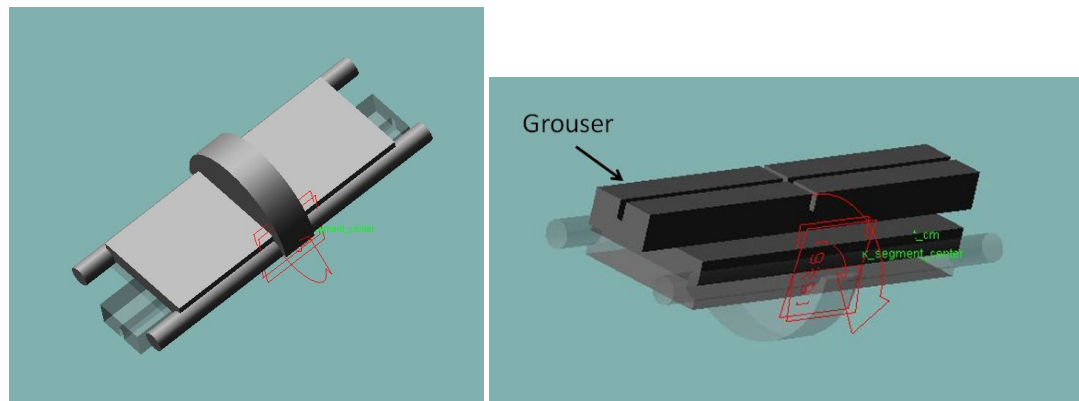


Fig. 5.8. Collision geometry that contacts the rolling parts (left) and the terrain (right)

5.3.5 Compliant Track Chain

There are two different approaches for modeling the pins that connect each track shoe to its neighboring shoe. In large, slow moving tracked vehicles such as mining excavators, the connecting pins are large and the low speed of operation leads to a minimal deflection of the pins. Thus, the track shoe pins can be modeled as revolute joints with friction. The track shoes are allowed one DOF with respect to each other, rotating along the axis of the connection pin [37-39]. The connections between track shoes in high-speed tracked vehicles are slightly different, and usually consist of a metal pin and rubber bushing. This type of connection can also be modeled as revolute joints under the assumption of low and constant operating speeds as shown in [29]. However, most high-speed tracked vehicles experience large forces and deflections in the running gear and a compliant track chain model is more appropriate.

In this model, a compliant single pin and bushing is used to link the individual shoes in the track chain. The pin and bushing connection act as a force element which is a function of the coordinates of the two track shoes. Figure 5.9 shows a two-dimensional illustration of two connected track shoe bodies, i and j . Each track shoe has two reference frames associated with it, a body reference frame and a bushing reference frame. The body reference frame is located at the center of gravity of the individual track shoe. The bushing reference frame is located a fixed distance from each body center. In Fig. 5.9, i_b and j_b denote the body reference frames while i_f and j_f are the reference frames of the force-based connection for track shoes i and j , respectively. When there is no force acting between the two track shoes via the pin and bushing connection, the locations of i_f and j_f

coincide and have a relative rotation matrix denoted by Θ in Fig 5.9 . When there is a displacement and/or velocity between reference frames i_f and j_f , the stiffness and damping of the bushing exerts a force between the two track shoes. The relative displacement and velocity between the two reference frames is denoted by r^{ij} and \dot{r}^{ij} , respectively, where,

$$\begin{aligned} r^{ij} &= j_f - i_f \\ \dot{r}^{ij} &= \dot{j}_f - \dot{i}_f \end{aligned} \quad (5.1)$$

and the dot denotes a derivative with respect to time. The bushing force exerted on track shoe j by body i in terms of the reference frame j_b can be calculated by:

$$\begin{bmatrix} Q^j \\ Q_0^j \end{bmatrix} = \begin{bmatrix} K & 0 \\ 0 & K_0 \end{bmatrix} \begin{bmatrix} r^{ij} \\ \delta\theta^{ij} \end{bmatrix} \begin{bmatrix} C & 0 \\ 0 & C_0 \end{bmatrix} \begin{bmatrix} \dot{r}^{ij} \\ \dot{\delta\theta}^{ij} \end{bmatrix} \quad (5.2)$$

where K , K_0 , C , and C_0 are the three-dimensional bushing stiffness and damping matrices, $\delta\theta^{ij}$ is the change in rotation from the zero torque rotation Θ shown in Fig 5.9, Q^j and Q_0^j are the translational and rotational force and torque vectors, respectively. The reaction force and torque exerted on track shoe i by body j is equal and opposite in direction to the values found from Equation (5.2).

Experimental measurement techniques to determine the value of the compliance parameters discussed in this section are readily available in the literature [30], but an investigation of the actual compliance parameters of the model is not the focus of this thesis and will be omitted. However, the compliance parameters were considered representative since the track chain tension forces obtained in the simulations were similar to the experimental values obtained from a similar tracked vehicle in [31].

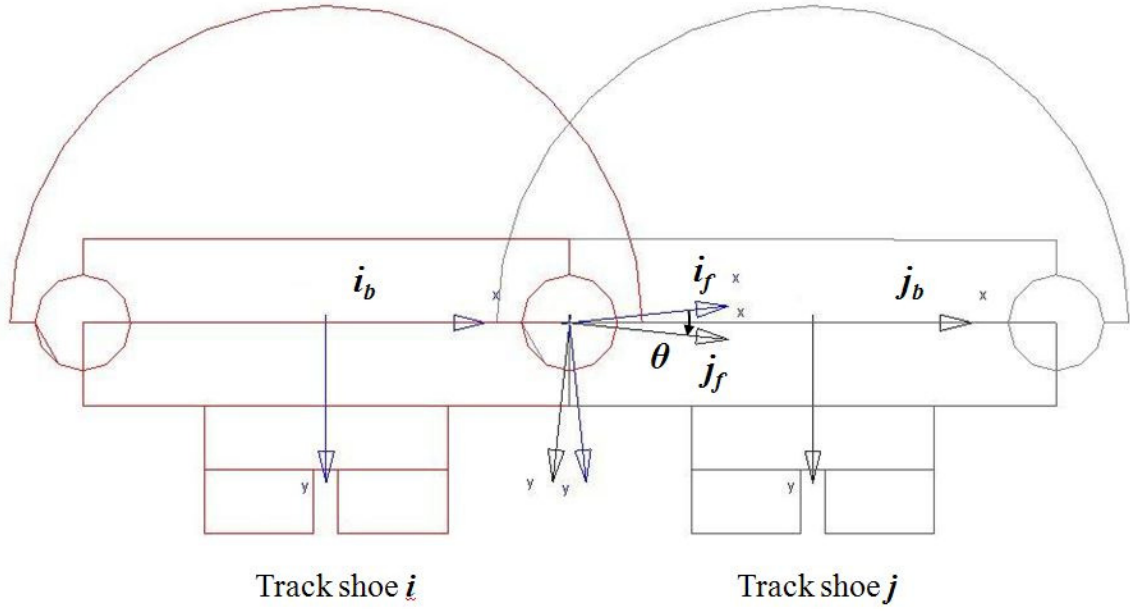


Fig. 5.9. References frames for track shoes *i* and *j*. Subscripts '*b*' and '*f*' indicate body and pin reference frames; θ is angle between \mathbf{i}_f and \mathbf{j}_f that causes zero torque.

5.4 Tracked Vehicle Model

The vehicle model was implemented in the software program ADAMS/Car, using the ADAMS Tracked Vehicle (ATV) plug-in that adds tools to specifically model and simulate tracked vehicles on hard or soft terrain. Similar to the modeling methodology of the HMMWV described in section 3.3, the same file types are created from a fully defined model which are used by the ADAMS/Solver to produce simulation results. The only difference in the data flow as shown in Fig. 4.1 is that FTire is not used for tracked vehicle simulations. Subsystems are combined to create the full model assembly; the assembly will be discussed to emphasize the importance that rigid body frictional contacts play in this type of simulation. The formulation for rigid body contacts is a penalty type approach, which will be discussed in section 5.4.2.

5.4.1 Assembly Topology

As the tracked vehicle is assumed to be symmetrical about its centerline, a half-vehicle is used to describe the assembly topology. Furthermore, Chapter 7 discusses applying the stochastic simulation framework on a tracked vehicle running on soft-soil, which utilizes a half-vehicle model. The assembly consists of: the hull, five suspension units and attached road wheels, one support roller, one tensioning system and attached idler, one drive sprocket and powertrain, and a track shoe chain made up of 73 track rigid bodies with compliant bushing type connections. Fig. 5.10 illustrates each subsystem as part of the full vehicle assembly.

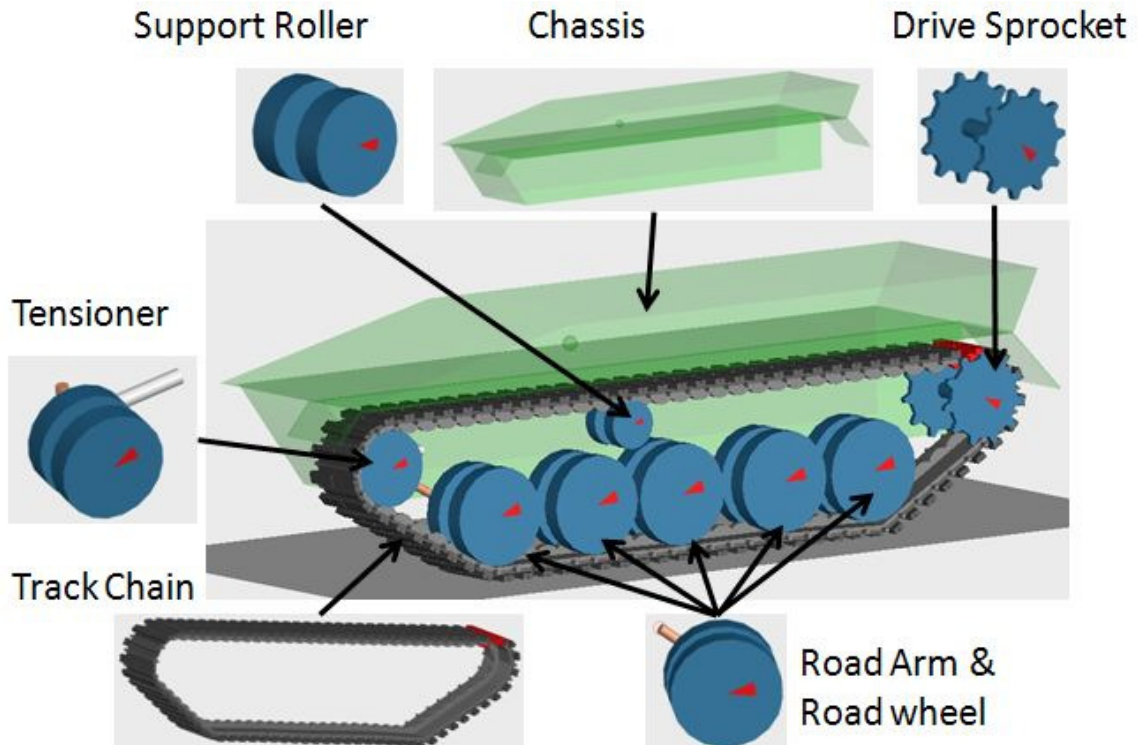


Fig. 5.10. Subsystems that are part of the full tracked vehicle assembly. From top left clockwise: Support roller, hull, powertrain and drive sprocket, road wheels, track chain and idler.

All of the rolling elements are connected to the chassis through a series of kinematic joints. The track chain is compliant and each track shoe is connected to its neighbor using a force element to model a pin and rubber bushing. The inner surface of the track chain and the rolling elements interact through rigid body frictional contacts, which are discussed in the next section. The outer surface of the track chain interacts with the terrain with rigid body contacts if the soil is considered hard and non-deformable. If the soil is soft and deformable, a soft-soil model is implemented. This model consists of three main elements: the Bekker pressure-sinkage relationship shown in equation (2.8), the Janosi-Hanamoto shear stress-shear displacement relationship shown in equation (2.10) and the repetitive loading effects shown in equation (2.12). The Bekker model is used to produce vertical forces and the Janosi-Hanamoto produce horizontal forces in the lateral and longitudinal directions. The repetitive loading effects only apply to vertical forces as repetitive loading effects for shear displacements are minimal. Bulldozing effects are not considered; however, the application of this soft soil model uses dry sand which has a small amount of sinkage in comparison to other soils such as snow. Therefore it is reasonable that the bulldozing effects are ignored.

5.4.2 Rigid Body Frictional Contacts

Many of the constraints in the tracked vehicle model consist of classic kinematic constraints, e.g. revolute and translational joints. Formal definitions can be found in texts on kinematic and dynamics of mechanical systems, for example in [25]. However, the presence of many rigid-body frictional contacts has a large effect on the response of the system and will be described in detail.

There are multiple ways to model colliding bodies, ranging from penalty based methods to sophisticated optimization based methods [40]. This investigation uses the penalty based method since it is a widely used and accepted method in the multi-body dynamics field. The method treats the interaction between colliding bodies as a very stiff spring/damper which results in a repulsion force.

There are three basic steps to handle colliding rigid bodies in the penalty approach. First, the collisions themselves must be detected. This includes detecting bodies in contact and determining the volume of intersection between the colliding bodies. MSC/ADAMS utilizes the collision detection engine RAPID for this purpose [41]. Once the volume of intersection is known, the centroid of the intersection volume is determined. The centroid of the intersection is the center of mass of the intersecting bodies with the assumption of uniform density. The closest point on each solid to this centroid is calculated, and a line connected these two points is known as the penetration depth, d and is used to find the normal contact force, F_n , associated with the colliding bodies using the following equation:

$$\begin{aligned} F_n &= Kd^e - c_{\max} \dot{d} & d \geq d_{\max} \\ F_n &= Kd^e - c_{step} \dot{d} & d < d_{\max} \end{aligned} \quad (5.3)$$

where K is the contact stiffness, c_{\max} is the maximum damping coefficient, e is the contact exponent (a positive real number), d_{\max} is the penetration depth at which full damping is turned on, \dot{d} is the time derivative of d and c_{step} is an interpolation of a third order polynomial, i.e., $c_{step} = f(d)$. The interpolation of the third order polynomial for the

damping coefficient is used to avoid a discontinuity in the damping force at the onset of a collision[42]. Figure 5.11 illustrates how the penetration depth is found from the volume of intersection. Two spheres are colliding, both with radius r . The closest point of the solid blue sphere's centroid to the volume of intersection is denoted x , and the depth of penetration d is the subtraction of x from r . RAPID approximates the collision geometry as a mesh of polyhedrons, and uses the approximated shapes to compute the intersection volume when computing the repulsion force.

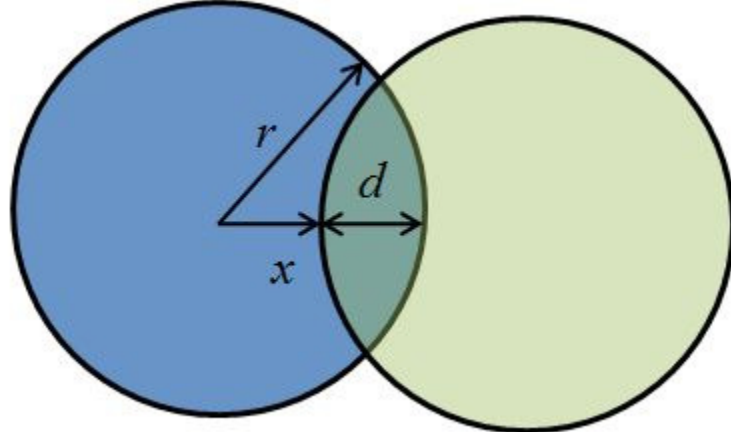


Fig. 5.11. Two colliding spheres with radius r and penetration depth d

It should be noted that there are many sources of modeling uncertainty associated with the penalty based approach for handling rigid body contacts. For example, colliding bodies in tracked vehicle simulations typically experience large forces over a relatively small contact area. This leads to very high contact stresses on the bodies near the point of contact, and would almost certainly lead to deformation of the bodies, which violates the

rigid body assumption. On the same note, the fact that the penalty method allows an intersection volume to compute the repulsion force is another violation of the same assumption. The geometry representation to calculate the volume of intersection is not exact as the method is general and RAPID approximates the exact geometry with a surface mesh of polyhedral. The volume of intersection is a function of the timestep, therefore different contact forces will result depending on the selected value of the timestep during a collision event. The added damping values in equation (5.3), which improve the robustness of the integrator, also introduce uncertainty to the system. These types of modeling uncertainties in conjunction with the fact that it is difficult to experimentally determine contact stiffness and damping parameters illustrate the fact that the penalty based method for calculating rigid body frictional contacts is laden with possible uncertainties from multiple sources.

5.5 Summary

This chapter discussed the important aspects when creating a model of a tracked vehicle. An overview of a few of the chief methods used for tracked vehicle analysis was given and the individual subsystems included in the model were described. The topology of the assembled vehicle model was illustrated, with special consideration given to the rigid body frictional contact forces which dominate the response of the system. The stochastic simulation framework applied to the HMMWV model was discussed in depth in Chapters 3 and 4, and its extension to a completely different vehicle model for a separate investigation is simple and straightforward. The vehicle model that will be used for the investigation is based on the tracked vehicle discussed in this chapter, shown in

Fig. 5.10, which is designed to give a tactical mobility advantage when traversing off-road terrain. Thus, the vehicle-terrain interaction is of key importance and is the motivation for carrying out a sensitivity analysis on the soft-soil parameters used in the simulation.

Chapter 6

Application 1: Reliability Prediction using a HMMWV Model

6.1 Introduction and Objectives

This Chapter addresses some aspects of an on-going multiyear research project of Ghiocel Predictive (GP) Technologies (Pittsford, NY) in collaboration with University of Wisconsin-Madison for the US Army Tank-Automotive Research, Development and Engineering Center (TARDEC). The focus of this research project was to enhance the overall vehicle reliability prediction process. The stochastic simulation framework played a key role in its development. Stochastic models, for both the vehicle and operational environment, are utilized to determine the range of the system dynamic response. Results from the vehicle simulations are used as inputs into a finite element analysis to determine stresses on subsystem components which are ultimately used for fatigue stress and damage modeling and reliability prediction calculations. The stochastic vehicle dynamics part of this project was carried out by the author, and GP Technologies carried out the FEA and reliability predictions. A majority of this chapter will be concerned with the role the stochastic vehicle framework played in the project, but the overall project will also be discussed in order to illustrate how the framework can be applied as a part of a larger, real-world project.

An integrated vehicle reliability prediction approach has to incorporate the following computational steps: i) modeling the stochastic operational environment, ii) vehicle multi-body dynamics analysis, iii) stress prediction in subsystems and

components, iv) stochastic progressive damage analysis, and v) component life prediction including uncertainty effects from maintenance activities, and finally, vi) reliability prediction at the component and the system levels. The stochastic framework presented in this work applies to i) and ii) in the overall process. To efficiently and accurately solve the challenges coming from using large-size computational mechanics models in a high-dimensionality stochastic parameter space, a novel HPC stochastic simulation based approach was developed and implemented. The HPC approach for the full project is outside the scope of this work, but details can be found in [43].

Of key importance for an accurate reliability prediction is the integration of various types of uncertain information sources, and the incorporation of lack of data effects. These types of uncertainties were discussed in Section 1.4. However, if uncertainties are considered, the dimensionality of the vehicle reliability problem increases since any single model has to be replaced by a set of stochastic models that correspond to the model space which includes the uncertainties. This transition is illustrated in Fig. 6.1, where the left column uses a single model in each step of the simulation process, represented by flat circles. The right column uses 3D circles to represent each step in the process, and the depth represents the increased dimensionality of the problem. It should be noted that the stochastic model space is usually a high-dimensional parameter space since it includes various model parameters which are considered random quantities. If test data is available, results from dynamic simulations and FEA should be compared with this data, and models should be updated accordingly, as shown by the “Update Response” arrows in Fig. 6.1.

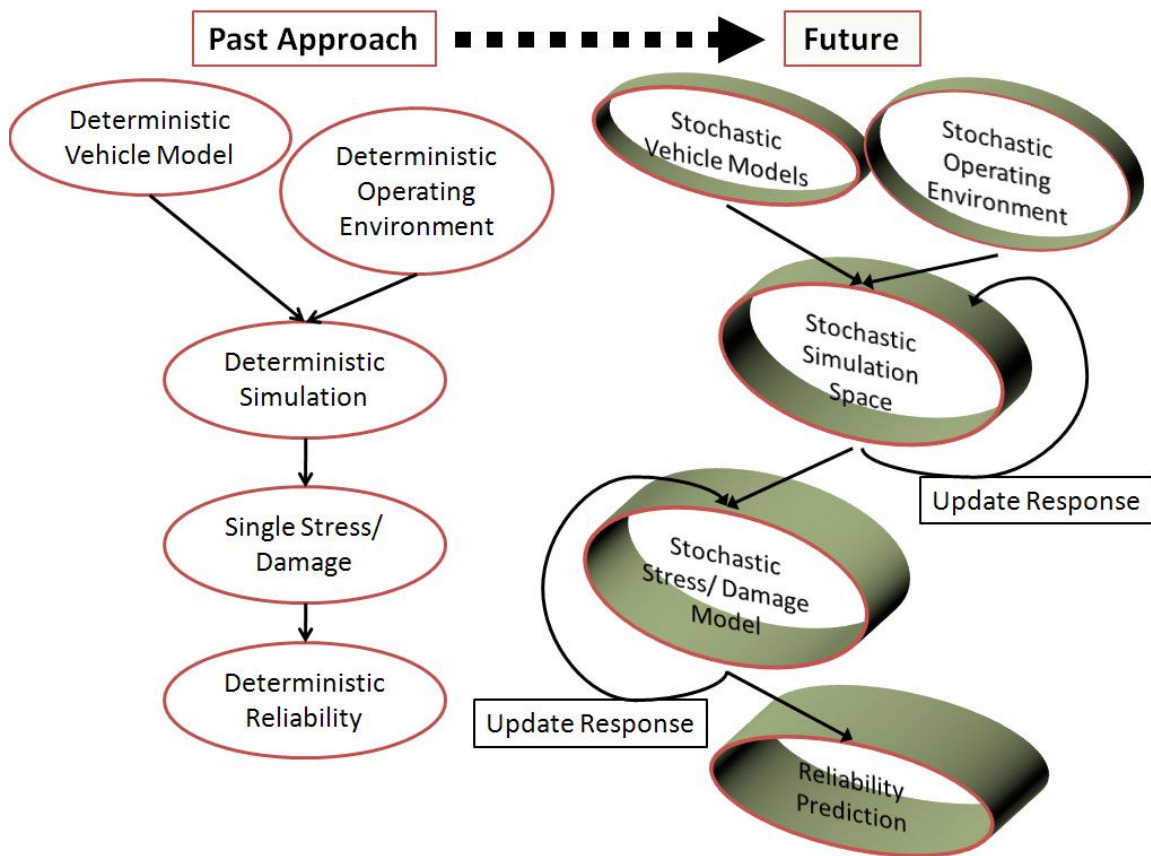


Fig. 6.1. Transition from a deterministic reliability prediction to a stochastic reliability approach

First, the types of variation that were introduced to the operating environment, i.e. road profiles, will be discussed. Next, the choice of uncertain vehicle parameters will be presented with details on the implementation of the variation of these parameters. Finally, simulation results illustrating the impact of uncertainty on the vehicle dynamic response will be shown.

6.2 Stochastic Operating Environment Models

Based on various road measurements it is noted that the road surface variations are highly non-Gaussian [43]. This presents a problem as traditionally, the road surface profiles have been idealized by simple zero-mean one-dimensional Gaussian stationary processes such as a PSD (discussed in Section 2.2) or a Covariance Function (CF). Unfortunately, the PSD or CF estimates are not sufficient for describing non-Gaussian road surface variations which are seen from real measurements. This is the motivation for creating road profiles with non-Gaussian non-stationary properties along its length, which most likely has a large impact on component fatigue and damage failure calculations. The effects of macro-scale road surface variations, such as curve and hill topology, along with varied average vehicle speeds were investigated as well.

The stochastic modeling of the vehicle operational conditions includes the following three variation components.

- 1) Stochastic road profiles idealized by a 10 Dimension-1 Variable vector process with 10 components that describe the statistical road surface amplitude variations on parallel track lines along the road.
- 2) Stochastic road topography idealized by a 1 Dimension-3 Variable stochastic vector process with 3 components that describes the statistical variations in 3D space of the slowly varying road centerline.
- 3) Stochastic vehicle average chassis speed levels along the road trajectory that include the randomness that is produced by a particular driver's maneuvers for

different roughness and topography of road segments, and different drivers' random maneuvers for the same road profile segment.

The implementation of road profiles includes the superposition of two stochastic variations listed above: 1) the road surface variation (micro-scale continuous, including smooth variations and random bumps or holes), and 2) the road topography variation (macro-scale continuous variations, including curves and hills). It is assumed that these two variations are statistically uncorrelated and the average road surface is horizontal and therefore no inclination in the transverse direction is considered. The road surface profile is idealized as non-Gaussian, non-stationary vector-valued stochastic field models with complex spatial correlation structures; the details of this process are beyond the scope of this work and are omitted, but details can be found in [43]. The third stochastic variation, the average vehicle speed along the road, was implemented in vehicle driver model.

Figure 6.2 shows modeled road surface segments with high spatial correlation (HC) and low spatial correlation (LC) in the transverse direction of the road. The longitudinal variation of the centerline is the same for both HC and LC roads. The HC road corresponds to a situation when the wheel inputs are about the same for two parallel wheel lines, so that wheels on the same axle see about the same input. In contrast, the LC road assumes that the inputs on wheels on the same axle are different. Thus, it is expected that a LC road profile will produce much larger vehicle dynamic responses in all directions, especially in the lateral direction. It should be noted that the road surface variation is typically highly non-Gaussian, being highly skewed in the direction of large

positive amplitudes. The LC and HC variations have different degrees of non-Gaussian skew.

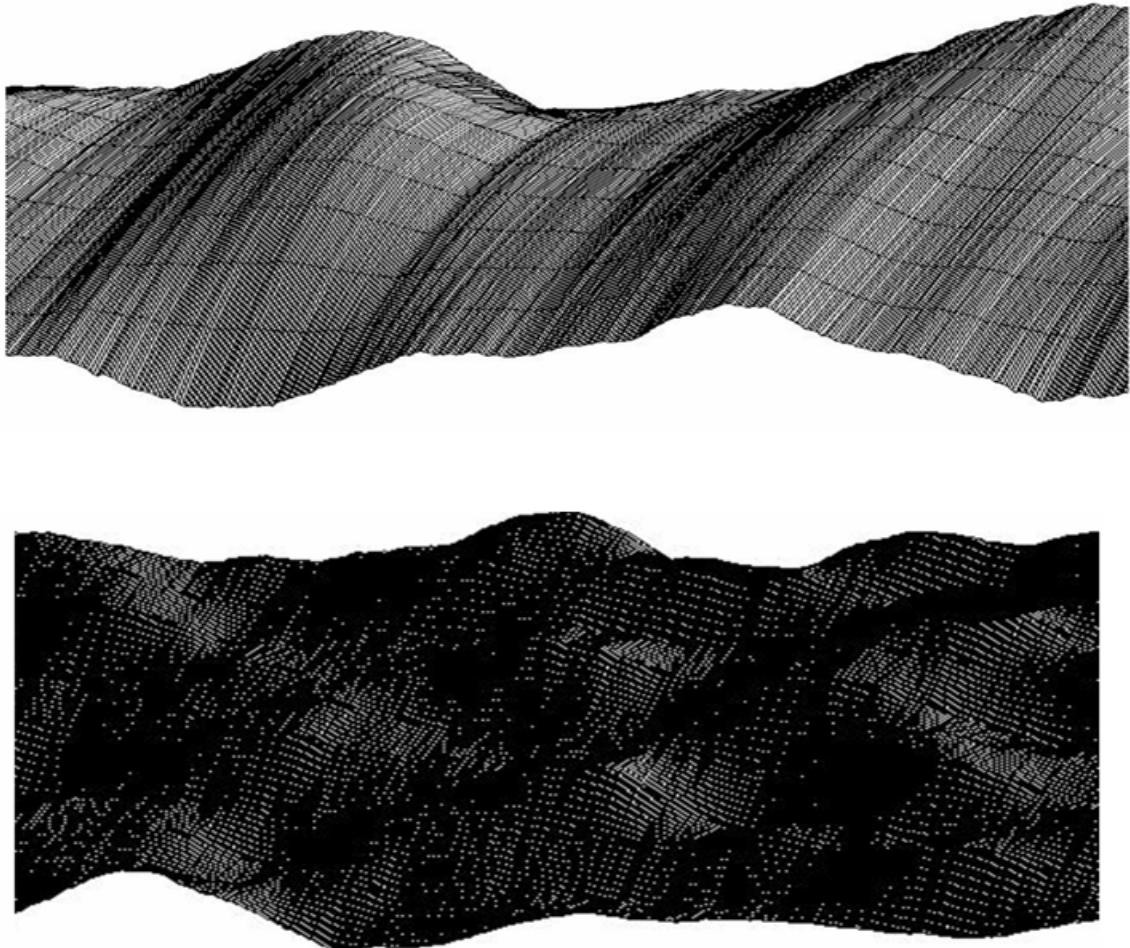


Fig. 6.2. Road surface models with high (top) and low (bottom) spatial correlations. The lateral direction is roughly top to bottom and the longitudinal direction is right to left.

6.3 Stochastic Vehicle Models

To reduce the number of simulations that had to be run, the vehicle parameters that were varied were only in the suspension units (which include the tires). There were 13 elements that were modified in each suspension unit, and a total of 54 modified

parameters in the entire vehicle model. Each modified parameter was considered to be a normally distributed variable whose mean is the nominal value present in the deterministic model. These parameters include: the shock absorber stiffness and damping, tire pressure and the tire model's in- and out-of-plane bending stiffness parameter and the stiffness and damping of the bushings on the upper control arm (UCA) and lower control arm (LCA) that connect the suspension to the chassis. There are two bushing elements on each of the upper and lower control arms.

There were a total of 40 sets of normally distributed variables, divided into groups of 10. For each simulation, the first set of random variables from the first group are applied to the front left suspension; the first set from the second group are applied to the front right suspension; the first set from the third group are applied to the rear left suspension and the first set from the fourth group are applied to the rear right suspension. Thus, all four suspension units are modified by a set of randomly distributed variables. An example of one group of 10 sets of variables used for a single suspension unit is shown in Table 6.1.

Vehicle simulations fall into one of three categories, each of which focused on a certain type of uncertainty. The first category utilized the deterministic vehicle model in every simulation, and only varied the roads using combinations of all three road variation components described in Section 6.2. The second category had a stochastic vehicle model whose parameters were varied as discussed in Section 6.3, but were only simulated on two types of roads at two different average vehicle speeds. The third category is

essentially a combination of the first two categories, whereas the stochastic vehicle was used while varying the road profile with all three road variation components.

Table 6.1. Example set of random distribution coefficients for a suspension unit

SPRING-SHOCK ABSORBER		TIRE			BUSHING UCA				BUSHING LCA			
STIFF	DAMP	PAR 1	PAR 2	PAR 3	STIFF1	STIFF2	DAMP1	DAMP2	STIFF1	STIFF2	DAMP1	DAMP2
1.0046	1.0252	0.8483	1.1049	1.0716	0.9860	0.8979	0.7884	1.1412	0.9560	0.8763	0.9331	1.0428
1.0170	0.9233	0.9034	1.1533	1.0442	1.1512	0.9959	1.1277	1.1785	0.9356	0.7864	0.9588	1.1241
1.0263	0.9224	0.9619	0.8663	1.1349	0.9198	0.9738	0.7934	0.9495	1.1268	0.9292	0.7712	1.0154
1.0250	0.8826	0.9332	1.0963	0.9320	1.1233	1.0434	1.0009	0.9780	1.0331	0.8679	1.1380	1.2354
1.0655	0.9600	1.0767	1.1483	0.9730	1.0422	1.0474	0.9030	0.9874	0.9234	0.8460	1.1254	1.0853
0.8834	1.0012	0.9436	0.8863	0.9126	1.1390	1.2008	1.0600	0.8831	1.2318	1.1183	0.9270	0.8846
0.9718	0.9928	1.0367	0.8705	0.8072	0.9921	0.9028	0.9260	0.8768	1.0374	0.8974	1.0160	1.1076
1.0401	1.0288	1.2577	1.0742	0.8515	1.2938	0.8654	1.1658	1.0048	0.9202	0.8021	0.8877	0.9028
0.9714	1.0110	0.9962	1.0619	1.1171	0.9602	1.0146	0.8774	1.0631	1.0497	1.0655	1.0235	1.0369
1.0784	1.0001	1.1865	1.0407	0.9509	1.0045	1.2185	1.0015	0.9672	1.0450	1.0060	0.9484	1.0460

Categories 2 and 3 were re-run using a ‘degraded’ vehicle, which saw the nominal values of the varied suspension parameters reduced by a factor of 0.85 and 0.7 for stiffness and damping parameters, respectively. However, the tire parameters were not modified with the degradation parameter. Also, the variance of the random variables of the degraded vehicle runs were twice the value of the variance used for the original vehicle. In total, over 500 simulations were run, which required a stochastic vehicle simulation framework to create all the models, run the simulations and post-process the data.

6.4 HMMWV Simulation Results

The results section is split into four separate sections. The first two cover vehicle simulation categories 2 and 3 using the original stochastic vehicle model. The third and

fourth sections cover the same categories of vehicle simulations, but utilize the degraded vehicle. It should be noted that all results presented pertain to the front left suspension unit, which includes the front left tire.

6.4.1 Category 2 Results – Original Vehicle Model

The stochastic variables in the category 2 simulations varied vehicle/tire parameters by multiplying their nominal values by the normally distributed variables, and simulation were performed on medium roughness and high roughness roads. The high roughness road is denoted with ‘Seg6000’ in all subsequent figures. Table 6.2 shows a selected group and set of tire variables; notice the higher tire pressure and out-of-plane stiffness for the group 3 variables. One would assume that a vehicle running on a tire with a high inflation pressure would exhibit a smaller tire deflection than a tire with lower pressure, and would flex less when encountering obstacles due to the higher stiffness of the tire model. However, for each simulation each suspension unit was modified with 13 variables, totaling 52 variable changes in the model for each simulation. Therefore conclusions cannot be drawn by simply isolating one suspension element and equating the results to the random variables that affect that element. As shown in Fig. 6.3, the front-left tire associated with Group 2 in table 6.2 deflects less on average than the Group 3 tire when simulated on the same road profile. The lower pressure tire even deflects less when traversing obstacles as shown in Fig. 6.4. These counter-intuitive results highlight the effect the random variables have on the system behavior of the vehicle and the coupling present in the system.

Table 6.2. Selected stochastic variable factors. Only tire parameters are shown.

Variable Group, Set	Tire Variables		
	Tire pressure	In-plane stiffness	Out-of-plane Stiffness
Group 2, Set 1	0.9726	0.9933	0.9259
Group 3, Set 1	1.1193	0.9995	1.1122

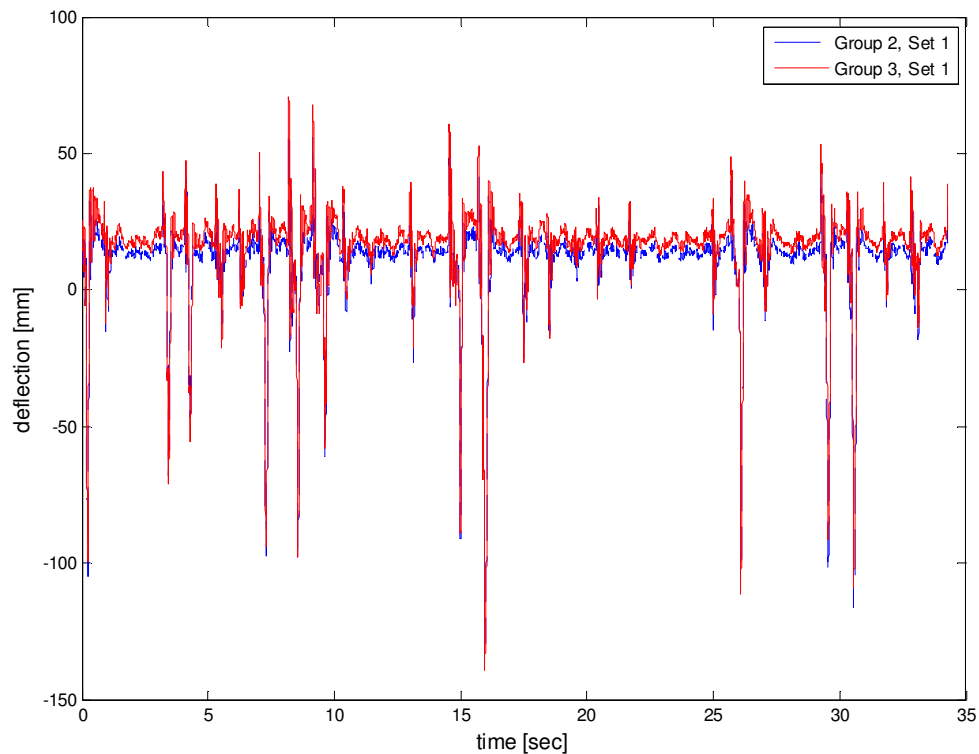


Fig. 6.3. Tire deflections of the front-left tire; positive deflections indicate compression of the tire

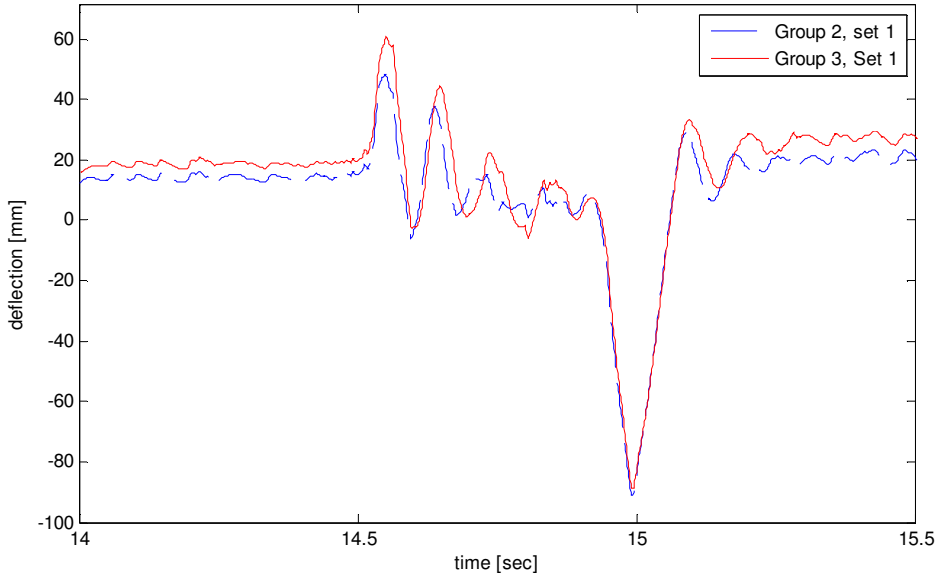


Fig. 6.4. Zoomed in section of Fig. 6.3 illustrate tire deflection when traversing an obstacle

6.4.2 Category 3 Results – Original Vehicle Model

Adding topology to the medium and high roughness roads used in the category 2 simulations gives results as shown in Fig. 6.5, where the vehicle pitch is greatly affected by the superposition of rolling hills topology on the medium roughness road. On the same note, adding topology to the high roughness road has the same effect. The effect of road roughness on chassis pitch is still evident as shown in Fig. 6.6, where the high roughness road sees more oscillations in its chassis pitch. Adding topology to the stochastic vehicle/tire models has a large effect on the overall vehicle response, but the road profile roughness still has a large impact on the loading cycles in the suspension elements. This is shown in Fig. 6.7, where the peak loads in the damping element of the shock absorber are much larger for the high roughness road than the medium roughness road. Figure 6.8

and Fig. 6.9 also show the importance of road roughness on peak loads in the LCA and UCA ball joint forces, respectively.

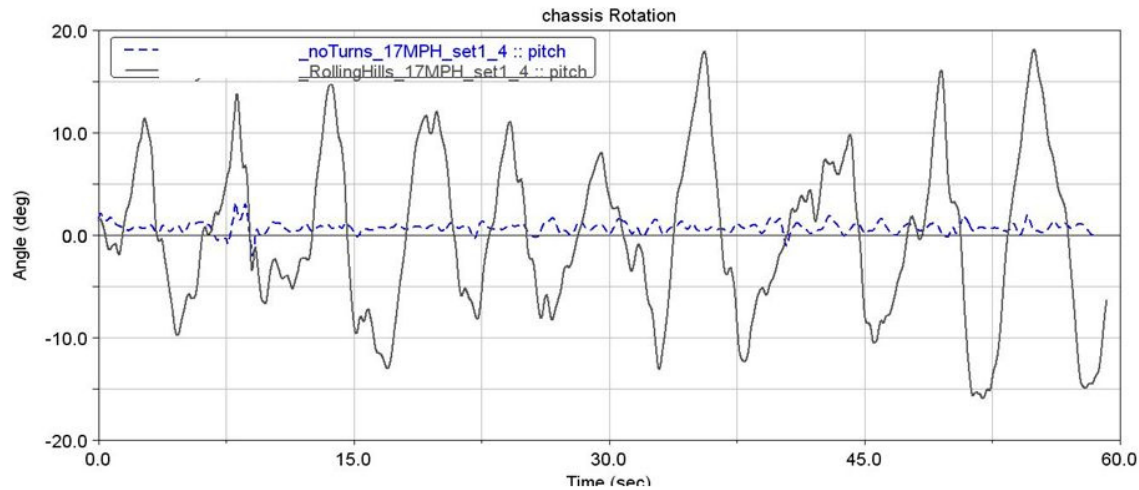


Fig 6.5. Effect of rolling hills topology on chassis pitch for the medium roughness road

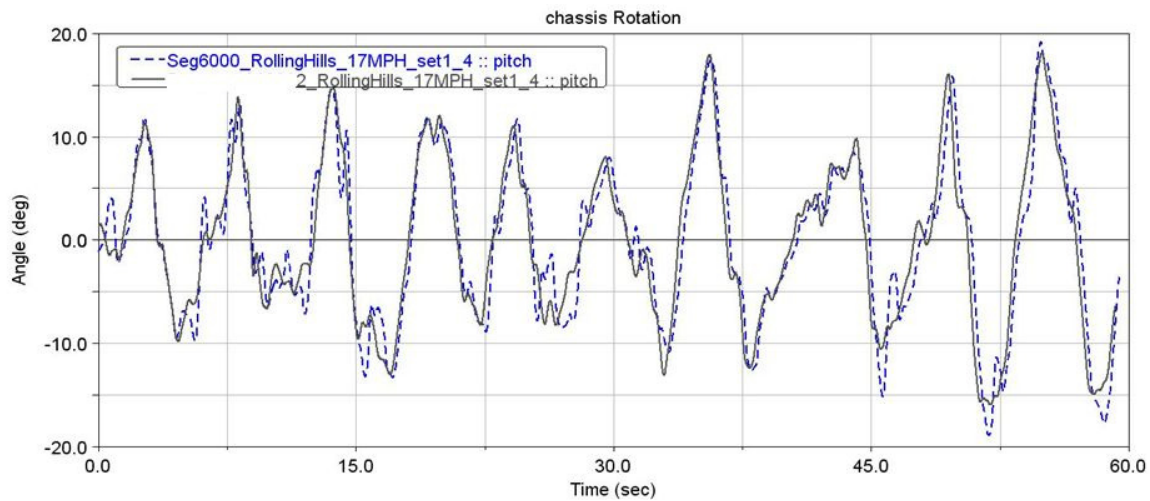


Fig. 6.6. Chassis pitch for medium and high roughness road simulations

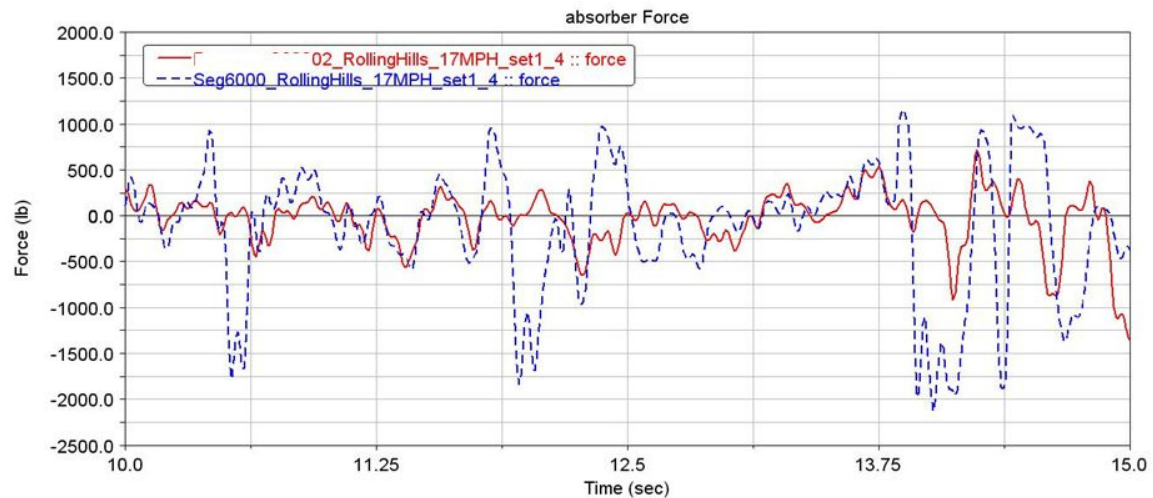


Fig. 6.7. Shock absorber force for medium and high roughness roads

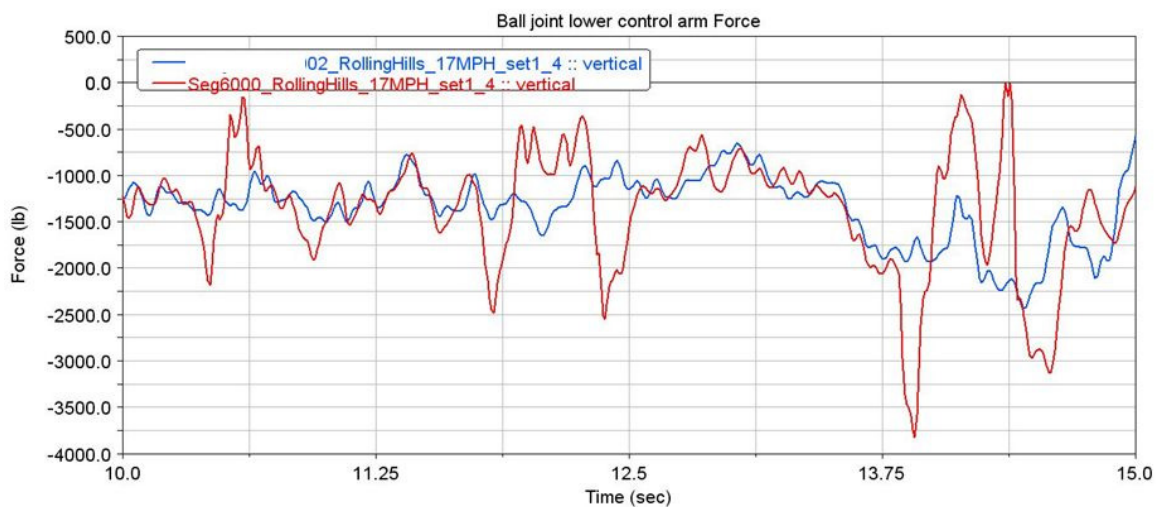


Fig. 6.8. LCA ball joint vertical force for medium and high roughness roads

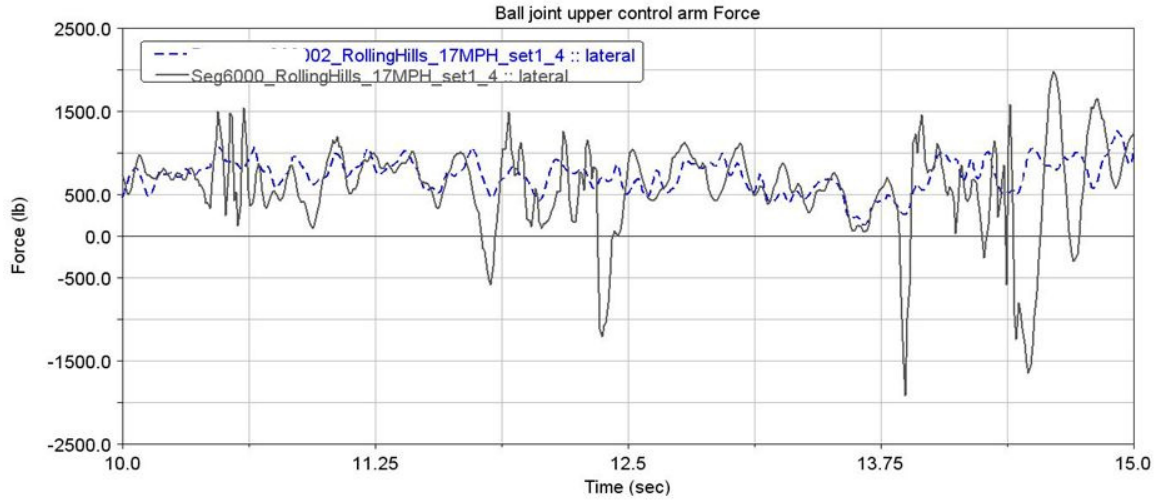


Fig. 6.9. UCA ball joint lateral force for medium and high roughness roads

6.4.3 Category 2 Results – Degraded Vehicle Model

As the degraded vehicle essentially has overall lower values for the vehicle suspension parameters, some of the important outputs are compared between the degraded and original vehicle simulations. There are obvious ramifications of lowering the stiffness and damping by a factor of 0.85 and 0.7, respectively, such as the spring force in the shock absorber should be lower across all degraded vehicle simulations. This can be seen in Fig. 6.10, where the spring force of the front left shock is lower throughout the simulation when compared to a simulation with the original vehicle model which operated on the same road with the same topography and average speed.

The degraded vehicle has some surprising results, such as the vertical force component in the LCA ball joint, as shown in Fig. 6.11. When the vehicle is not traversing any large bumps, the degraded vehicle has a larger (i.e., more negative in the figure) vertical force on the LCA ball joint; however, the original vehicle sees a larger

force spike when the vehicle traverses an obstacle, at time = 7.5 and 8.7 seconds. One possible explanation for this behavior is the larger variance associated with the uncertain vehicle parameters of the degraded vehicle. The suspension unit that contains the LCA ball joint force reported in Fig. 6.11 could have higher stiffness and higher damping values which could cause a larger force on the LCA ball joint during normal operation and less when encountering obstacles.

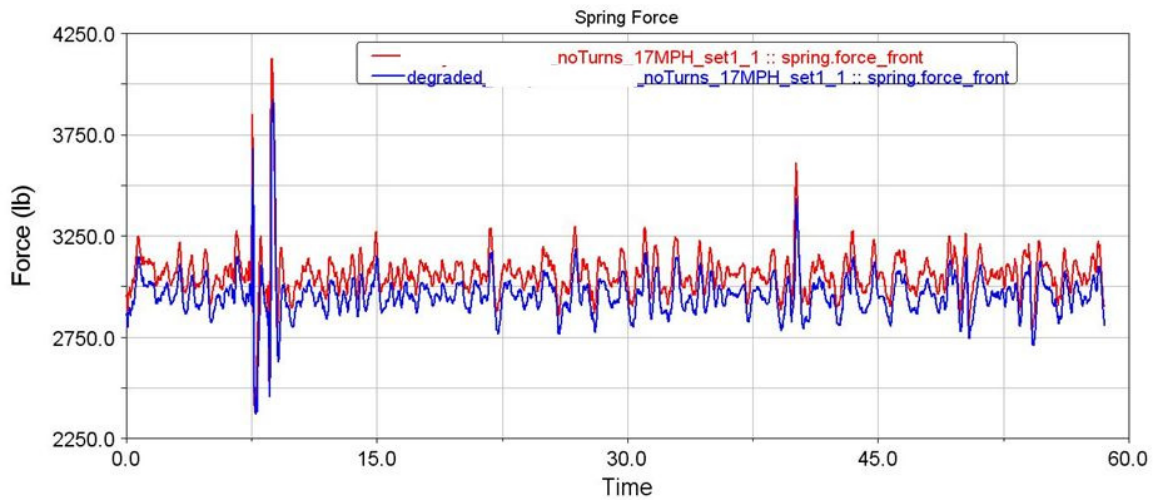


Fig. 6.10. Front left shock spring force is lower in the degraded model simulation

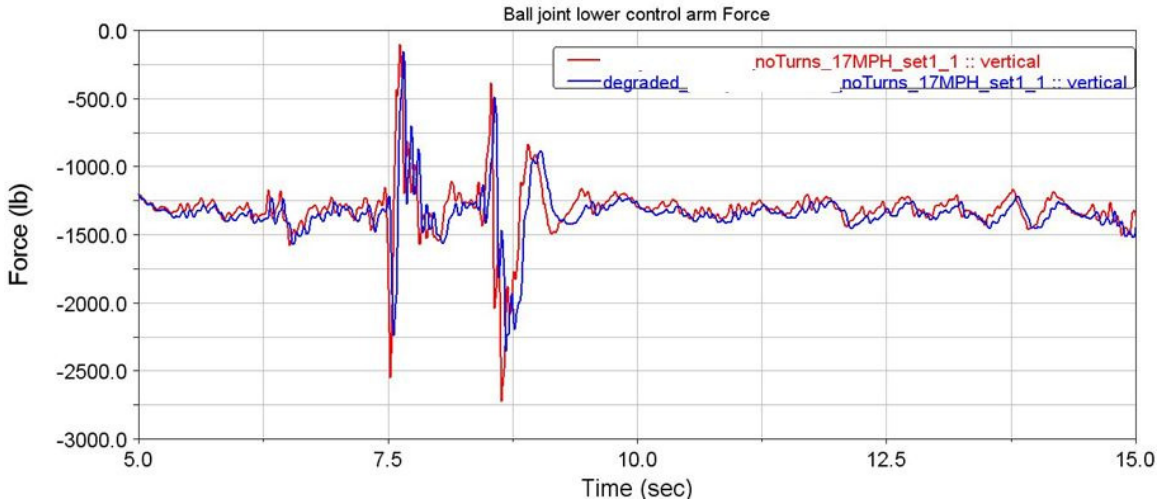


Fig. 6.11. Vertical force in the LCA ball joint is lower and higher in the degraded model

6.4.4. Category 3 Results – Degraded Vehicle Model

The third category of degraded vehicle simulations combines the degraded vehicle with modified parameters as well as multiple road profiles, some of which include superimposed rolling hills topology. Fig. 6.12 shows the chassis pitch angle of the degraded vehicle with the non-degraded vehicle on a road with rolling hills topology. At first glance, it seems that the degraded vehicle parameters don't play a large role in the chassis pitch angle, but the chassis pitch angular acceleration comparison shown in Fig. 6.13 indicate that the non-degraded vehicle has substantially larger chassis pitch angular acceleration peaks at some points, such as at time = 5.8 and 7.8 seconds.

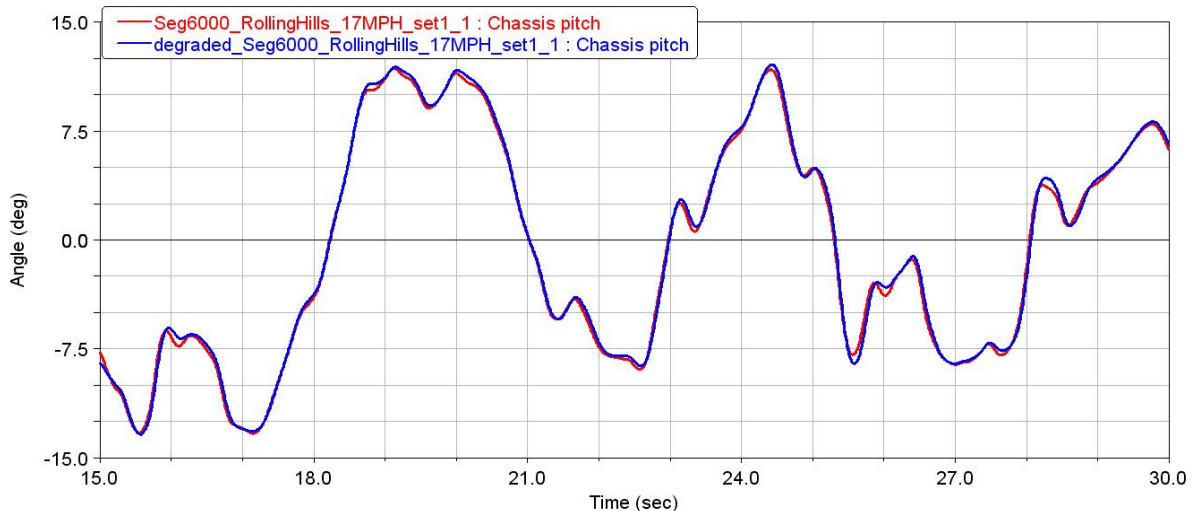


Fig. 6.12. Chassis pitch angles of the degraded and original vehicle model

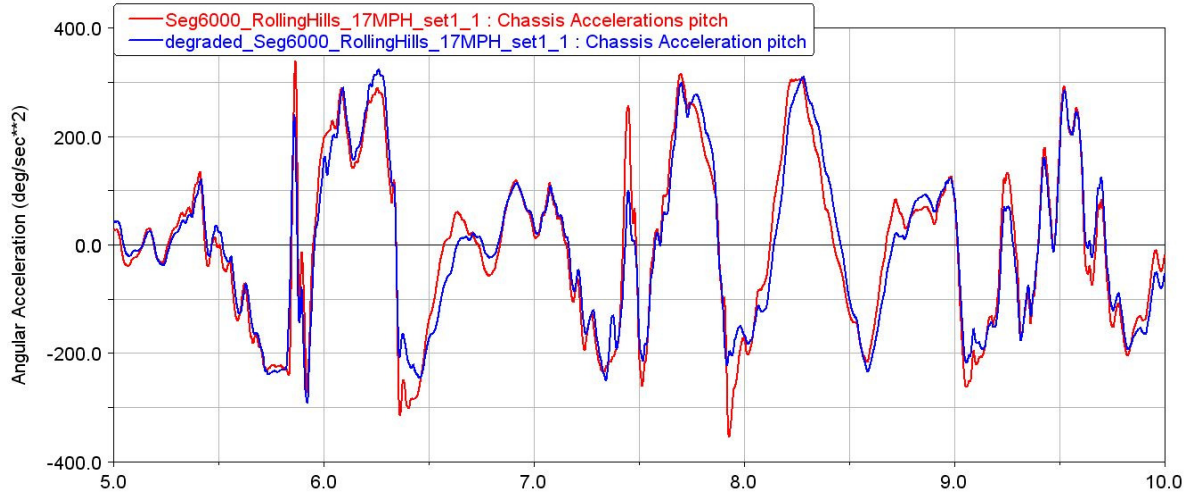


Fig. 6.13. Chassis pitch angular acceleration of the degraded and original vehicle model

The degraded vehicle has substantially less damping in the suspension elements, such as the bushing and shock absorber damper components. Thus, it would be expected that the overall dissipative forces in the degraded vehicle would be substantially lower than that of the non-degraded vehicle. Fig. 6.14 illustrates this fact, as the peaks of the damper force are much higher on the original vehicle, which indicates that the degraded vehicle dissipates less force from the many hills and turns caused by the rolling hills topology. This leads to larger peaks in the joint forces in the degraded vehicle as shown in Fig. 6.15 at time = 7.65 seconds, where the UCA ball joint lateral forces are plotted for both vehicle models. In this particular case, the lateral force in the UCA ball joint of the degraded model experiences 300 lbs more force at the peak than the original model. This force peak is almost 15% larger than in the non-degraded vehicle, and could have large effects on the fatigue and damage calculations used for reliability estimates.

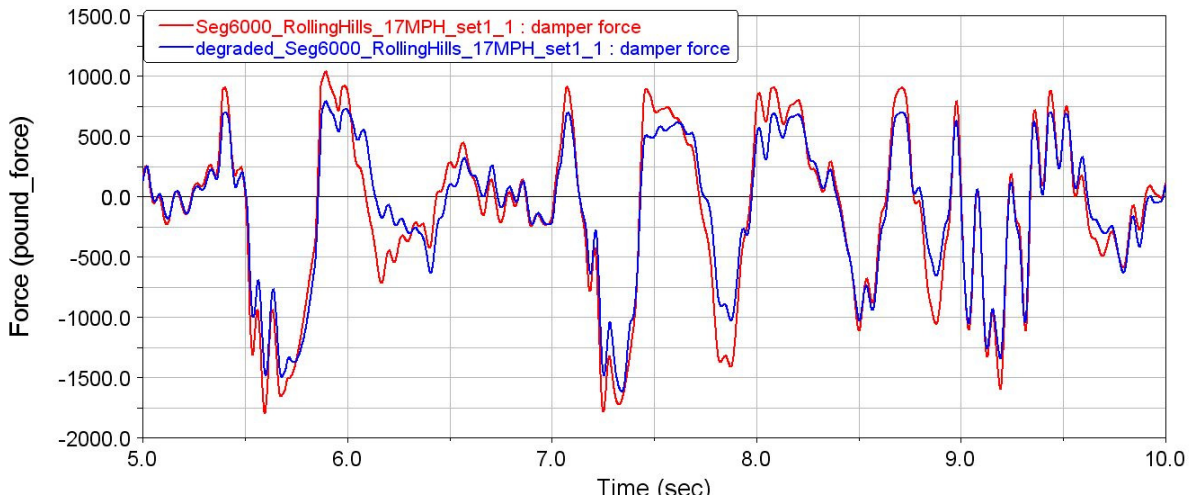


Fig. 6.14. Damper force comparison for roads with rolling hills topology

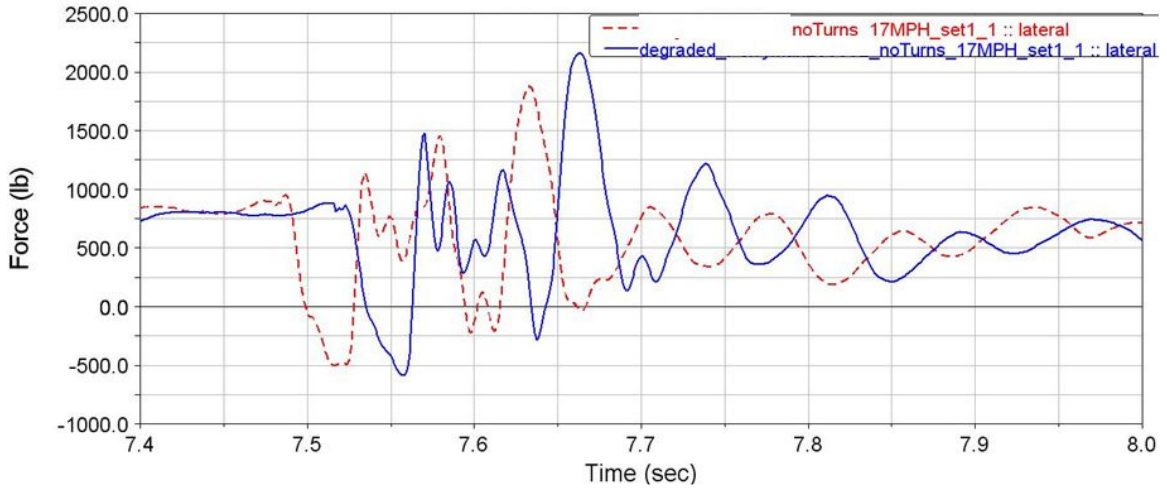


Fig. 6.15. UCA ball joint lateral force in the original and degraded vehicles

6.5 Summary

Vehicle responses to stochastic model parameters and operating conditions were simulated in a co-simulation environment using a multi-body dynamic model of the Army's HMMWV in conjunction with a high-fidelity tire model. These simulations were run using the stochastic simulation framework discussed in chapters 3 and 4. The

dynamic response outputs of the simulations were used as an input into a FEA to determine local stresses on the component level, which were not performed by the author and are outside the scope of this work. However, the stochastic stress loading cycles serve as an input into the stochastic progressive damage models which can ultimately be used for reliability predictions, which are the ultimate goal of the project with GP Technologies.

Stochastic modeling of the operating conditions included variations in height and topography of the road profiles. Vehicle chassis velocity and the inherent randomness of a particular driver's trajectory were also treated as stochastic variables. A representative HMMWV and tire model were created, and various tire and suspension component parameters were varied. Sample results from vehicle dynamics simulations are presented and discussed, with an emphasis on the effects of the varied road and vehicle parameters on the response.

Chapter 7

Application 2: Tracked Vehicle Response Sensitivity to Soft Soil Parameters

7.1 Introduction and Objectives

This chapter shows the application of the stochastic framework to the tracked vehicle model of chapter 5 when using the soft soil models discussed in section 2.3. The objective of this investigation is twofold: 1) extend the stochastic framework to a different vehicle model and note the differences, and 2) understand how experimental uncertainty in the soft-soil parameters affects the response of the system. The first objective was fairly straightforward to address because the entire simulation environment is contained in the ADAMS/Car software program. A few slight modifications (mostly simplifications) are made to the stochastic simulation framework discussed in chapter 4, and will be commented on in the following section.

The second objective was slightly more difficult to address, as the computational bottleneck due to the many rigid body frictional contacts in the model caused half-vehicle simulations to take more than 7 hours of computation time for a mere 5 seconds of output data. The simulation was implemented in a COTS software package which utilized a penalty approach to solve the contact problem as discussed in section 5.4.2; thus, there was no opportunity to implement a more efficient contact algorithm. However, more efficient approaches for handling many contacts do exist, such as the linear complementarity problem approach [40]. A space-filling Latin Hypercube (LH) sampling was used to generate meaningful results without needing a large number of simulations.

A brief overview of the design generated by the LH approach will be given and the resulting sampling set of soft-soil parameters will be presented. Finally, simulation results pertaining to mobility and track chain reliability of the tracked vehicle model run on the soft-soil terrain models will be discussed.

7.2 Stochastic Tracked Vehicle Simulation

The extension of the stochastic framework utilized for the HMMWV simulations was straightforward to implement because the same vehicle simulation software (ADAMS/Car) was used. Also, the soft soil models discussed in sections 2.3.2 and 2.3.3 were implemented by leveraging a plug-in to the program, the ADAMS Tracked Vehicle Toolkit, which contains a module that calculates the terrain forces according to the soft-soil models [44]. Finally, there was no need for a co-simulation environment since the road wheels were considered rigid.

The data flow diagram for the stochastic simulation implementation is shown in Fig. 7.1. Similar to the case involving the HMMWV, model files from a single deterministic vehicle are used as inputs into a MATLAB script to create multiple instances of the model files. A single, flat road profile was used and is omitted from the data flow diagram, but is shown in Fig. 7.2. The nominal soft-soil parameters are based on a dry sand terrain reported in [1] and a few of the parameters for that soil are listed in Table 2.1. The road profile shown in Fig. 7.2 has the surface area divided into equally sized rectangular elements. Each element keeps track of the maximum vertical沉降 (sinkage) in order to calculate the correct vertical forces on the vehicle due to repetitive loading effects discussed in section 3.2.3.

The tracked vehicle begins at rest after performing a series of equilibrium analyses, and a motion is applied to the drive sprocket which reaches a maximum value of 270 degrees/sec at 1.0 seconds into the simulation.

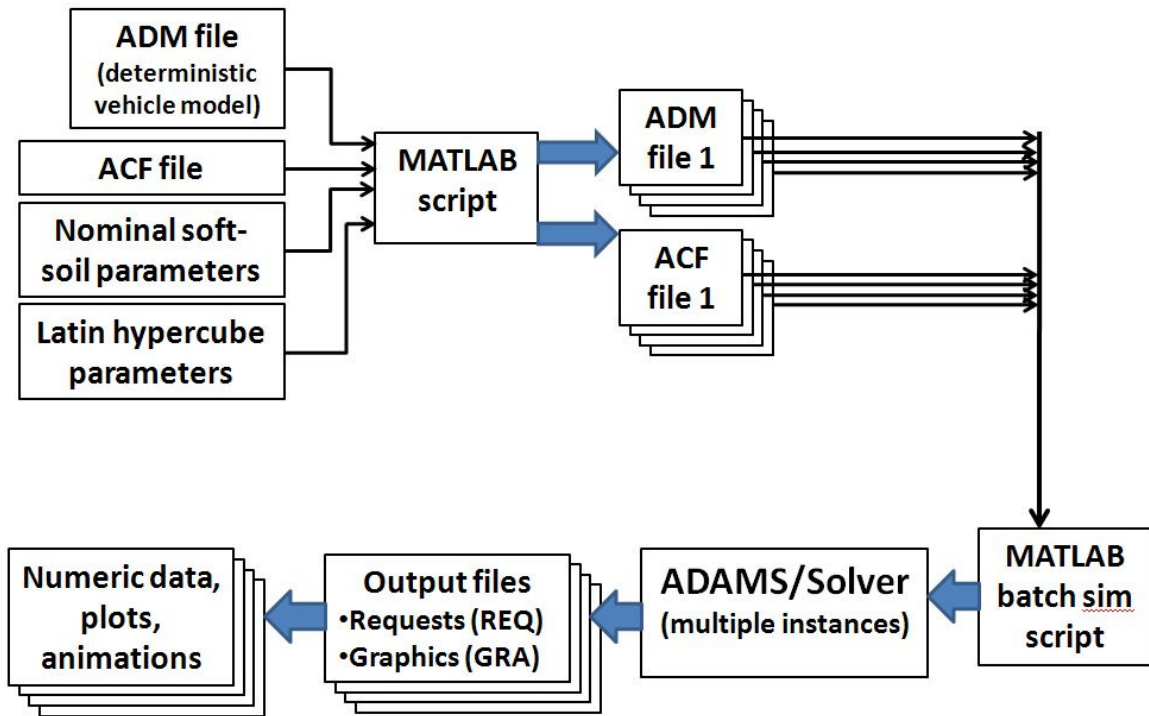


Fig. 7.1. Data flow diagram for a stochastic set of tracked vehicle simulations

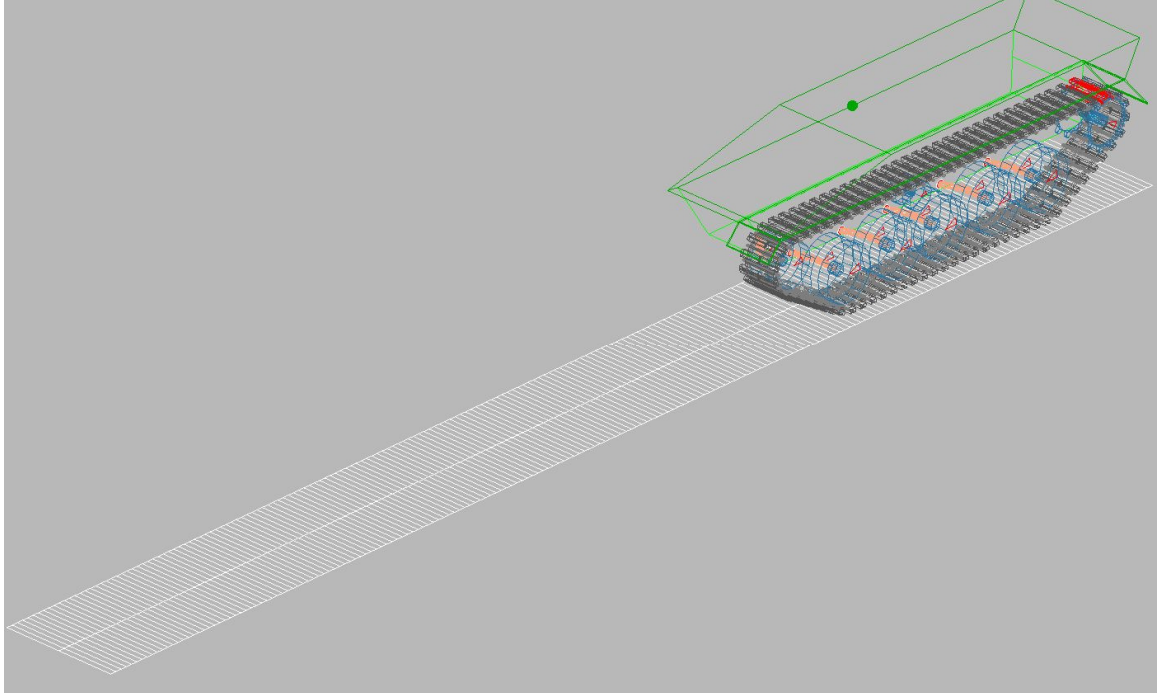


Fig. 7.2. Tracked half-vehicle model shown on the flat road profile.

7.3 Latin Hypercube Sampling Design

The Latin Hypercube (LH) sample is constructed by assuming a set of variables X_k , where $k = 1, \dots, d$, has support $[a_k, b_k]$ with any assumed distribution $D_k(\bullet)$. Now, the k^{th} axis is divided into n parts with equal probability $1/n$ under $D_k(\bullet)$ [45]. Each variable has n equally spaced divisions and for each permutation, the sample variables fall into one of the n divisions once over all the samples. In this case, d is the number of parameters that are varied in the soft-soil model, n is the total number of simulations that are run, and the support $[a_k, b_k]$ is the interval due to an assumed amount of experimental error.

Each soft-soil parameter is assumed to have a range of error around its median value; +/- 5% experimental error was assumed. There are seven soil parameters that are modified, thus $d=7$. Due to the long simulation time involved, only 25 total simulations were run; thus, $n=25$. An example of this LH sampling design for two parameters is shown in Fig. 7.3, and each variable only uses a value in each $1/n$ partition once. However, the design shown in Fig. 7.3 leaves many areas of the latin cube empty, and is a non-space filling hypercube design. The actual implementation uses a random number generator to create a design with better space-filling properties. The actual soft-soil values derived from the LH design used in the simulations is given in Appendix B. It should be noted that when each parameter is assigned to a $1/n$ sized partition, the selected value is randomly distributed within the partition. Simulation results of applying the LH sampling of soft-soil parameters to the deterministic tracked vehicle model are shown in the next section.

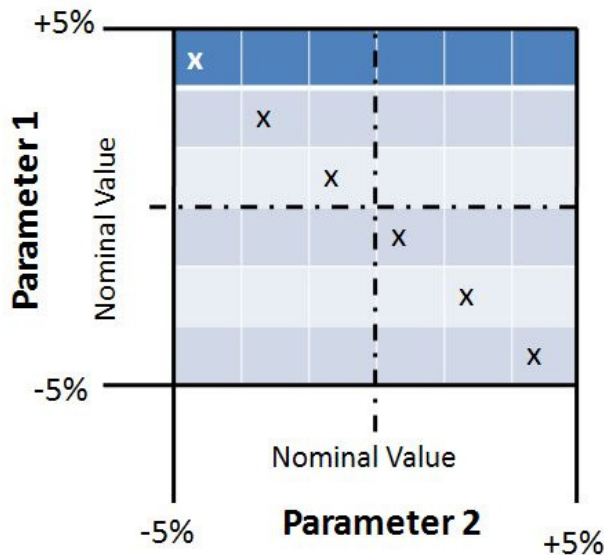


Fig. 7.3. An example of a non-space filling LH design with two parameters

7.4 Tracked Vehicle Simulation Results

The results for this tracked vehicle analysis will focus on two important aspects in order to gauge how the response of the system is affected by uncertainty stemming from measurement error in the soft-soil parameters. The aspects of interest are: vehicle mobility and reliability of track chain components. To gauge the mobility of the tracked vehicle on the various permutations of the soft soil model, the behavior of forward chassis velocities during acceleration and at quasi-steady state operating conditions will be investigated. A main cause of tracked vehicle failure is due to “throwing” a track shoe, where one of the bushing elements between two track shoes fails, which renders the vehicle completely immobile. Thus, bushing force results between track shoe connections will be addressed.

7.4.1 Tracked Vehicle Results: Mobility

The vehicle forward velocity was measured and data from all 26 simulations was saved to evaluate the effect that varied soft-soil parameters has on this particular tracked vehicle model’s mobility. A plot of the mean forward chassis velocity is shown in Fig. 7.4. Note that the velocity increases cubically from the initial position to time = 1 as the imposed rotational velocity of the drive sprocket is ramped up to its maximum value of 270 deg/sec in the first second. Due to a combination of non-steady state conditions, the slip does not reach a maximum until a short amount of time after the maximum drive sprocket speed is achieved. Combining this with the fact that the vehicle does not settle immediately, the steady-state velocity is reached at approximately time = 3 seconds.

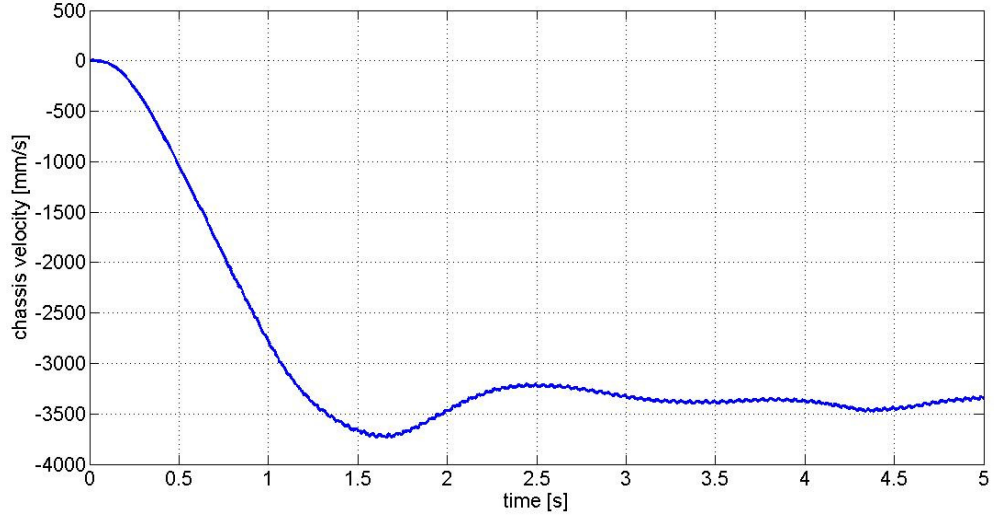


Fig. 7.4. Average longitudinal velocity of the tracked vehicle

Taking a closer look at the time span at steady state velocity, the individual chassis velocities are plotted in Fig. 7.5. Note the oscillatory nature of the data; this can be at least partially attributed to the behavior of the track chain tension in conjunction with the tensioning system, which is seen in tracked vehicles operating on non-deformable terrain models [39].

The variation of velocity is the most important aspect of mobility in these tracked vehicle simulations, and the standard deviation of chassis velocities shown in Fig. 7.5 are taken over the steady state time interval and plotted in Fig. 7.6. The values over the entire range of steady state operation are very low, and it can be concluded that for this model, the assumed measurement error of the soft-soil parameters does not have a large effect on the mobility of the vehicle. However, during acceleration the variation in the chassis velocity is much larger as shown in Fig. 7.7. Thus, further studies on the impact of varied

soft-soil parameters on vehicle mobility should be in relation to the acceleration of the vehicle rather than its steady state velocity.

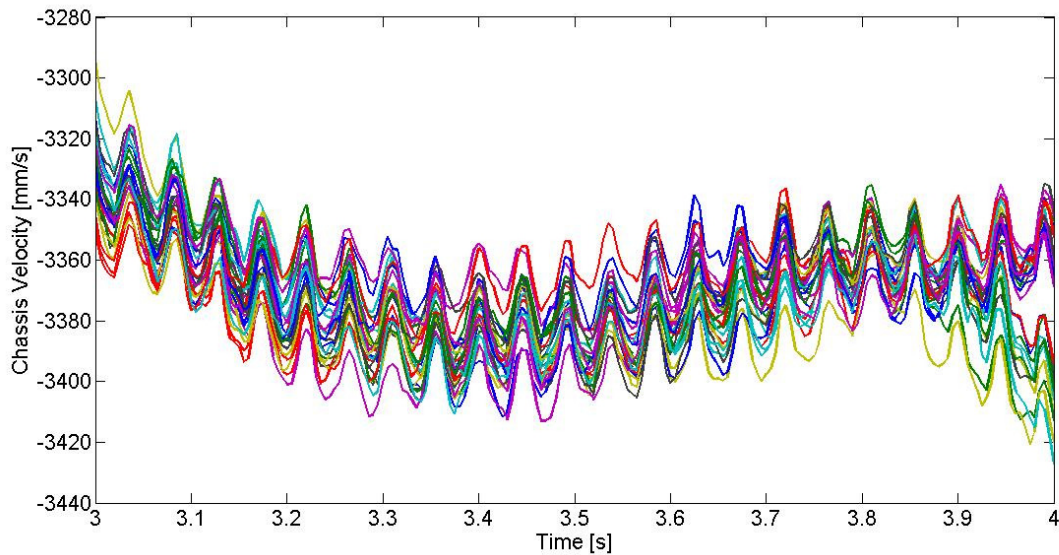


Fig. 7.5. Individual chassis velocities during quasi-steady state operation

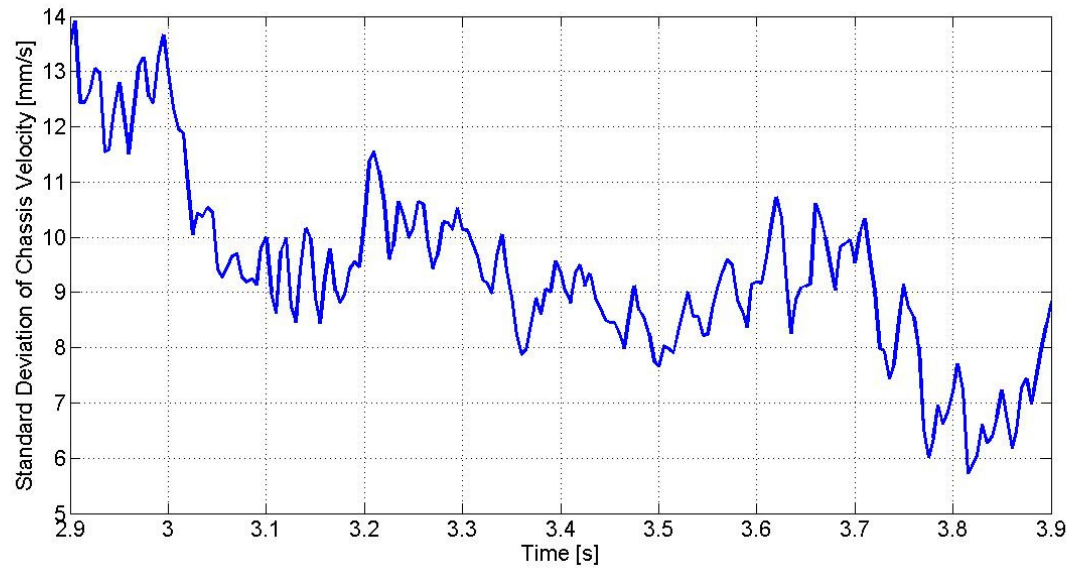


Fig. 7.6. Standard deviation of chassis velocity during quasi-steady state operation

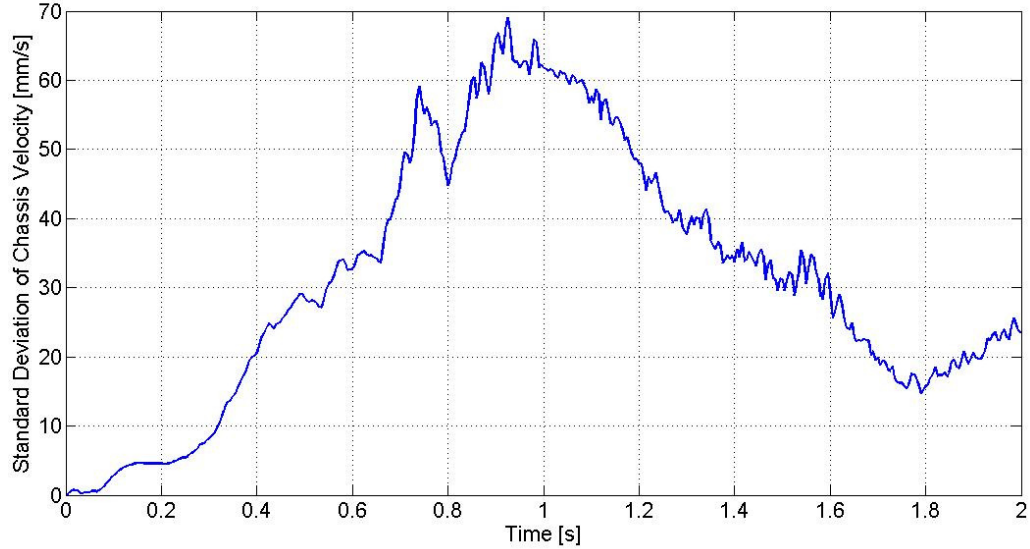


Fig. 7.7. Standard deviation of chassis velocity during initial acceleration

7.4.2 Tracked Vehicle Results: Bushing Forces

The bushing connection force data is inherently noisy due to the fact that each track shoe is under the influence of: its two neighbors via bushing elements, the soft-soil exerting vertical and horizontal forces on the bottom face of each track shoe, and the road wheels constantly impacting the top face. Since the maximum forces exerted on the bushings are desired, the magnitude of the bushing force is calculated by summing the vector of vertical and horizontal forces; the lateral forces are negligible since a straight line simulation was run with a half-vehicle model. All results concern to the track shoe shown in Fig. 7.8; the bushing forces reported are those in the bushing that lags the direction of travel of the track shoe in Fig. 7.8. The calculated bushing force magnitude for all 26 simulations is shown in Fig. 7.9.

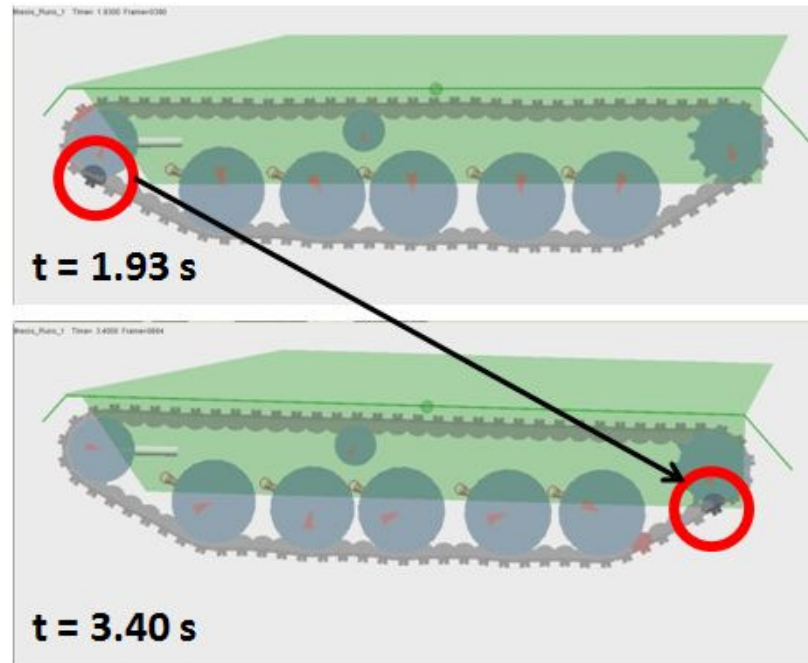


Fig. 7.8. Simulation screen shots of the selected track shoe

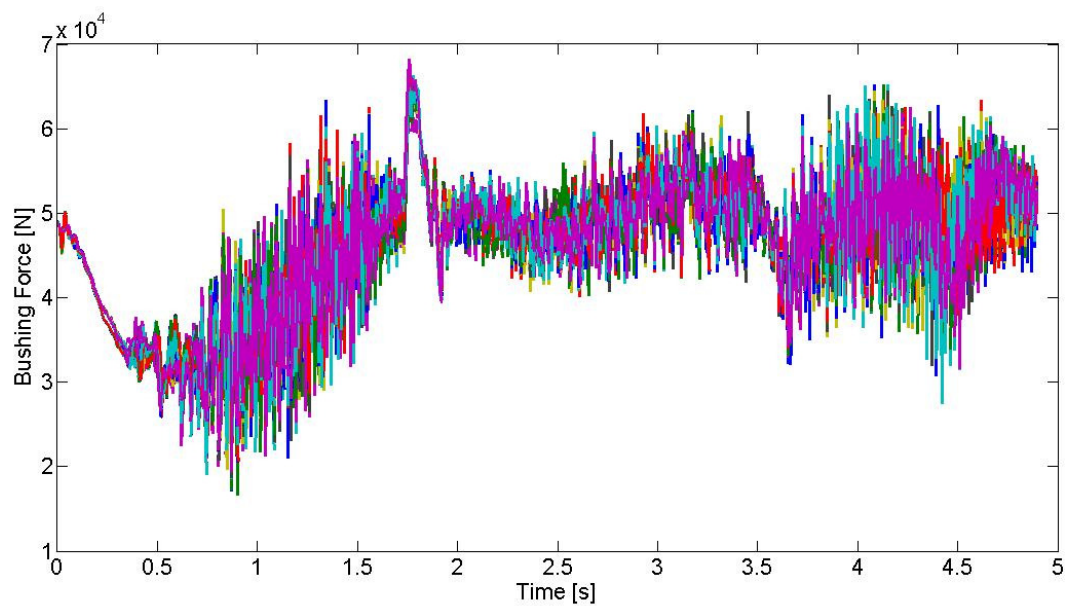


Fig. 7.9 Bushing force of the track shoe shown in Fig. 7.8

The maximum, minimum and average bushing forces are reported in Fig. 7.10, and it is clear that there is a large difference between the maximum and minimum values from different simulations at each time step. A standard deviation of the bushing forces during the time span of quasi-steady state operating conditions is shown in Fig. 7.11, and substantial differences are noted in the bushing forces among the 26 simulations.

Fatigue failure is usually attributed to stress cycles, where the average force and the amplitude and frequency of force oscillations are typically the causes of failure. Fig. 7.10 indicates that there are large oscillations in the bushing force and Fig. 7.11 shows that there are large differences in bushing forces at any given time across the 26 simulations. A stress cycle analysis should be conducted for all 26 simulations to determine the effect of the varied soft-soil parameters on the reliability of the track shoe bushing; however, this type of in-depth analysis is outside the scope of this work and could be an area of future work.

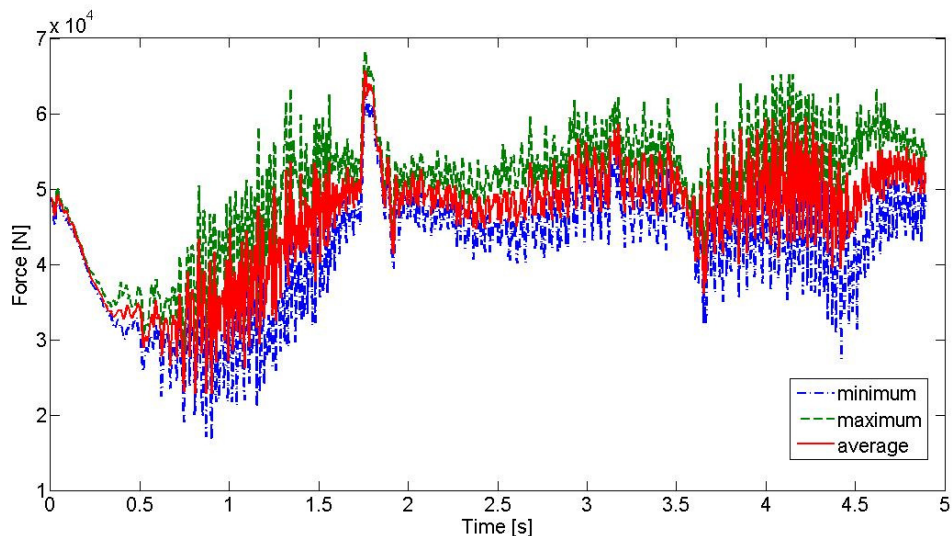


Fig. 7.10. Maximum, minimum and average bushing forces

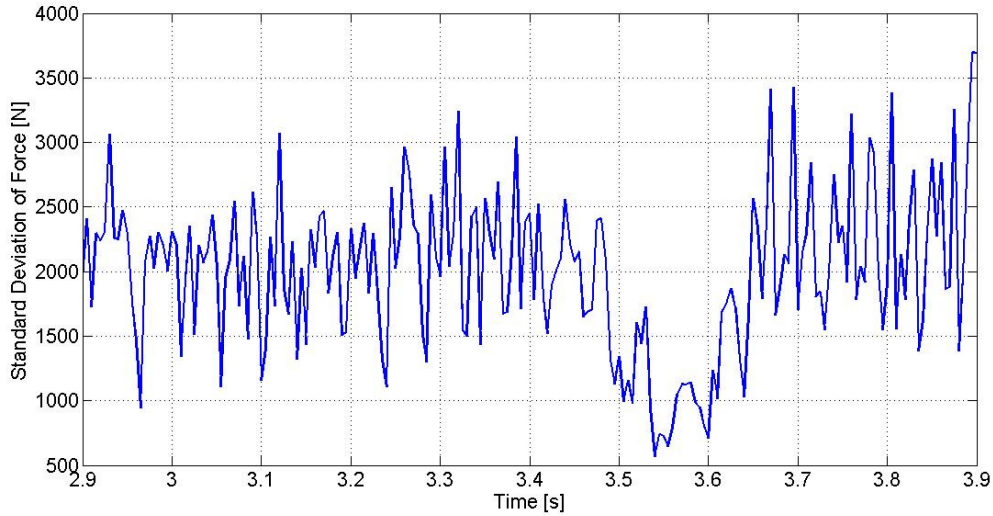


Fig. 7.11. Standard deviation of bushing forces during quasi-steady state operation

7.5 Summary

This chapter illustrated the extension of the stochastic simulation framework to a completely different vehicle system. Rather than simulating a HMMWV vehicle model on non-deformable terrain, the tracked vehicle model of chapter 5 was used which operated on a soft soil model that was discussed in section 2.3. The objective of this investigation was to understand how experimental uncertainty in the soft-soil parameters affects the response of the system. Modifying the stochastic simulation framework was straightforward because the same simulation software program, ADAMS/Car, was used. The modifications made to the original stochastic simulation framework discussed in chapter 4 were mostly simplifications due to focusing on a single source of uncertainty in the soft-soil parameters.

A computational bottleneck (i.e., a calculation that greatly increases the required number of computations) due to formulation of the rigid body frictional contact problem in the software caused a single 5 second simulation to take more than 7 hours of computation time; therefore only a small number of simulations could be run to assess the impact of uncertainty. A Latin Hypercube design was used to generate a space-filling sample of soft-soil models from a set of measurement data for a dry sand terrain. A single tracked half-vehicle model was simulated on the original dry sand model and on the 25 variations created from the Latin hypercube samples. Simulation results pertaining to mobility and track chain reliability of the tracked vehicle model run on the soft-soil terrain models were discussed. It was determined that the uncertainty affected the acceleration of the vehicle more-so than its quasi-steady state velocity. There were large differences in the force magnitudes of a selected track shoe bushing element among the simulations, and an in-depth fatigue analysis due to stress cycles would be appropriate to determine how the uncertainty in measured soft-soil parameters affects the reliability of the track chain due to fatigue failure in the bushing elements.

Chapter 8

Summary and Conclusions

Over the last decade, simulation-based engineering in the form of virtual prototyping has been increasingly utilized by engineers in the design process of mechanical systems. In the field of ground vehicle modeling and simulation, the continual increase in computing power has lead to applications involving increasingly complex and accurate representations. In the past, small sets of simulations were run to understand the general behavior of deterministic vehicle system models. In recent years there has been an increasing demand to understand complex problems such as uncertainty propagation, sensitivity analysis and reliability prediction. As such, single deterministic vehicle and operating environment models must be extended into stochastic sets of models and simulations in order to capture the added dimensionality that is associated with these types of problems. To address these issues, methods and tools were created to utilize models that are simulated in commercial software, and enabled a stochastic simulation framework. Deterministic vehicle and environment models are extended into sets of stochastic models and simulations using the tools in conjunction with information about the nature of the uncertainty.

The original motivation for creating the tools which implement a stochastic simulation framework stems from a research project where the effect of various uncertainties on the reliability calculations of a HMMWV model was investigated. This project was a joint effort between the author and engineers at GP Technologies. A single

deterministic HMMWV model was created from physical measurement and design data in the commercial software program ADAMS/Car and extended into a large number of models which were subsequently simulated using the stochastic simulation framework. The outputs from these numerous vehicle simulations were used as inputs into a HPC finite element analysis framework to understand the stresses on subsystem components which are ultimately used for fatigue stress and damage modeling and reliability prediction calculations. Results from these simulations which took different types of uncertainty into account were presented to illustrate the impact the uncertainty has on various components in the vehicle model. In this work, the framework was applied to a wheeled vehicle operating on non-deformable terrain, but the tools are general and could be modified and applied other types of vehicle simulations.

The tools that were created and presented were meant to be able to be extended to different types of ground vehicle systems with relative ease. After a slight modification, they were successfully applied to a tracked vehicle model to characterize how the uncertainty in parameters of the soft soil model affects certain forces (connection bushing forces) and velocities (chassis velocities) of interest.

References

1. Wong, J.Y., *Theory of Ground Vehicles*. 3rd ed. 2001, New York: Wiley Interscience.
2. Datar, M., *Uncertainty Quantification in Ground Vehicle Simulation, M.S. Thesis*, in *Mechanical Engineering*, University of Wisconsin-Madison: Madison. 2008
3. Madsen, J., D. Ghiocel, D. Gorsich, D. Lamb, and D. Negruț, *A Stochastic Approach to Integrated Vehicle Reliability Prediction*, in *ASME-IDETC*, ASME: San Diego, CA. 2009
4. Schmitt, K., J. Madsen, M. Anitescu and D. Negruț. *A Gaussian Process Based Approach for Handling Uncertainty in Vehicle Dynamics Simulations - IMECE2008-66664*. in *2008 ASME International Mechanical Engineering Congress and Exposition*. 2008. Boston, MA: ASME.
5. Kryloff, N. and N. Bogoliuboff, *Introduction to Non-Linear Mechanics*. 1949: Princeton University Press.
6. Helton, J. and F. Davis, *Sampling-based methods*. Sensitivity Analysis, 2000: p. 101-153.
7. Helton, J. and F. Davis, *Latin Hypercube sampling and the propagation of uncertainty analyses of complex systems*. Reliability Engineering and System Safety, 2003. **81**(1): p. 23-69.
8. Sandu, A., C. Sandu and M. Ahmadian, *Modeling multibody systems with uncertainties. Part I: Theoretical and computational aspects*. Multibody System Dynamics, 2006. **15**: p. 373-395.
9. Gorsich, D., M. Chaika, D. Gunter, R. Karlsen, and B. Haueisen, *Terrain Roughness Standards for Mobility and Ultra-Reliability Prediction*, in *SAE World Congress*: Detroit, MI. 2003
10. Gipser, M., *FTire Documentation Manual*. 2007(http://www.ftire.com/docu/ftire_ft.pdf).
11. Bekker, M.G., *Theory of Land Locomotion*. 1956, Ann Arbor, MI: University of Michigan Press.
12. Fröhlich, O.K., *Druckverteilung im baugrunde*. 1934: Springer.
13. Koolen, A.J. and H. Kuipers, *Agricultural Soil Mechanics*. 1983, Germany: Springer-Verlag.
14. Ayers, P.D. and J. Van Riper, *Stress distribution under a uniformly loaded rectangular area in agricultural soils*. Trans. of the ASAE, 1991. **34**(3): p. 706-710.
15. Feda, J., *Stress in Subsoil and Methods of Final Settlement Calculation*. 1978, Amsterdam: Elsevier.
16. Bekker, M.G., *Introduction to Terrain-Vehicle Systems*. 1969, Ann Arbor, MI: University of Michigan Press.
17. Bekker, M.G., *Off-the-Road Locomotion*. 1960, Ann Arbor, MI: University of Michigan Press.

18. Wong, J.Y. and M.G. Bekker, *Terrain Vehicle Systems Analysis*, Monograph, Department of Mechanical and Aerospace Engineering: Carleton University, Ottawa, Ont., Canada. 1976-78, 1980 and 1985
19. Wong, J.Y., "Evaluation of Soil Strength Measurements," Report no. NRCC 22881, Division of Energy, National Research Council of Canada, 1983.
20. Wong, J.Y., *Terramechanics and Off-Road Vehicles*. 1989, Amsterdam: Elsevier Science.
21. Wong, J.Y. and J. Preston-Thomas, *On the Characterization of the Shear-Stress-Displacement Relationship of Terrain*. Journal of Terramechanics, 1983. **19**(4).
22. Wong, J.Y., M. Garber and J. Preston-Thomas, *Theoretical Prediction and Experimental Substantiation of the Ground Pressure Distribution and Tractive Performance of Tracked Vehicles*. Transport Engineering, 1984. **198**(no. D15).
23. Aardema, J., *Failure Analysis of the Lower Rear Ball Joint on the High-Mobility Multipurpose Wheeled Vehicle (HMMWV)*. 1988.
24. Frame, E. and M. Blanks, "Emissions From a 6.5 L HMMWV Engine on Low Sulfur Diesel Fuel and JP-8," Report Number TFLRF No. 376, U.S. Army Corps of Engineers, 2004.
25. Haug, E.J., *Computer-Aided Kinematics and Dynamics of Mechanical Systems. Volume I:Basic Methods*. 1989, Boston, MA: Allyn and Bacon.
26. Gipser, M., *FTire: a physically based application-oriented tyre model for use with detailed MBS and finite-element suspension models*. Vehicle Systems Dynamics, 2005. **43**(Supplement/2005): p. 76 - 91.
27. Datar, M. and D. Negrut, "Virtual Prototyping of Ground Vehicles: Technical Report TR-2007-03 " Simulation-Based Engineering Laboratory, University of Wisconsin, Madison., 2007.
28. Ma, Z. and N.C. Perkins, *A Track-Wheel-Terrain Interaction Model for Dynamic Simulation of Tracked Vehicles*. Vehicle System Dynamics, 2002. **37**(6): p. 401-421.
29. Rubinstein, D. and R. Hitron, *A detailed multi-body model for dynamic simulation of off-road tracked vehicles*. Journal of Terramechanics, 2004. **41**: p. 163-173.
30. Ryu, H.S., D.S. Bae, J.H. Choi and A.A. Shabana, *A compliant track link model for high-speed, high-mobility tracked vehicles*. International Journal for Numerical Methods in Engineering, 2000. **48**: p. 1481-1502.
31. Ryu, H.S., K.S. Huh, D.S. Bae and J.H. Choi, *Development of a Multibody Dynamics Simulation Tool for Tracked Vehicles (Part I, Efficient Contact and Nonlinear Dynamics Modeling)*. JSME International Journal, 2003. **46**(2).
32. Rula, A.A. and C.J. Nuttall, "An Analysis of Ground Mobility Models (ANA-MOB)," Technical Report M-71-4, U.S. Army Corps of Engineers Waterways Experiment Station, 1971.
33. Shoop, S.A., "Terrain Characterization for Trafficability," 93-6, CRREL, US Army Corps of Engineers, 1993.
34. McCullough, M.K. and E.J. Haug, *Dynamics of High Mobility Track Vehicles*. ASME Paper No. 85-DET-95, 1985.

35. Sandu, C. and J.S. Freeman, *Military tracked vehicle model. Part I: multibody dynamic formulation*. International Journal of Vehicle Systems Modelling and Testing, 2005. **1**(1/2/3): p. 48-67.
36. Ma, Z. and N.C. Perkins, *A Super-Element of Track-Wheel-Terrain Interaction for Dynamic Simulation of Tracked Vehicles*. Multibody System Dynamics, 2006. **15**: p. 351-372.
37. Eberlein, M., R. Musiol and H. Haut, *Kinematic analysis of the crawler travel gear of a bucket wheel excavator using multibody simulation*. World of Mining, 2008. **60**(4): p. 232-241.
38. Choi, J.H., H.C. Lee and A.A. Shabana, *Spatial Dynamics of Multibody Tracked Vehicles Part I: Spatial Equations of Motion*. Vehicle System Dynamics, 1998. **29**: p. 27-49.
39. Madsen, J., "High Fidelity Modeling and Simulation of Tracked Elements for Off-Road Applications Using MSC/ADAMS: Technical Report TR-2007-02," Simulation-Based Engineering Laboratory, University of Wisconsin, Madison, 2007.
40. Anitescu, M. and F.A. Potra, *Formulating dynamic multi-rigid-body contact problems with friction as solvable linear complementarity problems*. Nonlinear Dynamics, 1997. **14**(3): p. 231-247.
41. Gottschalk, S., M.C. Lin and D. Manocha, "OBB-Tree: A Hierarchical Structure for Rapid Interference Detection," University of North Carolina, 1996.
42. *ADAMS Standard Documentation and Help*, MSC Software Corporation, MD/ADAMS R3 2007
43. Madsen, J., D. Ghiocel, D. Gorsich, D. Lamb, and D. Negrut, *A Stochastic Approach to Integrated Vehicle Reliability Prediction (DETC2009-87487)*, in *2009 International Design Engineering Technical Conferences ASME*: San Diego, Ca. 2009
44. Slattengren, J., *Utilization of ADAMS to Predict Tracked Vehicle Performance*, in *SAE World Congress*, SAE: Detroit, MI. 2000
45. Santner, T.J., B.J. Williams and W. Notz, *The Design and Analysis of Computer Experiments*. 2003: Springer.

Appendix A

ADAMS Post-Processing Commands

pages2_jpgs_name.command

This command is executed in the ADAMS Command Window, and exports and saves all created plots as JPG files.

(Derived from ADAMS KnowledgeBase article KB8014834)

```

! TO USE:
! Create all plots using the plot config file
! Open the command window (F3)
! run the command: fi com re fi = "pages2jpgs_name.command"
!---set hardcopy defaults you want (ex. jpg)
defaults hardcopy &
language = jpg &
send_to_printer = no &
black_and_white_graphics = no

!---set a temporary variable to store the page names
var set var=.gui.plot_print_panel.my_pages
object_value=(eval(DB_CHILDREN((DB_DEFAULT(.system_defaults,
"page").parent), "page")))

!---Use a FOR/END loop construct to:
!     1. display a page
!     2. store its shortened name in a temporary variable
!     3. print it to a file using the short name
!
for var=h start=1
end=(eval(ROWS(.gui.plot_print_panel.my_pages))) inc=1
    interface plot window page_display
page=(eval(.gui.plot_print_panel.my_pages[h]))
    variable set variable = .gui.plot_print_panel.short_name &
        string =
(eval(db_short_name(.gui.plot_print_panel.my_pages[h])))
    hardcopy page=(eval(.gui.plot_print_panel.my_pages[h])) &
        file=(.gui.plot_print_panel.short_name)
end !for

!---delete the temporary variable

```

```
var del
var=.gui.plot_print_panel.my_pages,.gui.plot_print_panel.short_name
!
```

exportHMMWVdata.command

Exports all the data in plots that were created with a plot configuration file. Please note that this is only a code snippet, and the file should be modified to account for all the data that is utilized to create the plots using the plot configuration file.

```
! A macro that will write all the plot data from the HMMWV
simulations to individual .dat files
! RUNNING THE MACRO:
! The request data should have already been imported, and the
plots MUST have been created (most likely by using the plot
config file) since this macro uses plot data
! Open the command line (press F3), and issue the command: fi com
re fi = "exportHMMWVData.command"
! Lots of data files (.dat format) will be written to the ACar
directory
!
! Created by: Justin Madsen, University of Wisconsin-Madison
! Revised: Nov 8 2008
!

if cond=("numeric" == "analysis" || "numeric" == "request" ||
"numeric" == "results" || "numeric" == "graphics")
    interface container execute container =
.gui.ppt_file_export.c_analysis undisplay = no
else
    interface container execute container =
.gui.ppt_file_export.c_numeric undisplay = no
numeric_results write  &
    result_set_component_name =
.lca_balljoint_disp.Dx_longitudinal.y_data,
.lca_balljoint_disp.Dy_lateral.y_data,
.lca_balljoint_disp.Dz_vertical.y_data  &
    &
    order = ascending  &
    write_to_terminal = off  &
    file_name = "lca_balljoint_disp.dat"  &
    &

end
```

Adams_output.command

Automates the post-processing of stochastic simulations by deleting old plots, importing a new request file, creating a new set of plots from the imported data, then exports the plots as JPG files and saves the output data. Note that small changes are required for each instance of this file, but it can be easily created using the same scripts that create multiple instances of the vehicle model files.

```

! run the command: fi com re fi = "Adams_output.command"

! delete old plots
group modify group=SELECT_LIST
objects=.gui.ppt_main.sash1.sash2.gfx.page_uca_balljoint_force
interface plot window page_display
page=.gui.ppt_main.sash1.sash2.gfx.page_uca_balljoint_force
group modify group=SELECT_LIST
objects=.gui.ppt_main.sash1.sash2.gfx.page_uca_balljoint_force, &
.gui.ppt_main.sash1.sash2.gfx.page_uca_balljoint_disp,
.gui.ppt_main.sash1.sash2.gfx.page_spring_force, &
.gui.ppt_main.sash1.sash2.gfx.page_spring_disp,
.gui.ppt_main.sash1.sash2.gfx.page_spindleUpRight_torque, &
...
.gui.ppt_main.sash1.sash2.gfx.page_absorber_disp
if cond = (db_count( "select_list", "objects") == 0)
    group object add group=select_list &
        objects = (eval(select_objects( (none), "*",
"Plotting")))
    if cond = (db_count("select_list", "objects") == 0)
        return
    end
end
undo begin
mdi delete_macro
undo end

! Import new REQ file

interface dialog display dia=.gui.ppt_file_import
parameter="request"
file request read  &
```

```

    file_name =
"file://C:/Army_Road_Project/Year2_Results/degraded_road260002_no
Turns_17MPH_set1_5/Roadname_noTurns_17MPH_set1_6.req"  &
    model_name = .HMMWV_final_ARB_pitman  &
    &
    disk_based_results = no  &
    &
    time_step_skip = 9

!
if condition = ((request=="analysis")||("request"]=="request"))
    interface plot panel mode_set mode = request
elseif condition = ("request"]=="results")
    interface plot panel mode_set mode = result
end ! IF
!
if condition = ((request=="analysis")||("request"]=="graphics"))
    interface plot window load_view  &
        analysis_name = (eval( db_default( .system_defaults,
"analysis" )))
end ! IF ON results or graphics
interface plot panel reload
interface tree_navigator refresh=TRUE
if condition =1
    interface dia undisp dia=.gui.ppt_file_import
end

! New plots

int dia disp dia=.gui.ppt_file_import parameter="plot_cfg"
variable set
variable=.gui.ppt_file_import.plot_cfg.analyses_check &
integer_value=0
if condition=(.gui.ppt_file_import.plot_cfg.analyses_check &&
"no"=="no")
    variable set variable=.gui.ppt_file_import.plot_cfg.continue &
    integer_value=(eval(alert("question","For multiple analyses,
Cross Plotting is enforced. Would you like to:","Continue", "", "Cancel",1)))
    if condition=(.gui.ppt_file_import.plot_cfg.continue == 3)
        variable set
variable=.gui.ppt_file_import.plot_cfg.errorFlag integer_value=1
        return
    end
    interface toggle set
toggle=.gui.ppt_file_import.plot_cfg.t_cross_plotting state=on
end
acar postprocessing plots create &

```

```
analysis_names=.HMMWV_final_ARB_pitman.Roadname_noTurns_17MPH_set
1_6 &

config_file_name="mdids://humvee/plot_configs.tbl/HMMWV_output.pl
t" &
&
cross_plotting=no &
execute_macros=no
interface plot panel reload
interface tree_navigator refresh=TRUE
if condition =1
    interface dia undisp dia=.gui.ppt_file_import
end
if cond = (db_count( "select_list", "objects") == 0)
    group object add group=select_list &
        objects = (eval(select_objects( (none), "*", "
"Plotting")))
    if cond = (db_count("select_list", "objects") == 0)
        return
    end
end
undo begin
mdi delete_macro
undo end

! export jpgs, data
fi com re fi = "pages2jpgs_name.command"
fi com re fi = "exportHMMWVData.command"
```

Appendix B

Latin Hypercube Design Values

Table B.1. Nominal soft-soil parameters for dry sand model

k_c [N/m ⁿ⁺¹]	k_ϕ [MN/m ⁿ⁺²]	n [-]	A_u [N/m ⁴]E ⁸	c [N/m ²]	ϕ [-]	K [mm]
999.9	1.5284	1.1	5.030	1040	0.4887	10

Table B.2. LH sample values for soft-soil parameters

Sample #	k_c [N/m ⁿ⁺¹]	k_ϕ [MN/m ⁿ⁺²]	n [-]	A_u [N/m ⁴]E ⁸	c [N/m ²]	ϕ [-]	K [mm]
1	1033.9	1.5936	1.0687	5.0405	998.45	0.47832	9.7541
2	995.96	1.5462	1.1034	5.1924	1063.8	0.46942	9.5480
3	955.16	1.5856	1.1109	5.1625	1073.6	0.49364	10.323
4	959.98	1.6012	1.1542	5.0220	1051.5	0.46708	10.040
5	966.91	1.5637	1.1177	4.7818	1003.9	0.46471	10.497
6	965.05	1.4799	1.1490	5.1195	994.20	0.48052	9.8278
7	1040.9	1.4996	1.0452	5.2139	1089.2	0.48536	9.6059
8	1029.5	1.4626	1.1112	4.8329	1016.4	0.49781	10.186
9	983.06	1.5376	1.1419	4.9469	1087.5	0.48603	10.420
10	986.47	1.5896	1.0748	4.8964	1028.1	0.50718	10.160
11	1006.7	1.5508	1.1410	5.0124	1044.3	0.47674	9.7257
12	1002.9	1.5583	1.1304	4.9019	1009.8	0.50869	9.8978
13	981.48	1.4836	1.0643	5.2764	1078.9	0.50972	9.7834
14	1031.8	1.5011	1.1255	4.8583	1034.1	0.47504	9.5118
15	970.51	1.5213	1.0612	4.8589	1020.3	0.49203	10.082
16	1042.5	1.5093	1.0564	5.2290	1023.8	0.49647	10.341
17	992.38	1.5764	1.0919	5.0753	1048.6	0.50219	9.9510
18	1020.8	1.5739	1.0972	4.9708	1029.7	0.47360	9.6337
19	977.40	1.4890	1.1018	4.9246	1062.1	0.48310	10.399
20	951.13	1.5137	1.0821	5.0891	1055.0	0.50473	10.264
21	1047.6	1.5333	1.0876	5.1519	989.86	0.48801	10.257
22	1001.8	1.5295	1.1198	5.1285	1007.4	0.49950	10.121
23	1016.2	1.4743	1.1342	5.2577	1038.3	0.47086	10.007
24	1012.1	1.4576	1.0512	4.8024	1068.9	0.48988	9.6922
25	1022.7	1.4671	1.0770	4.9833	1081.7	0.51121	9.9339